

A STUDY OF EARLY STAGES IN PROTEIN AGGREGATION

By

Srabasti Acharya

A DISSERTATION

Submitted to
Michigan State University
in partial fulfillment of the requirements
for the degree of

Physics - Doctor of Philosophy
Quantitative Biology - Dual Major

2014

ABSTRACT

A STUDY OF EARLY STAGES IN PROTEIN AGGREGATION

By

Srabasti Acharya

Protein aggregation has been widely associated with neurodegenerative diseases like Alzheimer's and Parkinson's. One of the challenges associated with treating these diseases is that by the time people go to the doctor, the aggregation process has already spread all over their brain and killed a big chunk of the brain cells. The biochemical changes start happening at least a decade before the actual symptoms occur. In order to treat these diseases, it is essential to catch the aggregation process very early. This thesis presents a novel biophysical approach of attacking the aggregation problem, which is aimed at early detection of neurodegenerative diseases.

My findings suggest that monomer reconfiguration controls early steps in protein aggregation. When reconfiguration is fast, bimolecular association is not stable and can be disrupted easily, but as reconfiguration slows, association is more stable and the likelihood of aggregation increases. This hypothesis is tested in both A β peptide and α -synuclein. Furthermore, we find that mutations that have been associated with these diseases promote aggregation by slowing down reconfiguration. On the other hand, good mutations that inhibit aggregation speed up reconfiguration and thus reduce the chances of the protein from getting trapped into making stable intermolecular interactions. This suggests that speeding up reconfiguration can be used as an effective strategy of rescuing proteins from aggregation. Using this technique, we have identified an inhibitor molecule which can become a potential drug candidate for fighting neurodegeneration.

ACKNOWLEDGEMENTS

The central factor that kept me from losing my sanity during the course of my graduate years was my advisor Dr. Lisa Lapidus. When I joined her lab, I had absolutely no prior experience in conducting independent research. She walked me in baby steps, ushering me to a point where I can design, conduct and analyze experiments independently. Her perpetual tolerance towards my ignorance has encouraged me to shed all inhibitions in raising questions and clarifying daily doubts. The long open discussions I had with her often transcended beyond research, triggering a bond of camaraderie and comfort. Without her constant guidance, support and motivation, this research journey would not have been possible.

I am thankful to my committee members for providing me with constructive feedback on my research projects and presentations. I am especially grateful to Dr. Mahanti, who has been a father figure to me from the day I started at MSU. He has been a very kind mentor and has always addressed my concerns regarding courses, research and even future plans.

I would like to thank all my lab members, past and present, for creating such an amicable work environment. I have been surrounded by exceptionally talented colleagues, always willing to share their scientific wisdom. I am especially grateful to Kinshuk for his invaluable research tips and suggestions; the frequent scientific discussions with him have been very fulfilling and inspired me to read more papers. I would also like to thank Aimee and Dena for being such great friends and giving me splendid memories of working together.

My mother shielded me through thick and thin, and was always just one phone call away. Without the financial support of my father, I would not have made it to grad school. I am obligated to both of them for never giving up on me.

I am endlessly indebted to my husband, Ritesh, for supporting me through moments of extreme hopelessness and desperation. I would have quit grad school long ago, hadn't it been for his undying conviction in my potential. He gifted me with a daily dose of fun and laughter, sometimes in person and sometimes through skype. His occasional trips to East Lansing rejuvenated my spirits and motivated me to invest more time into research; that turned out to be the driving force behind my accomplishments.

TABLE OF CONTENTS

LIST OF TABLES	vii
LIST OF FIGURES	viii
Chapter 1	1
Introduction to Protein Aggregation	1
1.1 Protein Folding.....	1
1.2 Protein Misfolding and Aggregation	2
1.3 Reconfiguration and Aggregation.....	6
Chapter 2.....	11
Measuring Intramolecular Contact Formation.....	11
2.1 Method	11
2.2 Data Analysis Using SSS theory.....	16
2.3 Boltzmann Energy Reweighting	21
2.4 The Charge Effect.....	24
Chapter 3.....	26
Protein Aggregation in Alzheimer's disease.....	26
3.1 A β Production	26
3.2 Intracellular A β Accumulation	27
3.3 A β Associated with Alzheimer's disease.....	28
3.4 Neurotoxic Effects of A β	29
3.5 Structure of A β Monomer.....	30
3.6 Dimers and Trimers	31
3.7 Higher Order Aggregates.....	31
3.8 Comparison of A β_{42} and A β_{42}	34
3.9 Expression and Purification Protocol.....	35
3.10 Thioflavin T Assay	38
3.11 Trp Cys Quenching Measurement	39
3.12 Mutation Sites	40
3.13 Measuring Reconfiguration	44
Chapter 4.....	56
Protein Aggregation in Parkinson's disease	56
4.1 Introduction.....	56
4.2 Physiological Function.....	58
4.3 Effects of Oligomers on Neurotoxicity.....	59
4.4 Structure.....	61
4.5 Mutations Associated with PD.....	64
4.6 Expression and Purification Protocol.....	68
4.7 Contact Quenching Experiment.....	69

4.8 Effect of Good and Bad Mutations on Reconfiguration	69
4.9 Effect of Inhibitors on Reconfiguration	79
4.10 Molecule that Slows Down Reconfiguration	81
4.11 Molecule Tweezer.....	84
Chapter 5	95
Conclusion	95
BIBLIOGRAPHY	98

LIST OF TABLES

Table 3.1 Parameters for two different polymeric models that best fit the experimental data	55
Table 4.1 Parameters obtained from Gaussian analysis for aggregation prone mutations.....	93

LIST OF FIGURES

Figure 1.1 Two amino acids forming a peptide bond by removal of a water molecule (http://molecularsciences.org/files/images/peptidebond.jpg).....	9
Figure 1.2 Energy landscape connecting protein folding and aggregation [11] (http://www.ncbi.nlm.nih.gov/pmc/articles/PMC2706318/#!po=45.1220).....	9
Figure 1.3 Kinetic scheme describing the early phases of aggregation [17] (http://pubs.rsc.org/en/Content/ArticleLanding/2013/MB/c2mb25334h#!divAbstract).....	10
Figure 1.4 Oligomer formation rate with time at different reconfiguration rates [17] (http://pubs.rsc.org/en/Content/ArticleLanding/2013/MB/c2mb25334h#!divAbstract).....	10
Figure 2.1 Determination of the rate of contact formation between the probe, tryptophan (W), and the quencher, cysteine (C), at the ends of a flexible peptide. Pulsed optical excitation leads to population of the lowest excited triplet state of tryptophan. Tryptophan contacts cysteine in a diffusion-limited process with rate k_{D+} , and then either diffuses away or is quenched by the cysteine.....	13
Figure 2.2 A typical Gaussian polymer chain made of N rigid rods connected together by flexible pivot points.....	17
Figure 2.3 A schematic representation of worm like chain model showing the constraint parameters parameter length l_p and excluded volume diameter d_s	20
Figure 2.4 Experimental setup for measuring contact quenching.....	25
Figure 3.1 Sequence of A β ₄₂ WT with arrows showing the positions of Trp and Cys mutations for the 2 loops created.....	42
Figure 3.2 Thioflavin T fluorescence spectra of A β ₄₂ WT along with the 2 Trp/Cys containing mutants.....	42
Figure 3.3 The CD spectra of A β ₄₂ WT, and the 2 loops containing Trp/Cys, both for A β ₄₂ and A β ₄₀	43
Figure 3.4 Decay of Trp triplet states W19C35 at pH 7.5, 0 C as monitored by the decay of absorption of 445 nm light and captured through oscilloscope.....	50

Figure 3.5 The fast lifetimes of Trp triplet at pH 7.5 for various viscosities and temperatures as marked. a) A β_{42} M35C, F19W loop, pH 7.5 b) A β_{42} F4C, F19W loop, pH 7.5 c) A β_{40} M35C, F19W loop, pH 7.5 d) A β_{40} F4C, F19W loop, pH 7.5 e) A β_{42} M35C, F19W loop, pH 10 f) A β_{42} M35C, F19W loop, pH 7.5: Curcumin.....51

Figure 3.6 Comparison of intramolecular diffusion of the 2 loops of A β_{40} and A β_{42} (peptide concentration =30 μ M) a) Measured reaction-limited rates, as determined from the intercept of plots such as Fig. 9 (a, b, c, d) versus temperature b) Measured diffusion-limited rates as determined from the slope of plots such as Fig. 9 a, b, c, d normalized to the viscosity of water at each temperature. Errors from the linear fits are shown as error bars in (a) and (b). c) Average Trp-Cys distance calculated from the reweighted worm-like chain (WLC) model as described above d) Intramolecular diffusion coefficients determined using the WLC model.....52

Figure 3.7 Modulation of reconfiguration of A β_{42} by altering solution conditions and adding an inhibitor a) Measured intramolecular diffusion coefficients at pH 7.5 and pH 10 for A β_{42} M35C, F19W loop b) Average Trp-Cys distance at pH 7.5 and pH 10 for A β_{42} M35C, F19W loop determined using the WLC model from measured reaction and diffusion-limited rates obtained from plots shown in Fig. 9e c) Measured intramolecular diffusion coefficients for A β_{42} M35C, F19W loop, with and without inhibitor Curcumin (peptide: Curcumin=1:1) d) Average Trp-Cys distance for A β_{42} M35C, F19W loop, with and without curcumin, determined using the WLC model from measured reaction and diffusion-limited rates obtained from plots shown in Fig. 9f.....53

Figure 3.8 Formation of oligomer [O] versus time for A β_{42} (black) and A β_{40} (red) which was calculated using previously reported kinetic model that correlates reconfiguration with oligomer formation.....54

Figure 4.1 ($1/k_{obs}$) versus viscosity at pH 7.5, at various temperatures as marked, for α -synuclein a) Y39W-A69C loop in the wild type sequence b) A53T mutant c) V74E mutant. Protein concentration=30 μ M.....76

Figure 4.2 Effects of Aggregation-Enhancing, PD-Causing, Familial Mutations (A53T, E46K, and A30P). a) Reaction-limited rates. b) Diffusion-limited rates, normalized to the viscosity at water at that temperature. c) Average root mean square distance between W39 and C69 determined from reaction-limited rates d) Intramolecular diffusion coefficients determined for each diffusion-limited rate.....77

Figure 4.3 Effects of Aggregation Reducing Mutations (V74E and T72P). a) Reaction-limited rates. b) Diffusion-limited rates, normalized to the viscosity of water at that temperature. c) Average root mean square distance between W39 and C69 determined for each reaction-limited rate d) Intramolecular diffusion coefficients determined for each diffusion-limited rate.....78

Figure 4.4 ($1/k_{obs}$) versus viscosity at pH 7.5, at various temperatures for inhibitor with α -synuclein Y39W-A69C loop a) Molecular tweezer, CLR01 b) inhibitor Baicalein c) inhibitor EGCG. Protein concentration=30 μ M.....88

Figure 4.5 Effects of Natural Inhibitors on α -synuclein. a) Reaction-limited rates. b) Diffusion-limited rates, normalized to the viscosity of water at that temperature. c) Average root mean square distance between W94 and C69, determined from the reaction-limited rates d) Intramolecular diffusion coefficients determined from diffusion-limited rates..... 89

Figure 4.6 Effect of EGCG on α -synuclein. a) Reaction-limited rates. b) Diffusion-limited rates, normalized to the viscosity of water at that temperature. c) Average root mean square distance between W94 and C69, determined from the reaction-limited rates d) Intramolecular diffusion coefficients determined from diffusion-limited rates.....90

Figure 4.7 Concentration dependant effect of Molecular Tweezer on α -synuclein. a) Reaction-limited rates. b) Diffusion-limited rates, normalized to the viscosity of water at that temperature. c) Average root mean square distance between W94 and C69, determined from the reaction-limited rates d) Intramolecular diffusion coefficients determined from diffusion-limited rates.....91

Figure 4.8 Molecular Tweezer CLR01 molecule.....92

Figure 4.9 Effect of binding of CLR01 on Trp94 fluorescence of α -synuclein. Protein concentration was fixed at 1 μ M and the CLR01 concentration was gradually increased.....92

Figure 4.10 Calculated effect of CLR01 binding on α -synuclein conformation. a) Re-weighted probability distributions, $Z(r)$, for $\sigma = 0$, $\gamma = 20$ for α -synuclein alone (blue), α -synuclein with one CLR01 bound at Lys10 (cyan), one CLR01 bound at Lys12 (magenta), and α -synuclein bound to two CLR01 molecules in positions 10 and 12 (red). In each case, the bound CLR01 are approximated by Lys \rightarrow Glu substitutions. b) Calculated (red triangles) reaction-limited rates using Eq. 9 and the probability distributions calculated in (a). The measured reaction-limited rates are plotted as black circles.....93

Figure 4.11 Intramolecular contact plots a) E46K and b) V74E. Each plot is the difference between the mutant and the wildtype sequence. The average distance is calculated from the reweighted ensembles using Eqs. 6 and 7 for $\gamma=9$94

Chapter 1

Introduction to Protein Aggregation

1.1 Protein Folding

Proteins are the major components of the living cell and play an important role in maintaining life. They are produced inside our cells by the process of translation, and comprise of amino acids linked by peptide bonds. There are 20 naturally occurring amino acids, and each comprise of a backbone that includes a carboxyl and an amino group and a distinctive side chain (R-group) bonded to the C_{α} atom (shown in Figure 1.1). Two amino acids may link together such that the OH of the carboxyl group of one amino acid and H of the amino group of another may be removed in the form of a water molecule giving rise to a peptide bond connecting the CO and NH_2 groups. This dipeptide may be joined by more amino acids forming a polypeptide chain, which is also called a protein. Each protein will contain one free amino group which is known as the N-terminus, one free carboxyl group known as the C-terminus, R groups referred to as residues, and the linked carbon, nitrogen and oxygen atoms in between C and N-terminus (except the R-group) referred to as the main chain or backbone. The R-group imparts unique physiochemical properties to each amino acid. They can be broadly classified as being aliphatic (alanine, glycine, isoleucine, leucine, proline, valine), aromatic (phenylalanine, tryptophan, tyrosine), acidic (aspartic acid, glutamic acid), basic (arginine, histidine, lysine), hydroxylic (serine, threonine) sulphur-containing (cysteine, methionine), amidic (asparagines, glutamine). However, they may also be classified based on their polarity, size, charge or hydrophobicity.

Most proteins fold into a unique 3-dimensional structure called the native state that is essential for its proper functioning. The hydrophobic collapse has been widely described as one

of the key factors that drive protein folding, apart from other factors like Vander Waals forces, electrostatic Coulomb interactions, hydrogen bonds, disulfide bridges, etc. Anfinsen in his famous experiment showed that the folding and unfolding of proteins is reversible and proved that a protein would spontaneously fold into the most stable state, which suggests that the information needed to determine the final native conformation is located in the sequence itself [1]. However, Levinthal's paradox states that it is impossible for proteins to sample all possible conformations in physiologically relevant time to attain its native state, and the fact that protein folding happens in millisecond timescale suggests that there must be a specific folding pathway guided by native-like interactions already present within the unfolded state. NMR and X-ray scattering studies have detected the presence of local and long-range contacts, native-like and non-native interactions within the unfolded states referred to as residual structures [2]. Experimental and computational studies have further shown that intramolecular diffusion of unfolded states of well behaved proteins is relatively slow, suggesting a rugged energy landscape, since a smooth landscape would enable unfolded conformations to reconfigure rapidly by diffusion without having to slow down [3][4][5].

1.2 Protein Misfolding and Aggregation

Protein aggregation is the process in which non-native conformations of two or more proteins interact, leading to their self-assembly into a variety of structures called aggregates. Protein-protein interactions leading to aggregation is unwanted because it often prevents the protein from adopting its functional state and detrimental because the resulting protein aggregates often have toxic properties and can lead to neurodegeneration[6]. Evidence collected over the years suggest that protein aggregation can initiate from different conformations ranging from a fully unfolded monomer to misfolded states or a partially folded conformation [7]. In all

the above cases, aggregation-prone segments that are normally buried in the fully folded state become exposed to the solvent, initiating intermolecular interactions which can lead to the formation of amyloid-like oligomers and fibrils. What makes one protein more aggregation prone than another? Sequence definitely plays a key role and generally sequences that have high hydrophobicity, low net charge and high β -sheet forming propensity are more likely to aggregate.

One of the most widely accepted mechanisms for assembly of monomers into aggregates is the previously reported ‘nucleation growth’ mechanism. According to this mechanism, the nucleus which could very well be a monomer, acts as a template for growth of an aggregate through the association of further monomers. Evidence have been found of proteins populating amyloid conformations at the monomeric level which were described as ‘ β -like’ structures that seemed increase with aggregation promoting conditions [8]. Study of insulin aggregation has revealed that monomers without undergoing any structural organization directly assemble at the end of a growing aggregate and lead to elongation of an amyloid like fibril [9]. However, in some cases evidence were found suggesting that native monomers initially convert into misfolded conformations, which initiate self-assembly through a template-independent mechanism with formation of an amyloid-like oligomer that acts as a nucleus, leading to higher order oligomer formation and then finally fibrils. This mechanism is referred to as ‘nucleated conformational conversion’ mechanism [7]. It was recently shown that the $A\beta_{40}$ monomers can rapidly form small spherical oligomers *in vitro* that are kinetically competent to slowly convert to amyloid fibrils following the nucleated conformational conversion [10]. The two models differ in many ways. In the former model, it is believed that the monomer may directly interact with the nucleus, the nucleus may be as small as a monomer and the rate-limiting step is considered to

be the formation of the nucleus. The latter model proposes that both the building block as well as the nucleus is the oligomeric species, and the rate limiting step is the conversion of the non-amyloid oligomer into an amyloid-competent oligomer; once that happens amyloid formation advances rapidly. One view that could possibly unify the two models is that the first step of aggregation requires the monomer conformational ensemble to be in a state which exposes their hydrophobic patches long enough to the solvent, which can initiate bimolecular association in between two proteins.

Funnel-shaped free energy landscapes provide a useful description of protein folding in isolation, but the behavior of proteins in the living cells are much more complex and competition between intramolecular and intermolecular interactions will result in increasing ruggedness to the energy landscape. Figure 1.2 shows a previously reported schematic representation of an energy landscape that takes into account both protein folding and aggregation [11]. It shows that a wide range of different conformational states and multitude of pathways may be available to each protein as it navigates through the landscape. Inside living cells, the relative depth of each well will depend upon the protein sequence, solution conditions, temperature and also protein concentration. Energy minima on the aggregation side of the energy landscape are also poorly defined. Sometimes, under same set of solution conditions, a multitude of fibrillar or oligomeric morphologies may be formed, which adds further complexity and multiplicity to the aggregation pathway. However one simple fact that emerges out of such complexity is that protein folding and aggregation are intimately connected, and somewhere along the folding pathway the sequence may take a wrong turn and aggregation happens as an off-pathway event or that some sequences favor the aggregation well over the folding well. Cells have sophisticated quality control mechanisms to ensure that a newly synthesized protein is properly folded before being

released. When misfolded proteins accumulate within cells, organelles like the endoplasmic reticulum (ER) activates a complex signaling network called unfolded protein response (UPR) to cope with the stress [12] [13]. UPR increases expression of chaperone proteins which help to fold the proteins properly and also directs the damaged proteins towards degradation via either ubiquitin–proteasome system or lysosomal autophagy. When such attempts to re-establish ER homeostasis fail misfolded proteins assemble into toxic aggregates, causing cellular dysfunction and death.

There is another interesting class of proteins called the intrinsically disordered proteins (IDPs) which challenges the widely accepted structure-function paradigm. Such IDPs lack stable secondary and or tertiary structures, yet fulfill regular biological functions. They could either exist in state of extended disorder due to repulsion from a net charge, which would resemble an ideal random coil, or a semi-collapsed state containing transient secondary structures referred to as pre-molten globule. Such natively unfolded proteins are typically characterized by a low overall hydrophobicity and large net charge [14]. In comparison with structured proteins, IDPs mostly lack structure-promoting residues (like cysteine, tryptophan, tyrosine, isoleucine, phenylalanine, valine, leucine, histidine, threonine, asparagine) and are relatively enriched in the disorder-promoting residues (aspartic acid, methionine, lysine, arginine, serine, glutamine, proline, and glutamic acid) [15]. Due to lack of a folded structure, the hydration of IDPs is significantly higher than that of globular proteins of similar size, suggesting that the chain has largely exposed interaction surfaces [16].

1.3 Reconfiguration and Aggregation

Aggregation may be defined as the physical process in which two or more proteins may bump into each other and end up clumping together. Within the crowded environment of the cells, the proteins have great chances of bumping across each other, so that raises the very important question as to why they don't always aggregate. Therefore there must be an escape route which needs to be taken into account while describing aggregation. One aggregation model that accommodates this idea has been reported recently [17]. This model talks about the very first step in aggregation from the view of monomer dynamics. A monomeric protein at any time may be sampling different kinds of conformations, a process called protein reconfiguration. Some of those conformations may be aggregation competent monomers (M^*), which may have hydrophobic patches sticking out at the surface; while some of them may be aggregation incompetent monomers (M). Assuming that there is no significant energy barrier between the states, at any time M and M^* may be inter-convertible by diffusive reconfiguration, the rate of which is given by $k_1 \approx k_{-1}$. The reconfiguration rate can be estimated by assuming that it is the rate to diffuse from one point on the chain across the chain diameter, given by $k_1 \sim 4D/(2R_G)^2$ where D is the intramolecular diffusion coefficient and R_G is the radius of gyration of the chain.

For the aggregation process to initiate, two M^* conformers have to first come together by a bimolecular diffusion controlled rate k_{bi} and form an encounter complex $[M^*M^*]$. While both monomers are in the encounter complex two things may happen; they may make stabilizing bimolecular interactions that lead to an oligomeric state O or one or both the monomers may escape by reconfiguration to the innocuous conformation M which makes stabilizing bimolecular interactions difficult and the complex comes apart. Thus there are three possibilities:

- 1) When $k_1 \gg k_{bi}$, the reconfiguration is really fast and before stable associations happen, one or both M^* conformers reconfigures back to an innocuous conformation M .
- 2) When $k_1 \ll k_{bi}$ the reconfiguration happens really slowly, because of which M^* takes a long time to form and so the likelihood of two M^* conformers coming together is really unlikely. Hence the encounter complex is rarely made.
- 3) When $k_1 \approx k_{bi}$ the reconfiguration happens with an optimum speed such that two M^* can react to form a stable encounter complex. When that happens, the encounter complex can proceed to form an oligomeric conformation O .

The previously reported kinetic scheme shown in Figure 1.3 takes into account these three possibilities [17]. It used the bimolecular association rate $k_{bi} \approx 10^5 \text{ s}^{-1}$ calculated for a solution of $100\mu\text{M}$ protein of average molecular weight in water and a range of k_1 values to solve the model. The model assumes that the rate of forming O is much slower compared to rate of formation of the encounter complex, because it would require further structural reorganization and may even need the addition of a third aggregation competent monomer M^* . Under this assumption k_O was chosen to be 100s^{-1} , an arbitrary rate that is slower than the bimolecular association rate and fast enough to allow solving the model within reasonable computation time. The kinetic equations governing the scheme were solved in Matlab to calculate the oligomer O formation rate with time. Figure 1.4 shows the plot of different oligomer formation rates at different k_1 values, ranging from 10^3 to 10^5s^{-1} . It has been previously reported that the reconfiguration rate of α -synuclein is $k_1 \approx 10^5\text{s}^{-1}$ at 40°C [18]. Interestingly, Figure 4 shows that the oligomer formation rate is most rapid when bimolecular association rate matches the reconfiguration rate of α -synuclein such that $k_1 \approx k_{bi} \approx 10^5\text{s}^{-1}$. The physical significance of this is that aggregation results from kinetic competition between reconfiguration and bimolecular

association. When reconfiguration happens at an optimum speed, the aggregation competent monomers get enough time to interact and stick, thus forming stable bimolecular associations in the form of aggregates.

The rate of forming O is assumed to be slower than reconfiguration, but an increased k_o does not affect the overall trend of maximal oligomerization occurring when $k_1 \approx k_{bi}$. Also the escape rate k_{-1} may be different from the diffusive reconfiguration rate k_1 . To take that possibility into account the model was also solved in the scenario such that $k_{-1} \approx x k_1$ where x is some fraction determined by the equilibrium constant for M and M*. That increased the oligomer formation rates, but the overall trend of maximal k_1 remained unchanged, suggesting that $k_1 \approx k_{-1}$ assumption is not unreasonable. Clearly this aggregation model is quite simple and the real process could be more complicated. However, since it has been able to predict the aggregation behavior of α -synuclein correctly and also it is the only model in current literature that explains aggregation from the monomer point of view, I will use this model in good confidence to explain my experimental measurements in subsequent chapters.

In this thesis, I will describe the experimental technique to measure protein reconfiguration in chapter 2 and then go on to test the above mentioned aggregation hypothesis using two sequences, namely A β peptide and α -synuclein protein. In chapter 3, I will talk about A β peptide aggregation in connection with Alzheimer's disease and using aggregation model, I will compare the early aggregation propensity of A β peptide based on its length, pH and addition of an aggregation inhibitor. In chapter 4, I will talk about α -synuclein protein in connection with Parkinson's disease and then show that its reconfiguration rates can be moved around using inhibitors or point mutations.

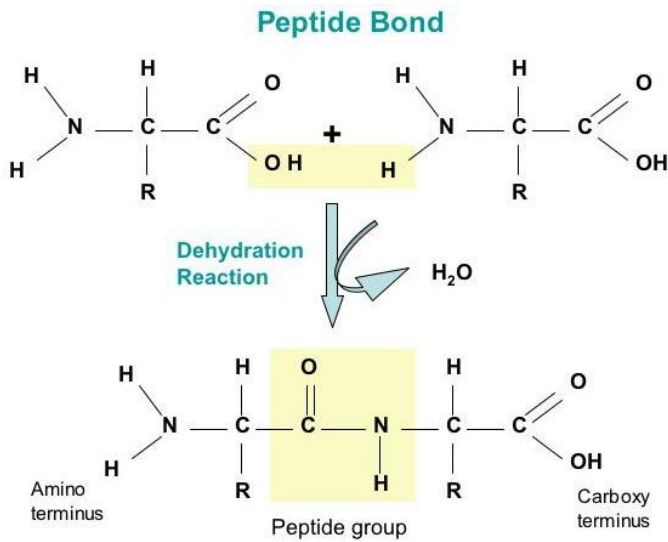


Figure 1.1 Two amino acids forming a peptide bond by removal of a water molecule

(<http://molecularsciences.org/files/images/peptidebond.jpg>)

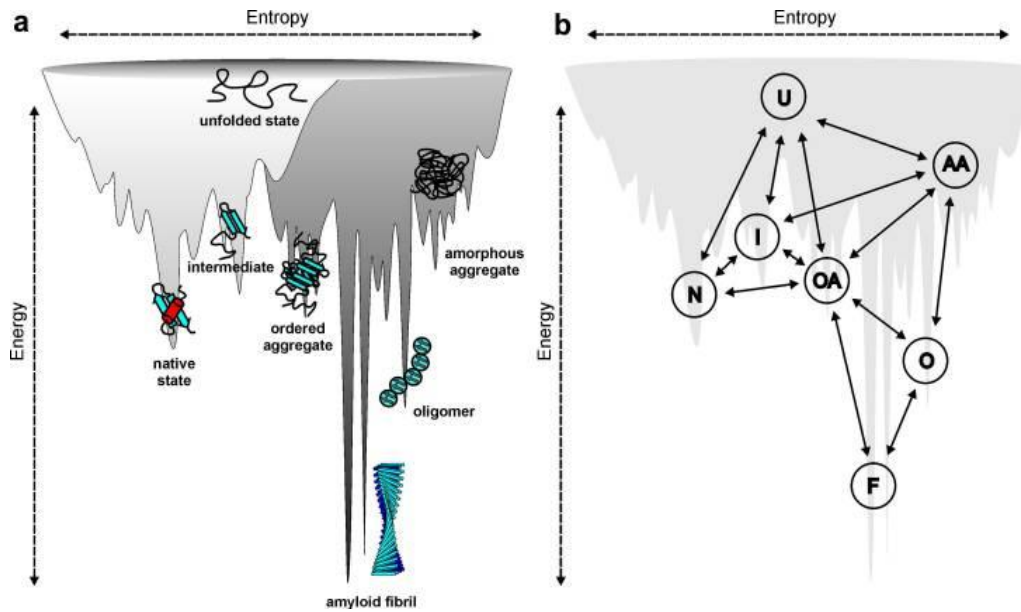


Figure 1.2 Energy landscape connecting protein folding and aggregation [11].

(<http://www.ncbi.nlm.nih.gov/pmc/articles/PMC2706318/#!po=45.1220>)

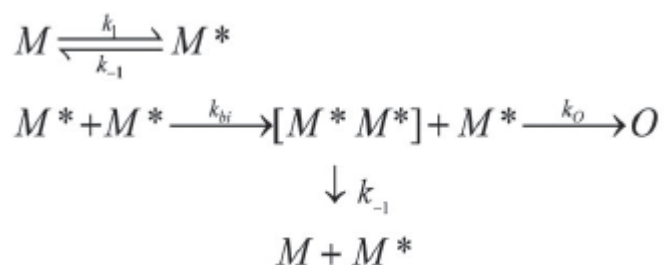


Figure 1.3 Kinetic scheme describing the early phases of aggregation [17].

(<http://pubs.rsc.org/en/Content/ArticleLanding/2013/MB/c2mb25334h#!divAbstract>)

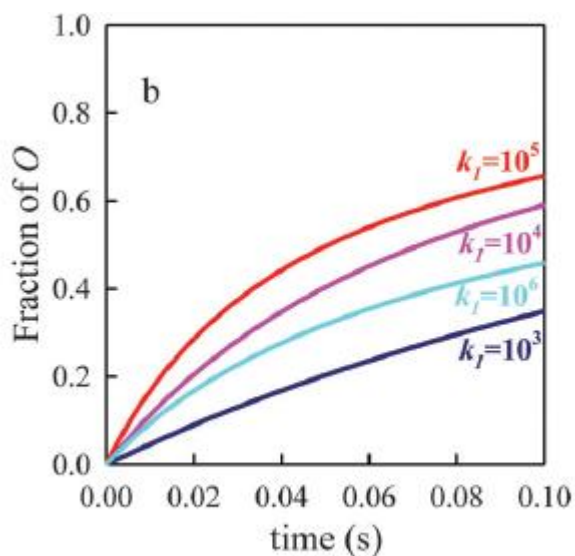


Figure 1.4 Oligomer formation rate with time at different reconfiguration rates [17].

(<http://pubs.rsc.org/en/Content/ArticleLanding/2013/MB/c2mb25334h#!divAbstract>)

Chapter 2

Measuring Intramolecular Contact Formation

In this chapter I will describe the experimental technique for measuring protein reconfiguration and the computation methods of analyzing the data.

2.1 Method

Intramolecular loop formation is one of the very early stages in protein folding. It can be probed by using a pump probe laser spectroscopy method that has been described previously [19]. The mechanism involves introducing two probes into the sequence and then monitoring contact formation between the two probes. We have used two naturally occurring amino acids, namely tryptophan (Trp) and cysteine (Cys) as the two probes, which were incorporated into the protein sequence in a manner which caused negligible perturbation to the original structure and aggregation propensity of the sequence. Sequences should ideally contain only one Trp and Cys so that the measured quenching rate reflects only one intrachain contact formation. Normally multiple Trp-Cys loops are created in different mutants to cover the entire protein length, and also to account for positional dependence of the probes, if any.

Tryptophan is an ideal probe in this case, since it can be excited to long-lived triplet energy states upon absorption of 289 nm UV light. Reportedly, tryptophan triplet life time is about 40 μ s in water and even longer in the hydrophobic core of the folded protein [20]. Cysteine is a very efficient quencher (400 fold faster than other amino acids) and can quench the excited state of tryptophan when nearby, thus cutting short the triplet state life time. The mechanism of quenching reportedly occurs by electron transfer and has an exponential dependence[21] on the intramolecular Trp-Cys distance and is given by the following equation:-

$$q(r) = q_0 \exp[-\beta(r - a_0)] \quad (1)$$

Where r is the intramolecular distance, a_0 is the distance of closest approach (4Å), $q_0=4.2\text{ns}^{-1}$ and $\beta = 40\text{nm}^{-1}$.

The triplet state of tryptophan absorbs visible light at 442nm wavelength, which can be used as a probe to monitor the population of the triplet state. The observed decay rate is a combination of several decay rates:

$$k_{obs} = k_0 + \sum_i k_i^{uni} + \sum_i k_i^{bi} [i] \quad (2)$$

Where k_0 is the decay rate in the absence of any quencher, k_i^{uni} and $k_i^{bi}[i]$ are the unimolecular and bimolecular quenching rates respectively. Since the bimolecular rate ($2 \times 10^8 \text{ M}^{-1}\text{s}^{-1}$) is concentration dependent, by keeping the concentration low (around 30 μM) we ensure that the contribution of the bimolecular rate is negligible[19]. Secondly, the Trp and Cys have to be engineered close enough in sequence so that the unimolecular contact rate is much faster than k_0 ($2 \times 10^4 \text{ s}^{-1}$) and dominates.

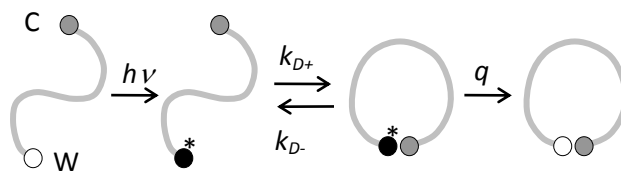
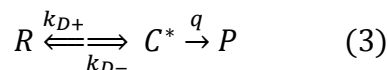


Figure 2.1 Determination of the rate of contact formation between the probe, tryptophan (W), and the quencher, cysteine (C), at the ends of a flexible peptide. Pulsed optical excitation leads to population of the lowest excited triplet state of tryptophan. Tryptophan contacts cysteine in a diffusion-limited process with rate k_{D+} , and then either diffuses away or is quenched by the cysteine.

The microsecond-nanosecond intramolecular loop formation can be explained well by the simple 2-step kinetic model that has been illustrated in Figure 2.1. Tryptophan is first excited to its triplet state by UV light; since the sequence diffuses freely the tryptophan and cysteine may come in close contact towards each other at a rate k_{D+} . Cysteine either quenches the tryptophan at a quenching rate q or diffuses away at rate k_{D-} .

Assuming the following equation approximates the above model:-



Steady state approximation leads to the following equations:-

$$\frac{dC^*}{dt} = 0 = k_{D+}[R] - (k_{D-} + q)[C^*] \quad (4)$$

$$\frac{dP}{dt} = k_{obs}[R] = q[C^*] = q \left(\frac{k_{D+}}{q + k_{D-}} \right) [R] \quad (5)$$

The observed rate k_{obs} is given by:-

$$k_{obs} = \frac{k_{D+}q}{q + k_{D-}} \quad (6)$$

Three situations may arise:-

(1) $q \gg k_{D-}$ (diffusion-limited) then $k_{obs} = k_{D+}$ (diffusion limited rate)

(2) $q \ll k_{D-}$ (reaction limited) then $k_{obs} = q \left(\frac{k_{D+}}{k_{D-}} \right) = qK = k_R$ (reaction limited rate)

(3) $q \sim k_{D-}$ (experimentally feasible):-

$$\frac{1}{k_{obs}} = \frac{1}{qK} + \frac{1}{k_{D+}} = \frac{1}{k_R(T)} + \frac{1}{k_{D+}(T, \eta)} \quad (7)$$

In the ideal case of a diffusion process, as shown by Smoluchowski, the reaction occurs only when the reacting pair comes within a center-to-center distance a (0.4nm) For distances less than or equal to a , reaction is instantaneous and irreversible, while at distances larger than a , reaction rate is assumed to be zero. The Smoluchowski rate is given by $k_{D+bi} = 4\pi D_{bi}a$, where D_{bi} is the sum of diffusion coefficients of the reactants. In real systems, there is distance dependence to this rate, as exhibited by equation (1) and hence a cannot be approximated in the same way as before. Also since the quenching rate q is comparable to k_{D-} , there is a good chance for tryptophan to escape quenching due to the encounter complex breaking apart. Hence the measured rate would be a mixture of reaction-limited and diffusion-limited rate and does not solely reflect diffusion dynamics. The former depends only on temperature (as temperature affects the chemical reaction speed, viscosity does not) while the latter depends on both temperature and viscosity of the solution. This gives us a chance to segregate the two rates by monitoring the observed rate as a function of various temperature and viscosities. Based on equation (7) we assume that $1/k_{obs}$ versus viscosity at a constant temperature exhibits a linear

relationship. Hence by plotting $1/k_{obs}$ versus η and fitting to a straight line at each temperature, the reaction limited rate $k_R=1/\text{intercept}$ and diffusion limited rate $k_{D+}=1/(\eta\text{slope})$. The linear $1/k_{obs}$ versus viscosity relationship may break down in some cases, and power law dependence of the form $1/k_{obs} \propto \eta^\delta$ needs to be applied [22], but for systems comprising of 5-20 residue long loops δ has been estimated to be very close to 1.

Figure 2.4 demonstrates the optical setup for measuring the transient absorption of the tryptophan triplet states using a pump-probe spectroscopy. Two different laser beams are involved in this collinear geometry setup. The Nd:YAG pulse laser (Continuum Surelite, pulse duration: 8 ns, interval time: 10 ms) is employed to pump the tryptophan to the triplet states. The wavelength of the pulse beam is shifted from 266 nm to 289 nm using a Raman cell (filled with methane at 250 psi) to minimize photodamage [23]. Between each pulse, a continuous wave (CW) 441 nm diode laser beam (add) is used to monitor the tryptophan triplet states. It is split into two parts: a reference beam and a sample probe beam. The probe beam is collimated with respect to the pulse beam so that it passes through the sample that contains the tryptophan molecules that have been excited by the pulse beam. The intensities of the probe beam and reference beam are measured using two silicon photodiodes (New-Focus) and LeCroy DA 1886A differential and SR445A, SRS Inc four channel preamplifier with 5 x gain at each stage (which adds two extra stages of amplification). It is then recorded with digital oscilloscopes (Tektronix TDS), subtracted and then stored in a computer using GPIB interface. The absorption decay trace reflects the lifetime of tryptophan triplet states which can range from nanosecond to millisecond. Two oscilloscopes are used to cover the time range; one with a 10 μ s window and one with a 10ms window. To eliminate any pulse leakage and high frequency cable noise, a

background with the pump but without the probe beam is recorded each time at the beginning of each experiment and thereafter subtracted from all other recorded decay traces.

The UV pulse also tends to generate hydrated electrons and neutral radicals that absorb light near 450 nm and decay within 3 μs [19]. Furthermore, O_2 is a good quencher of the tryptophan triplet state. Therefore, before each experiment, the free electrons are scavenged and oxygen molecules are removed by degassing the sample solution with N_2O , a free electron scavenger, for at least one hour to eliminate unwanted contribution from such photo-effects. Another undesired photo-effect is thermal lensing, in which the heat induced by pulse laser changes the refractive index of the solution, causing the probe beam to slightly refract and move across the detector. Thermal lensing may result in a pseudo-decay trace on the millisecond timescale. Ways to diminish the effect of thermal lensing include decreasing the power of the pulse laser, realigning optics of the pulse and probe beams and adjusting detector positions.

The sample cuvette is placed in a Peltier temperature controlled sample holder (Quantum Northwest) for the purpose of measuring sample at different temperatures. N-acetyl-L-tryptophanamide (NATA), which is an uncharged analogue of tryptophan, is used to optimize the alignment of the instrument. NATA has a 40 μs decay time in the presence of deionized water, in the absence of any additional quencher [20].

2.2 Data Analysis Using SSS theory

The polymer theory of Szabo, Schulten and Schulten (SSS) is the model used to explain the experimental results. SSS theory models intrachain diffusion dynamics as a motion on a 1-dimensional potential of mean force which depends on the probability distribution of intrachain distances [24].

$$U(r) = -k_B T \ln P(r) \quad (8)$$

Where k_B is the Boltzmann constant and $P(r)$ is the equilibrium Trp/Cys distance distribution, the observed rate of bringing two ends of the chain in close contact can be expressed as [25]:-

$$\frac{1}{k_{obs}} = \frac{1}{k_R} + \frac{1}{k_R^2 D} \int_{a_0}^{l_c} \frac{dr}{P(r)} \left\{ \int_r^{l_c} (q(x) - k_R) P(x) dx \right\}^2 \quad (9)$$

Where a_0 is the closest contact distance, l_c is the contour length of the loop, D is the intramolecular diffusion constant. The reaction-limited and diffusion-limited rate is given by the following equations:

$$k_R = \int_{a_0}^{\infty} q(r) P(r) dr \quad (10)$$

$$\frac{1}{k_{D+}} = \frac{1}{k_R^2 D} \int_{a_0}^{l_c} \frac{dr}{P(r)} \left\{ \int_r^{l_c} (q(x) - k_R) P(x) dx \right\}^2 \quad (11)$$

It is much easier to numerically solve the above equations instead of analytically to obtain the diffusion coefficient D. In order to do that, the only unknown in the equation 10 and 11 is the Trp/Cys distance distribution $P(r)$.

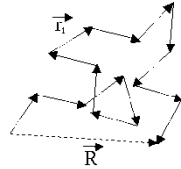


Figure 2.2 A typical Gaussian polymer chain made of N rigid rods connected together by flexible pivot points.

The simplest distribution that can be chosen is the freely jointed/Gaussian chain as depicted in Figure 2.2. The pivot points connecting the rigid rods are absolutely flexible, and have no orientational correlation whatsoever, and all configurations are possible. The typical $P(r)$ is of the following form:-

$$P(r) = 4\pi r^2 \left(\frac{2\pi \langle r^2 \rangle}{3} \right)^{-\frac{3}{2}} \exp\left(-\frac{3r^2}{2 \langle r^2 \rangle} \right) \quad (12)$$

Substituting equation 12 in equations 10 and 11 yields the following:-

$$k_R = \frac{4\pi q a_o^3}{\left(\frac{2}{3\pi} \langle r^2 \rangle \right)^{3/2}} \exp\left(-\frac{3a_o^2}{2 \langle r^2 \rangle} \right) \quad (13)$$

$$k_{D+} = \frac{4\pi D a_o}{\left(\frac{2}{3\pi} \langle r^2 \rangle \right)^{3/2}} \quad (14)$$

Equations 13 and 14 lead to two very important results that tell us that the reaction-limited rate is inversely proportional to the chain volume and also the diffusion limited rate is directly proportional to diffusion coefficient D and inversely proportional to the chain volume.

$$k_R \propto \frac{1}{\langle V \rangle} \quad (15)$$

$$k_{D+} \propto \frac{D}{\langle V \rangle} \quad (16)$$

Though a Gaussian chain is a very simple model, these qualitative relationships between rates and chain properties hold for even the sophisticated models of intramolecular diffusion studies.

A more sophisticated model that has been widely used for data analysis is the worm like chain (WLC) model with excluded volume illustrated in Figure 2.3. It is more realistic as it

imposes two important constraints on the simplified Gaussian chain model. Firstly, the real chain stiffness due to chemical bonds is taken into account by introduction of a new parameter called the persistence length l_p which is defined as the distance over which the polymer begins to lose memory of direction (as opposed to a Gaussian chain which has no orientational correlation) and ensures that the chain does not fold into itself over short distances. In the WLC model the peptide backbone is assumed to have a uniform rigidity k with persistence length $l_p = k/k_B T$. The second constraint imposed is the excluded volume effect by introduction of a hard sphere shell of diameter d_s to the end of each virtual peptide bond. Excluded volume of one molecule is defined as the volume that is inaccessible to other molecules due to the presence of the first molecule. A criteria to prevent clashes has been imposed that requires that the distance between two non-neighboring spheres must exceed d_s .

Worm like chains are computationally generated using the method described previously [25][26]. Typically 2-10 million chains with a persistence length of 4 Å and an excluded volume of 4 Å are generated and the position of every 10th link (corresponding to C^α) is calculated. A histogram of distances between two points within the sequence that represent the location of Trp and Cys distances is normalized to give probability distribution $P(r)$ where $d_s \leq r \leq l_c$ where l_c is the contour length of the chain. Chains are grown from the N-terminus by vectorially adding links to the chain that are 1/10th the length of a peptide bond (10 segments per peptide bond) with a random azimuthal angle ϕ between 0 and 2π radians and an axial angle θ . A Monte Carlo algorithm is applied in the construction of each chain, and every time a clash is detected (less than d_s distance between 2 non-neighboring residues) after the addition of 10 links, the chain is truncated 3 persistence lengths before the clash and the chain is regenerated. Otherwise additional links are added until the full length of the protein is reached.

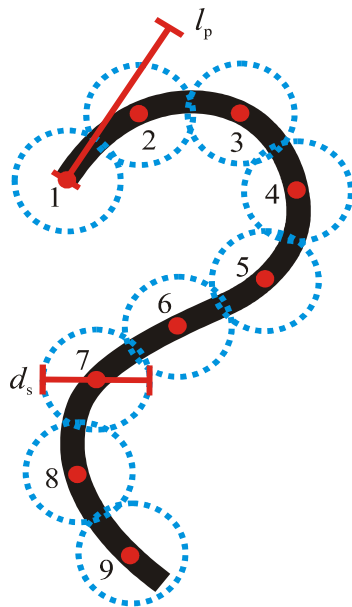


Figure 2.3 A schematic representation of worm like chain model showing the constraint parameters parameter length l_p and excluded volume diameter d_s .

There is considerable evidence that highly denatured states act globally like random, non-interacting chains [27] and a simple WLC model with SSS theory should be sufficient to describe these states. However experimental data suggest that under physiological conditions (mimicked by low denaturant concentrations) the polypeptide chain is much more compact (as evidenced by higher values of k_R). A compact conformation can be physically reproduced by the lowest possible values of d_s , but it was found in some sequences that even $d_s=0$ was not compacting the chain enough to yield experimentally observed values of k_R . This problem could occur due to of our initial assumption that denatured states can be described by random coil structures, and we were generating absolutely random worm-like chains in that regard. A growing number of studies of unfolded proteins that have shown residual structures under folding conditions such as low denaturants, contradicts our initial assumption [28]. These

observations suggest more complicated unfolded states with residual structures marked by transient intrachain interactions and secondary structure formation which may bias the unfolded states towards the native conformation. This leads to the conclusion that a homogenous worm like chain model is probably too simple a model to describe unfolded proteins under physiological conditions. MD simulations have been able to map long range interactions in sequences [29] but since our experimental method is much more sensitive to the short range interactions (tail of the distribution) we require much more than 10000 conformations that were generated and used by previous methods.

2.3 Boltzmann Energy Reweighting

To account for the above details, the WLC model was modified to reweight and bias the worm like chains generated, based on favorable intramolecular interactions. The worm like chains are generated the same way as before but then a bias is assigned to those chains which have residues of similar hydrophobicity near each other. This upgraded model is called the Energy-Reweighted WLC model, and has been able to reproduce experimental contact quenching rates measured under folding conditions in a computationally inexpensive manner [28].

To perform re-weighting, a new parameter E_{TOT} is defined as a total energy that is a sum of pair-wise interactions between C^α atoms:-

$$E_{TOT} = - \sum_{|i-j|>1} \frac{e_{i,j}}{|r_i - r_j|} \quad (17)$$

$$e_{i,j} = \begin{cases} 0, & |h_i - h_j| > 0.3 \\ \sigma, & |h_i - h_j| \leq 0.3 \end{cases}$$

Where i and j are the indices of two non-adjacent residues $|r_i - r_j|$ is the distance between these two residues which must be larger than d_s and less than 6.5\AA , which is the cutoff distance for hydrophobic associations [28]; h_i and h_j are the normalized hydrophobicities of the two residues as determined by a standard hydrophobic scale. $e_{i,j}$ is the strength of the hydrophobic potential between two residues which equal zero if one is hydrophobic and one hydrophilic, and equals σ , if both are hydrophobic or hydrophilic. σ is a tunable parameter that exhibits the strength of the hydrophobic interaction and depends upon various factors, such as temperature and solvent conditions, etc. The cutoff 0.3 is chosen based on the spread of normalized hydrophobicity distribution of different amino acids.

Using E_{TOT} and r as independent reaction coordinates, we can define a 2-D probability distribution $P(r, E_{TOT})$ such that:-

$$1 = \int dr \int dE_{TOT} P(r, E_{TOT}) \quad (18)$$

And the 1-d Trp-Cys distance distribution is defined as $P(r) = \int dE_{TOT} P(r, E_{TOT})$.

Let $Z(r)$ represent the energy re-weighted distribution of distance r between the Trp and Cys.

$$\begin{aligned} Z(r) &= N \cdot \int P(r, E_{TOT}) \exp(-E_{TOT}/kT) dE_{TOT} \quad (19) \\ &= N \cdot \int P(r, E_{TOT}) dE_{TOT} \cdot \int \frac{P(r, E_{TOT}) \exp(-E_{TOT}/kT) dE_{TOT}}{P(r, E_{TOT}) dE_{TOT}} \end{aligned}$$

$$= N \cdot P(r) \cdot \left\langle \exp\left(-\frac{E_{TOT}}{kT}\right) \right\rangle_r$$

$$\frac{1}{N} = \int_{d_s}^{l_c} P(r) \cdot \left\langle \exp\left(-\frac{E_{TOT}}{kT}\right) \right\rangle_r dr$$

N is the normalization constant.

Substituting $Z(r)$ for $P(r)$ in the SSS theory equations 10 and 11 we obtain the following:-

$$k_R = \int_{d_s}^{\infty} q(r) Z(r) dr \quad (20)$$

$$\frac{1}{k_{D+}} = \frac{1}{k_R^2 D} \int_{d_s}^{l_c} \frac{dr}{Z(r)} \left\{ \int_r^{l_c} (q(x) - k_R) Z(x) dx \right\}^2 \quad (21)$$

When this model was being developed, different forms of potentials were used to calculate hydrophobicity energy, and total energy terms with varied forms of r dependence (namely $\frac{1}{r^2}$ distance dependence, Leonard-Jones distance dependence, no distance dependence, etc) were tested and it was found that the overall trend remained unaltered in different sequences at different denaturant concentrations, though the σ values differed from one model to another. However if the energy function was not cut off at 6.5Å, the convergence of σ between sequences was seen to fall apart. This suggested that inclusion of long range interactions may introduce sequence-dependant complexity to the re-weighting functions. Also, another possibility was considered where only the hydrophobic residues lying near each other were given the bias (assuming that hydrophobic residues drive the collapse) but the convergence of σ was not found among the tested sequences.

2.4 The Charge Effect

In order to account for the charge effects, the total energy term needs to include the electrostatic energy term in addition to hydrophobic energy. The total energy term becomes:-

$$E_{TOT} = E_h + E_e = \gamma \sum_{|i-j|>1} \frac{q_i q_j}{|r_i - r_j|} - \sum_{|i-j|>1} \frac{e_{ij}}{|r_i - r_j|} \quad (22)$$

$$q_i = \begin{cases} 1, & \text{if } i \text{ is Arg or Lys} \\ -1, & \text{if } i \text{ is Asp or Glu} \end{cases}$$

Where q_i and q_j are the charges of two non-adjacent residues and $|r_i - r_j|$ is the free space distance between them. γ is the tunable parameter, and can be varied usually varied by holding σ constant or vice versa, to predict the measured quenching rates.

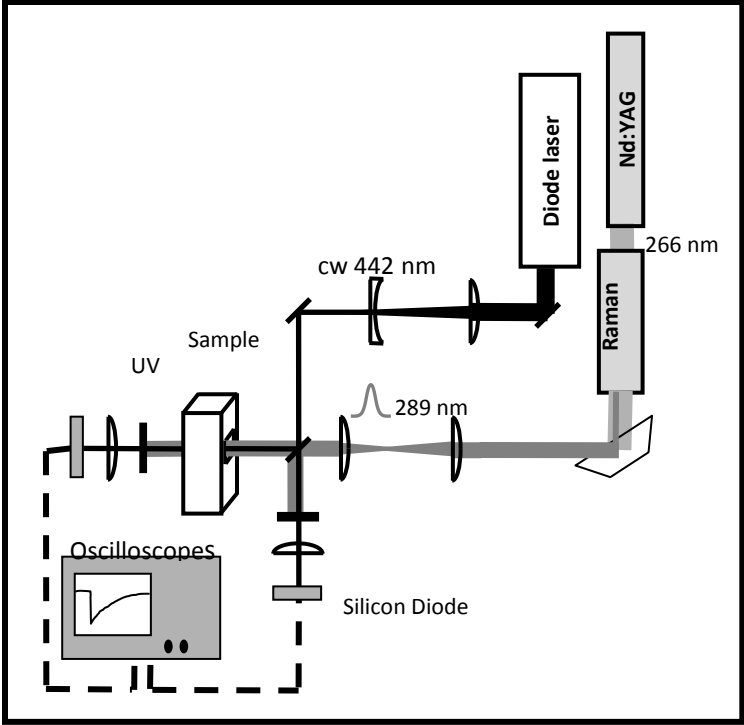


Figure 2.4 Experimental setup for measuring contact quenching

Chapter 3

Protein Aggregation in Alzheimer's disease

In this chapter, I will talk about A β peptide aggregation in connection with Alzheimer's disease and then compare the early aggregation propensity of A β peptide based on its length, pH and addition of an aggregation inhibitor. I will show that the aggregation model described in chapter 1 is commensurate with the data.

3.1 A β Production

APP (Amyloid beta precursor protein) is a transmembrane protein of approximately 120kDa ubiquitously expressed in mammalian cells. It may be attached to neuronal cell membranes with a transmembrane segment and may exist in different isoforms ranging from 695 to 770 residues, of which the 695, 751 and 770-residue isoforms predominate in the brain [30][31]. The A β region of APP is located partially within the ectodomain and partially within the transmembrane domain of APP. Though the biological function of APP is not entirely known, there is some evidence suggesting the involvement of APP in G-coupled cell signaling and being a regulator protein of cell-trafficking[32][33]. APP has selective metal binding sites in the N-terminal region for copper, and there have been studies showing that lowering the copper levels, lowered the gene expression of APP and also depletion of metals in drinking water gave lower A β fibril formation among rabbits *in vivo* [34]. This has led to suggestions that APP may be involved in regulation of copper levels and also in maintaining metal homeostasis.

The proteolytic cleavage of APP can follow either a non-amyloidogenic or an amyloidogenic pathway. In the non-amyloidogenic pathway, APP is cleaved by α -secretase at a position 83 amino acids from the C-terminus, producing a large N-terminal ectodomain (sAPP α)

which may be secreted into the extracellular medium. The remaining C83 fragment is retained in the membrane and cleaved by γ -secretase, producing two benign fragments P3 and AICD (Amyloid Precursor Protein Intracellular Domain). While during the amyloidogenic pathway, the initial proteolysis is mediated by β -secretase at a location 99 amino acids from C-terminus. This cut releases sAPP α into extracellular space, leaving the C99 fragment within the membrane whose first amino acid corresponds to A β . The next step is cleavage of C99 fragment by γ -secretase at positions anywhere between 38 to 43, which releases different isoforms of the A β peptide[35][36]. Out of the different isoforms the most abundant is the A β_{40} peptide, whereas a small proportion is A β_{42} isoform (approximately 10%)

3.2 Intracellular A β Accumulation

The A β peptide was first identified as a component of extracellular plaques in the mid-1980s [37] and also there was evidence suggesting the presence of A β as a normal product of APP metabolism throughout life, which could be measured circulating in extracellular fluids like cerebrospinal fluid and plasma [35]. However, soon studies showing the presence of intraneuronal A β started pouring in, elucidating roles of intracellular abeta in the AD pathology [36] [38][39]. Cell biology studies have demonstrated the presence of parent protein APP in plasma membrane, trans-Golgi network, endoplasmic reticulum (ER), endosomal, lysosomal and mitochondrial membranes. The liberation of A β reportedly occurs wherever APP and the β and γ -secretases are localized; the APP cleavage may happen within different cellular compartments thus giving rise to intracellular A β , or it may happen at the plasma membrane or in a secretory pathway, which would result in A β being released extracellularly[36][39]. There have been

studies showing that in addition to A β being produced intracellularly, A β secreted extracellularly can be taken up by cells and internalized into intracellular pools through receptors and transporters[40]. Exciting observations from mouse model studies have shown that fluorescently labeled A β injected into tail vein can cross defective blood brain barriers and accumulate intracellularly in the neurons of the cerebral cortex [41]. This has led to conclusions that neurons can take up extracellular A β thus contributing to the brain A β load and leading to pathogenicity in AD models. In the interstitial fluid of human brain, A β concentration is regulated by its rate of production from parent protein APP, influx into the blood brain barrier via various receptors, and its rapid clearance by enzymatic degradation [42]. A β accumulation in the brain beyond its critical concentration in the micromolar range favors aggregation [43] and continuous removal of A β species from brain by transport across blood brain barrier and metabolism is essential to prevent its reported neurotoxic effects[44].

3.3 A β Associated with Alzheimer's disease

Alzheimer's disease (AD) is a progressive and irreversible brain disorder that is known to destroy memory and cognitive skills. In 1907, German psychiatrist and neuro-pathologist Alois Alzheimer first described two striking pathological alterations in the brain of one of his female patients who died of unusual mental illness and severe dementia. Post mortem studies of her brain tissues revealed 1) peculiar extracellular deposits in specific brain regions, which is now referred to as senile plaques (SP's) and 2) neurofibrillary tangles (NFT's) occurring intraneuronally. These two observations turned out to be hallmark features of the disease and their presence during postmortem examination is still required to confirm AD diagnosis. During

mid-1980s biochemists discovered that the SP's comprised of aggregates of a small peptide A β [37] and that NFT's are composed of aggregates of the tau protein, which becomes abnormally phosphorylated [45]. Apart from SP's and NFT's, there are also significant other pathological changes that reportedly occur in the AD brain, including inflammatory responses and oxidative stress, all of which combined could lead to severe neuronal and synaptic dysfunction and loss.

Extensive research on A β peptide has generated considerable evidence connecting it to the AD pathology.

- 1) Various missense mutations have been identified in the three genes APP, PS1 and PS2- all of which have lead to increased A β production and accumulation, thus leading to early onset familial AD. For example, most of the APP mutations cluster at or near the cleavage sites within APP, thus favoring proteolytic processing of APP by β and γ -secretases [46] [35]. Other familial mutations such as Arctic mutation (E22G) reportedly increase the aggregation propensity of A β , thus causing genetically inherited early and aggressive onset of the disease [47].
- 2) Direct incubation of neuronal cells with A β or overexpression of APP results in cell death [43] [48][49].
- 3) Anti-Abeta antibodies have been able to reverse the histological and cognitive impairments in mice models, that overexpress A β or APP [50][51].

3.4 Neurotoxic Effects of A β

There are various ways in which A β has been reported to exert neurotoxic effects like oxidative stress, mitochondrial dysfunction, formation of ion-channels and membrane disruption,

synaptic dysfunction, activation of cellular processes such as apoptosis and inflammation [52][53][54][55]. Initially the ‘amyloid cascade’ hypothesis attributed dementia to nerve cell death caused due to toxicity of large insoluble amyloid fibrils. However research evidence in recent years suggests that it is actually the lower-order A β assemblies that are the neurotoxic species. To begin with, relatively weak correlations exist between fibrillar plaque density and severity of dementia among AD patients, whereas correlations between soluble A β levels and the extent of synaptic loss and cognitive impairment are reportedly stronger [56] [57]. Formation of soluble oligomers precedes AD symptoms and initial AD symptoms usually occurs much before plaque accumulation [53][58]. The concentration of soluble lower order A β oligomers are elevated in the human AD inflicted brain tissues [59] and oligomeric species as small as dimers and trimers have reportedly exhibited neurotoxic characteristics in mouse models and cell cultures [60][61][62]. There is also evidence showing that microinjections of as low as 1pM of cytosolic A β_{42} induced cell death of cultured human neurons, suggesting that intracellular A β may be neurotoxic in nature [63].

3.5 Structure of A β Monomer

The A β sequence has an amphipathic character, as its N-terminal segment is hydrophilic, and 12-14 residues in the C-terminal are extremely hydrophobic. In aqueous solution, a random coil structure of A β_{40} has been observed [64]. The A β_{42} assumes a beta sheet structure rapidly at physiological pH, in contrast to less hydrophobic specie A β_{40} which preserves the random-coil conformation over longer periods of time, before assembling into β -sheet-rich oligomers [53].

3.6 Dimers and Trimers

SDS-Stable A β dimers have been detected both *in vitro* as well as *in vivo* [53] and those isolated from human brain have a hydrophobic core diameter of about 3-4 nm [65]. The dimerization process begins intracellularly as reported by studies on cells obtained from human brains [66]. Soluble A β dimers extracted directly from the cerebral cortex of human AD inflicted brains inhibited long term potentiation (LTP), enhanced long term depression (LTD) and reduced dendritic spine density in normal rodent hippocampus and disrupted memory of a learned behavior in rats, whereas neither insoluble plaque cores nor A β monomers significantly altered synaptic plasticity [67]. Another study has reported the effect of soluble oligomers secreted by cultured cells expressing a mutant form of APP that causes aggressive forms of familial AD and have found strong evidence suggesting that trimers may be selective inhibitors of certain forms of hippocampus LTP in mice [68]. The above findings support the hypothesis that soluble oligomers as small as dimers or trimers could be the potential synapto-toxic species in course of AD pathogenesis.

3.7 Higher Order Aggregates

Different oligomers (globulomers, spheroids, annular) comprising of 3-50 A β monomer subunits have been observed *in vivo* AD patients, mouse models, A β secreting cell cultures as well as *in vitro* using AFM and SEC. They exhibit varying degrees of toxicity[53] [69]. An interesting study has shown that extra-cellularly accumulated soluble A β dodecamers of 56kDa (A β *56) isolated from the brains of middle aged mice caused memory deficits in them and even disrupted memory when administered to young rats, independently of plaques or neuronal loss [62]. Observations and characterization of annular A β oligomers *in vitro* and cell cultures led to

the channel hypothesis, according to which the annular oligomers cause membrane-disruption and may lead to Calcium influx into cells [53]. That can alter Calcium homeostasis by increasing levels of cytoplasmic Calcium levels, which in turn alters neuronal excitability and synaptic plasticity, while also exhibiting neurotoxicity [70][71].

A β -Derived Diffusible Ligands (ADDL's) are oligomers ranging in size from 17 to 42 kDa and may comprise of groups of small soluble oligomers; ADDL levels in CSF of living AD patients monitored with a nanoparticle-based detection technique, were reportedly much higher in concentration than non-demented age matched controls [72] thus supporting the hypothesis that soluble A β oligomers exhibit strong correlation with cognitive deficits of AD patients. ADDL's have also exhibited neurotoxic effects *in vitro* [53].

Protofibrils (PFs) are highly polydispersed structures in solution ranging from spheres that are 8 nm in diameter upto curvilinear structures upto 200 nm in length, mostly seen *in vitro* by EM or AFM. They are precursor of amyloid fibrils and bind to dyes such as Congo red and Thioflavin T suggesting high beta sheet content and could be potentially neurotoxic [53][69]. Their formation is dependent on concentration, pH and ionic strength, and they could either proceed to form fibrils due to addition of preformed fibrillar seeds or could dissociate into lower molecular weight A β oligomers [69].

Amyloid fibrils found *in vivo* and *in vitro* are 'thermodynamically stable', highly insoluble and structurally ordered aggregates, composed of repeating β -sheet units aligned perpendicularly to the fibre axis [53]. They have been observed to bind well to dyes such as Congo red and Thioflavin T and also exhibit Fourier transform infrared (FTIR) spectroscopy peak at around 1620, indicating the presence of beta sheet. They usually have a characteristically distinctive cross- β pattern that arises from X-ray diffraction studies. The term 'cross- β ' was

based on observation of two sets of diffraction lines, one longitudinal and one transverse, forming a characteristic 'cross' pattern. The two notable reflections are: a meridional at 4.7-4.8 Å that arises from the spacing between hydrogen bonded β -strands and an equatorial around 10-11 Å that occurs from the distance between the β -sheets and may vary according to the respective side-chains present. The stacks of beta sheets are usually short and traverse the breadth of the amyloid fibrils, while the length is decided by the number of aligned β -strands [73].

Combination of results from hydrogen-deuterium (HD) exchange, NMR, mutagenesis and solid state NMR (ssNMR) led to the conclusion that 3D structure of $A\beta_{42}$ and $A\beta_{40}$ amyloid fibrils consist of two parallel β -sheets joined by a β -turn, represented by a sheet-turn-sheet morphology [74][75][76]. NMR results have shown that $A\beta_{40}$ fibrils may have the following key features: Residues 1-10 are disordered, 12-24 form β -strand1, 25-29 initiate β -turn, 30-40 form β -strand2 connected to β -strand1 with help of β -turn. While HD exchange, NMR and mutagenesis results have shown that $A\beta_{42}$ fibrils may have the following key features: Residues 1-17 are disordered, 18-26 form β -strand1, 27-30 initiate β -turn, 31-42 form β -strand2 connected to β -strand1 with help of β -turn.

Each β -sheet may be stabilized as a result of different inter-molecular side chain interactions, such as hydrophobic interactions, salt bridges, etc. At least two sheets arising from two $A\beta$ molecules may be required to form a protofilament which can then interact at higher levels forming mature fibrils. The 3-D structure of $A\beta_{42}$ protofilament consists of two-stacked, parallel β -sheets that perpetuate along the fibril axis. The residues L17, F19 and A21 of β -sheet1 may mediate hydrophobic intermolecular contacts with even numbered residues of β -sheet2. The loop region of residues 27-30 is connected to β -sheet1 by means of intermolecular salt bridge

D23-K28, which also forms contacts to residues I32 and L34 of β -sheet2. Cryo-EM analysis have shown protofilament dimensions of around 25 Å thick and 45 Å long, and two protofilaments may wind and twist around each other with a hollow core in between.

Amyloid plaques found in AD patients' and mouse brains represent the final stage of A β aggregation process *in vivo*. They are large extracellular A β deposits composed of insoluble A β amyloid fibrils and could be as big as 50 μ m in size [53]. Seeding of A β has been found to be highly specific; seeds from other amyloidogenic proteins are not able to trigger A β fibrillization or plaque formation.

3.8 Comparison of A β_{42} and A β_{40}

The most abundant alloforms of the peptide co-exist under normal conditions in the brain in an A β_{42} /A β_{40} ratios of 1:9 [77]. Out of the two, the A β_{42} specie have been widely observed to be much more aggregation prone, both *in vitro* and *in vivo*. The critical concentration of fibril formation is typically measured by determining the concentration at which the rates of fibril formation and fibril dissolution are equal [43] and it has been observed that critical concentration of A β_{42} is five times lower than that of A β_{40} under physiological conditions. Lag time of fibril formation is determined by the time needed to reach to 10% of the maximum fibril growth (which is marked by maximum rise in ThT fluorescence intensity). It has been reported that the lag time of A β_{40} is around 2.5 hours [78] whereas lag time of A β_{42} is in the order of minutes [79] and A β_{40} is much more soluble than A β_{42} *in vitro*. There have been reports showing that minor increase in A β_{42} /A β_{40} ratios have led to the formation of neurotoxic oligomers, which can potentially lead to cell death [78] and may also lead to more aggressive forms of the disease compared to sporadic AD cases, affecting synaptic activity, viability of neuronal cells and

memory development in animal models [77]. A β_{42} plays a more important role in AD pathogenesis, since it aggregates faster and is reportedly more prone to forming neurotoxic species than A β_{40} [75][77]. The higher aggregation propensity of A β_{42} makes purification, handling and reproducibility a big challenge and a lot less number of studies have happened on A β_{42} specie as compared to A β_{40} [53].

3.9 Expression and Purification Protocol

Most researchers use chemically synthesized A β peptide for experimental studies because recombinant purification of the peptide has several challenges. However, a recent work showed that recombinantly produced A β_{42} aggregates much faster and is more neurotoxic than its chemically synthesized counterpart [80]. That motivated us to purify the peptide recombinantly for our experiments. A β is usually expressed with a fusion tag, which makes subsequent purification stages much easier. The fusion construct A β_{42} plasmid was a kind gift by Dr. Rudi Glockshuber, from ETH Zurich. The fusion construct consist mainly of a Histidine tag and a soluble polypeptide segment comprising 19 repeats of the tetrapeptide sequence NANP which is a previously reported solubilizing A β fusion partner, followed by the TEV protease recognition sequence ENLYFQ↓ (the arrow indicates the cleavage site). The A β_{42} sequence is at the end of the fusion tag [81][80].

Two different Trp/Cys pair-containing A β_{42} and A β_{40} mutants were created using the QuikChange site-directed mutagenesis kit (Stratagene, La Jolla, CA, USA) and DNA sequencing was used to ensure the presence of the desired mutations. The sequenced wild type and mutant plasmids were then extracted from the XL1 blue competent cells and transformed into *E. coli* BL21 (DE3) cells and plated out in LB-agar plates containing 100 μ g/ml Ampicillin.

E. coli BL21 (DE3) cells bearing the corresponding the plasmid for expressing the A β fusion construct was first grown in 5ml tube cultures of LB media containing 100 μ g/ml Ampicillin, while being shaken at 37°C at 220 rpm for 4 hours. It was then transferred to 1liter LB media flasks (Ampicillin concentration 100 μ g/ml) and was shaken overnight at 37°C at 150 rpm. Protein expression was induced after 16 hours by addition of filtered 1mM isopropyl- β -D-thiogalactoside (IPTG) after which the flasks were shaken for further 4 hours in 37°C at 150 rpm. The cells were then harvested by centrifugation at 4000 rpm for 20 minutes (rotor SLA-1500). The pellets formed were re-suspended in A β lysis buffer (20mM Tris, 6M GnHCl, pH 8.0), sonicated and then stirred at 4°C for 90 minutes. The cell debris was then removed by centrifugation (19000 rpm in rotor SS-34) at 4°C for 1 hour.

Using the supernatant, the His-tag containing fusion construct was purified with an affinity column. Ni-NTA agarose column (Nickel charged resins by Qiagen) was first equilibrated with 5 column volumes of A β equilibration buffer (20mM Tris, 10mM Imidazole, 6M GnHCl, pH 8.0) after which the supernatant was loaded and incubated with gentle shaking at 4°C for 1 hour to enable binding of the His-tagged fusion protein to the Nickel column. Following binding, the Nickel resins containing the bound protein were re-suspended in 5 column volumes of wash buffer (20mM Tris, 20mM Imidazole, 6M GnHCl, pH 8.0) and gently shaken at 4°C for half an hour to get rid of unbound bacterial protein. The washing step was repeated at least two to three times, until all unbound proteins were washed away and the supernatants were discarded each time. Finally the Nickel resins containing mostly fusion protein were re-suspended in 2 column volumes of elution buffer (20mM Tris, 250mM Imidazole, 6M GnHCl, pH 8.0) and gently shaken at 4°C for 1 hour, following which the supernatant containing

eluted fusion protein was collected and stored at -20°C until further use. The elution step can be repeated until all fusion protein has been recovered.

The next step in the purification is semi-preparative RP-HPLC (Reverse Phase- High Performance Liquid Chromatography) to get rid of guanidine and other impurities. The fusion proteins from the previous step was filtered and loaded into an Agilent Zorbax SB300 C8 semi-preparative HPLC column in 10% (vol/vol) acetonitrile containing 0.1% trifluoroacetic acid (TFA) at a flow rate of 1ml/min. The sample injection loop was washed many times at the same acetonitrile gradient to ensure that all fusion protein gradually bound to the column and all unbound proteins eluted, before the acetonitrile gradient was increased. Also, the high hydrophobicity of A β requires HPLC to be conducted at 60°C to enable better protein recovery than room temperature. Once the protein bound to the column, the acetonitrile gradient was gradually increased along with the flow rate, resulting in the elution of A β fusion protein at 40% acetonitrile and 0.1% TFA, at 60°C and a flow rate of 2 ml/min. The fusion protein was collected and lyophilized, and then stored at -20°C.

The next step was cleavage of the fusion protein to yield A β peptide. The ProTEV Plus enzyme was purchased from Promega (Catalog# V6101) which is a 48kDa, improved version of the tobacco etch virus (TEV) protease (more stable in terms of enzymatic activity). It is reported to be a highly specific proteolytic enzyme that cleaves at the position shown by the arrow: ENLYFQ↓D thus liberating A β whose first residue is D. The lyophilized A β fusion protein was directly dissolved in the A β cleavage buffer (10mM Tris, 0.5 mM EDTA, pH 8.0) and the cleavage reaction was carried out in the presence of 1mM DTT at 4°C with 16 hour incubation. Approximately 20 μ g of fusion was cleaved by using 5 units of the enzyme (1 μ l of 5units/ μ l enzyme) following the protocol provided by Promega. The DTT was added to prevent

Methionine oxidation/ Cysteine disulfide bond formation at position 35 that has been reported previously as a potential problem arising during purification[80]. As soon as A β was cleaved, it began aggregating; at the end of the 16 hour incubation period all the aggregated A β was sedimented by centrifugation (rotor F13S14X50Cy, 11000 rpm for 30 minutes) and then re-suspended in 70% (w/w) formic acid, filtered and immediately subjected to RP-HPLC. The peptide was loaded into an Agilent Zorbax SB300 C8 semi-preparative HPLC column in 10% (v/v) acetonitrile and 0.1% TFA at flow rate of 1ml/min. Following rounds of washing of the sample loop, the acetonitrile gradient was increased the same way as before. The fusion partner being more hydrophilic eluted first followed by the A β peptide at 40% acetonitrile and 0.1% TFA, at 60°C and a flow rate of 2 ml/min. It was collected, lyophilized and stored at -20°C. The presence of the peptide was confirmed by Electrospray Ionization Mass Spectrometry (ESI).

To ensure that A β peptide was completely monomeric for every experiment, the lyophilized peptide was dissolved in 2-10mM NaOH, sonicated for 2 minutes, filtered using 0.2 μ m syringe filter and lyophilized for further use[80][82]. Re-suspension of A β peptide at pH>10 helps to ensure that the starting condition of A β peptide is completely random coil in conformation which was confirmed by circular dichroism.

3.10 Thioflavin T Assay

The Thioflavin T fluorescence experiment was performed according to the protocol previously reported [80]. Monomerized A β peptide in lyophilized form was re-suspended into 10mM NaOH until a concentration of roughly 100-200uM was achieved as measured by A₂₈₀ absorbance (wild type ϵ_{280} = 1730 M⁻¹cm⁻¹ ; F4C, F19W and M35C, F19W mutants ϵ_{280} = 6990 M⁻¹cm⁻¹). It was further diluted into 10mM NaOH to a concentration around 80uM which were

kept on ice and immediately used for Thioflavin T fluorescence experiment. The reaction mixture for the aggregation experiment was mixed in a 1cm path length quartz cuvette comprising of the following:-

- 1) 100 μ l: monomerized 80 μ M A β stock solution (diluted into total volume 1000 μ l, hence final A β peptide concentration 8 μ M)
- 2) 900 μ l reaction mixture: 750 μ l of 20mM Sodium Phosphate buffer, pH=7.4 (final =10mM); 100 μ l of 10mM HCl (final= 1mM); 20 μ l of 5M NaCl (final=100mM); 20 μ l of 2.5 mM Thioflavin T (final=50 μ M); 10 μ l of 100mM TCEP (final=1mM).

The mixture was stirred continuously at 37°C and its fluorescence was recorded every 3min for approximately 30s (excitation: 440nm, emission: 482nm) using a Jobin Yvon Spex Fluorolog-3 spectrofluorometer equipped with a thermo stated cell holder. Just prior to recording each reading the cuvette was inverted about 5 times for homogenous suspension of fibrils.

3.11 Trp Cys Quenching Measurement

For this experiment, monomerized A β peptide in lyophilized form was re-suspended into 10mM NaOH kept in ice, filtered and diluted into 20-25 mM sodium phosphate buffer (pH=7.5), 1 mM TCEP (to prevent disulfide bond formation), and various sucrose concentrations (0, 10, 20 and 30% w/w) in an ice bucket. The final concentration of the mutant proteins was kept fixed at 30 μ M for each set of temperature and viscosity measurements. The buffer, sucrose and TCEP solutions were bubbled with N₂O for one hour to eliminate oxygen and scavenge solvated electrons created in the UV laser pulse.

3.12 Mutation Sites

A β peptide is an intrinsically disordered peptide lacking both Trp and Cys. In order to measure reconfiguration, two loops were created containing one Trp and Cys each, 15-16 residues apart in sequence. The natural decay lifetime of the excited state of Trp is slower than 40 μ s, hence the Trp and the Cys must be engineered close enough in sequence to ensure that the unimolecular quenching dominates (100ns-20 μ s) which can be attained by placing them less than 30 residues apart for a random coil. The Trp and Cys positions had to be chosen very carefully to ensure that it did not alter the aggregation propensity or structure of the original peptide. The Tango [83] and Zyggregator [84] algorithms were used to pick the mutation positions. Tango algorithm is an algorithm that predicts protein aggregation based on beta-sheet formation propensity of a sequence. The Zyggregator method uses the physio-chemical properties of amino acids to predict how they may influence growth of misfolded assemblies and also specific regions of sequences that promote aggregation. The 2 loops created were F4C, F19W (15 residue long) and F19W, M35C (16 residue long) as shown in Figure 3.1. These sites were finally picked because Phe and Met have similar hydrophobicity compared to Trp and Cys, and they are not charged. Additionally, Met is similar to Cys as they both contain sulfur atoms. The wild-type (WT) along with F4C,F19W and F19W,M35C loops were expressed and purified, after which experiments were run to verify that the mutants were similar to the WT.

Thioflavin T (ThT) is a dye which is widely used to stain and detect amyloid fibrils in senile plaques of postmortem AD brains[85][86]. The free dye absorbs light of 385 nm and emits fluorescence at 445 nm. However, as it associates with the fibrillar beta-sheet aggregates, the bound complex undergoes a 120nm shift in excitation wavelength, absorbing light around 440nm to give enhanced emission at 482nm. The ThT fluorescence profile is characterized by an initial

lag phase marked by negligible fluorescence intensity, since it cannot bind to monomer or oligomeric intermediates in course of the aggregation pathway. However, as soon as fibrils form, the ThT fluorescence starts rising and finally saturates after all monomers have been converted into fibrils. Lag time of fiber formation is defined as the time taken to reach one-tenth of the maximum fluorescence signal. Figure 3.2 shows the ThT fluorescence data for the A β ₄₂ WT along with the 2 mutants. The calculated lag time for A β ₄₂ WT was ~ 1890s, which is in agreement with previously reported data [79]. The lag time of the F19W, M35C mutant was ~ 2040s and the F4C, F19W mutant was ~ 1770s, which is well within 10% of the WT lag time.

Circular Dichroism (CD) spectroscopy is commonly used to probe the secondary structure of proteins. The differential absorption of left and right circularly polarized light, as it passes through a protein molecule possessing backbone asymmetry, is measured at different wavelengths and reported in milli-degrees. α -helical, β -sheet and random coil structures have previously reported signature CD spectra which can be compared with that of the protein, to analyze its secondary structure. Monomeric A β peptide is intrinsically disordered, exhibiting random coil like behavior. However as it aggregates, it has been reported to readily assemble into β -sheet structured aggregates which can be probed by changes in CD spectra.

Figure 3.3 shows the far-UV CD spectra of WT A β ₄₂, along with the 2 mutants of A β ₄₀ and A β ₄₂. The measurements were carried out in an Applied Photophysics Chirascan spectropolarimeter, using a 1mm path length cell. The time per point was ~2.5s and bandwidth was fixed at 1 nm. For this experiment, monomerized A β peptide in lyophilized form was re-suspended into 10mM NaOH, filtered and diluted 20 times into 20-25 mM sodium phosphate buffer (pH=7.5) kept in ice, to yield a final protein concentration of ~5 μ M. The dead-time between dissolving the peptide and data collection was ~10-15 min. All the mutants and wild

type protein yielded random coil like CD spectra, characterized by a minima around 196-198 nm and absence of any minima in the 210-230 nm region. This helped in ensuring that the structure of the mutant proteins was similar to the wild-type.

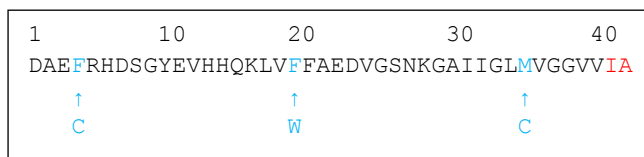


Figure 3.1 Sequence of A β_{42} WT with arrows showing the positions of Trp and Cys mutations for the 2 loops created.

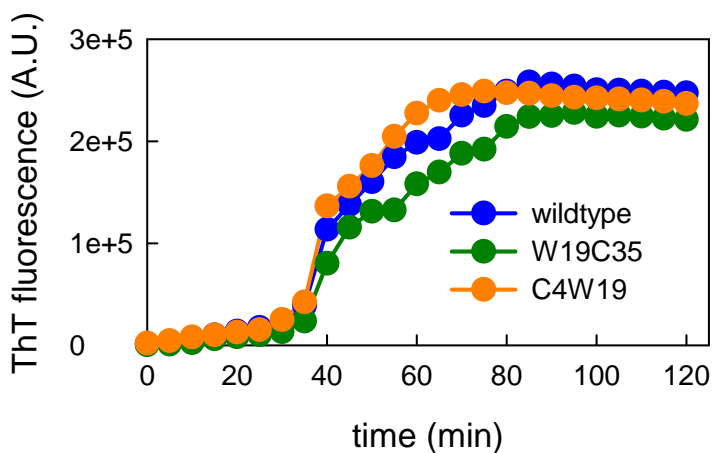


Figure 3.2 Thioflavin T fluorescence spectra of A β_{42} WT along with the 2 Trp/Cys containing mutants.

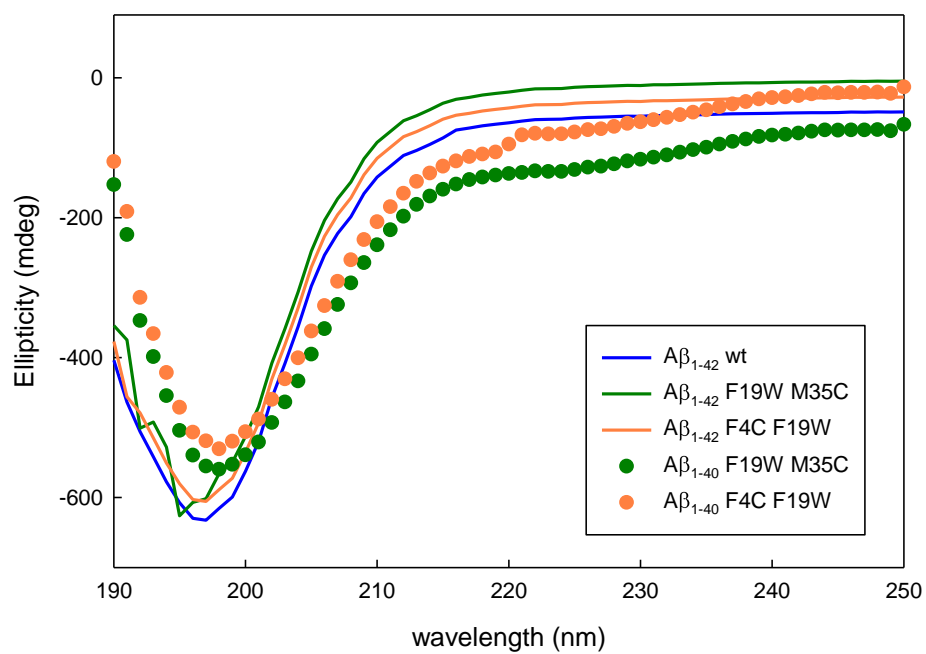


Figure 3.3 The CD spectra of $A\beta_{42}$ WT, and the 2 loops containing Trp/Cys, both for $A\beta_{42}$ and $A\beta_{40}$.

3.13 Measuring Reconfiguration

Figure 3.4 shows sample decay kinetics of Trp triplet excited state as quenched by Cys, for a typical A β mutant. It is best fit to a three exponential decay (as shown by the red line); a rapid decay on the microsecond timescale shows that the tryptophan triplet is being rapidly quenched by cysteine and this can be attributed solely to the reconfiguration of the monomer population, as the Trp is readily accessible to the Cys. A slower decay in the 10 microsecond timescale (faster than Trp natural lifetime) is observed that maybe attributed to the reconfiguration of an oligomeric population which may be gradually forming or imperfect monomerization. A very slow decay in the 100 μ s to 1 ms timescale may be due to different photo-physical processes[19]. However the amplitude of the fastest decay rate corresponding to the monomer population dominates, and is reported as k_{obs} . Figure 3.5 shows sample raw data plots of exponential decay times ($1/k_{obs}$) versus viscosity (η). Decay times at a single temperature can be fit to lines. Each experiment was repeated and eight points corresponding to each temperature were fitted to a line, from which k_R and k_{D+} were calculated.

The reaction limited rates shown in Figure 3.6a were calculated from intercept of the straight line fits from the plots shown in Figure 3.5 (a, b, c, d) such that $k_R=1/\text{intercept}$. The measured values of k_R for A β_{42} loops were an order of magnitude higher than that of the A β_{40} loops. Since k_R is inversely proportional to the chain volume (equation 15), our measurements show that A β_{42} is significantly more compact than A β_{40} at all temperatures, as shown in terms of decreased average Trp-Cys distances, which is plotted in Figure 3.6c. Our measurements show that the average Trp-Cys distances for both the loops of A β_{42} is smaller than that of A β_{40} as quantified by average r values, which means the A β_{42} ensemble is much more compact than A β_{40} .

Our results are in agreement with previously reported molecular dynamics (MD) simulation studies. Comparison between intra-molecular contact maps of A β ₄₂ and A β ₄₀ has revealed that the two additional hydrophobic residues at the A β ₄₂ C-terminus, Ile41 and Ala42 significantly increase contacts within the C-terminus and also between the C-terminus and the central hydrophobic cluster (CHC region: Leu17-Ala21). Additionally, the Tyr10 in A β ₄₂ also contacts residues 13-32 more frequently than A β ₄₀ [87]. Another reported MD simulation study has revealed many more close interactions between residues 25-37 and 12-20 for A β ₄₂ than for A β ₄₀ as shown by contact maps [88], which further supports the hypothesis that stronger C-terminus interactions caused between 39-40 and 41-42 residues of A β ₄₂ renders the rest of the residues in the hydrophobic patch (residues 29-39) to form interactions with other residues distant in sequence. Increased intra-molecular contact frequencies in A β ₄₂ sequence could be responsible for the compaction in chain which we have experimentally measured. In another analysis of MD trajectories in explicit water of A β ₄₂, non-local backbone H-bonds between the residues of Lys16Leu17 and Val39Val40Ile41 was observed being formed with time that caused a decrease in the number of water molecules around those residues, which could also lead to compaction. Due to such non-local backbone contacts being formed, those regions may become inaccessible to H bonding with water, facilitating inter-molecular side-chain interactions, which could initiate aggregation in the A β ₄₂ sequence [89].

The diffusion limited rates shown in Figure 3.6b were calculated from the slopes of the straight line fits shown in Figure 3.5(a, b, c, d) such that $k_{D^+}=1/(\eta \text{slope})$ and we normalize by the viscosity of water at that temperature. To find the intramolecular diffusion coefficient D, we need a probability distribution $P(r)$, such that Equation 10 predicts the measured k_R . Once an appropriate distribution has been chosen for a particular solvent condition, D can be calculated

using $P(r)$ and measured k_{D+} . For A β two models were chosen to generate $P(r)$. Based on our calculations, at all temperatures the measured D of A β_{42} ($D \sim 10^{-7} \text{cm}^2/\text{s}$) is lower by an order of magnitude than that of A β_{40} ($D \sim 10^{-6} \text{cm}^2/\text{s}$) which has been summarized in Table 3.1. Previous MD simulations (S^2 ordering parameter analysis) and NMR studies [90][91] have found that the C-terminus of A β_{42} is more structured than that of A β_{40} . It has been hypothesized that the formation of a β -hairpin in the sequence IIGLMVGGVIA involving short strands at residues 31-34 and 38-41 reduces the C-terminal flexibility of A β_{42} peptide, which may explain the slow intramolecular diffusion we have measured.

The simplest polymer chain model, a freely jointed chain, yields a Gaussian distribution as given by Equation 12. Table 3.1 below summarizes the D and r calculated from straight line fits shown in Figure 3.5, using the Gaussian distribution as $P(r)$. However a more sophisticated model is the worm-like chain model, which has been described in detail above. This model uses as a starting point a large number (20,000,000) of wormlike-chains [28] created by a Monte Carlo method, setting the persistence length to 4 Å. These chains are created with an excluded diameter for each link on the chain of 4 Å. The ensemble of worm like chains were then re-weighted to favor conformations in which residues of similar hydrophathy are near each other, using a tunable parameter σ (Equation 17). This re-weighted worm like chain probability distribution was normalized and then used to calculate D and average Trp-Cys distances as shown in Figures 3.6c, d and 3.7c, d. This model was further improved to take into account the charge effects [92] and was used to analyze the pH dependant effects of A β reconfiguration, which has been shown in Figures 3.7a, b. As shown by Equation 22 the charge effects introduced another parameter τ in addition to σ . The tuning parameters were adjusted to make the calculated reaction limited rates match the measured. When comparing measurements at pH7.5 and 10, we

initially set $\sigma=0$ and adjusted γ to make the ratios of the calculated rates at these two pH match the measured rate ratios, and then adjusted σ to get absolute agreement with the measured rates. As shown in Table 3.1, when the charge effects were introduced to analyze the data that were carried out under conditions of similar charge (such as pH 7.5) the calculated D and final average Trp-Cys distances did not change significantly, hence for conditions where charge effects did not play a role, we assigned $\gamma=0$.

Reconfiguration rate can be defined as the rate which allows the disordered chain to completely reconfigure by diffusion of the individual residues across the diameter of the chain and is given by:-

$$k_r \approx \frac{4D}{\langle 2r \rangle^2}$$

where r is given by average radius of the chain. Using our measured diffusion coefficient D and average Trp-Cys distance from WLC model as r , we obtain the reconfiguration rate of $A\beta_{42}$ as $4 \times 10^6 \text{ s}^{-1}$ and $A\beta_{40}$ as $2.2 \times 10^7 \text{ s}^{-1}$ at 40°C . Interestingly, our measurements show that the reconfiguration $A\beta_{42}$ is 5 times slower than $A\beta_{40}$ at all temperatures. This correlates to approximately 5 times higher concentration required for $A\beta_{40}$ to aggregate with the same lag time, and is in excellent agreement with previous reports showing that the critical concentration of $A\beta_{40}$ is 5 times higher than $A\beta_{42}$ [53][78][43][77].

Using Smoluchowski model of diffusion, the bimolecular diffusion rate k_{bi} for a $50 \mu\text{M}$ concentration of peptide is $1.7 \times 10^5 \text{ s}^{-1}$. Interestingly for $A\beta_{42}$, reconfiguration and bimolecular association formation rates are observed to be within a factor of 10, which further supports the hypothesis that when reconfiguration slows down to an optimum speed such that the

hydrophobic patches get to interact with each other and stick, that's when aggregation is most likely to occur[18][17]. As $A\beta_{40}$ reconfigures 100 times faster than its ability to form bimolecular association, stable association formation is much more difficult.

This correlation between reconfiguration and aggregation can be rationalized using a previously reported kinetic model described in chapter 1 [17]. It was solved in Matlab using reconfiguration rate k_r , calculated bimolecular association rate, k_{bi} , and a previously reported dimerization rate measured using self-quenching of tetramethylrhodamine (TMR) attached to $A\beta$ peptide, which showed a rapid loss of fluorescence within the lag time of fibril formation, which could be attributed to dimer and trimer formation. Solving the kinetic model using the previously reported values of $k_o=1.9s^{-1}$ for $A\beta_{42}$ and $k_o=0.5s^{-1}$ for $A\beta_{40}$, the rate of oligomer formation with time was computed and plotted, shown in Figure 3.8. The black colored plot represents $A\beta_{42}$ and red represents $A\beta_{40}$, comparing which we find that difference in reconfiguration between the two explains why the former is more aggregation prone than the latter.

Figure 3.5e shows the raw data plot of $1/k_{obs}$ versus viscosity for $A\beta_{42}$ peptide at pH10. The trend is very different from the data at physiological pH, as the slope decreases consistently at all temperatures. That translates into increase in diffusion with temperature, which is the usual trend that is observed in most proteins [28][26]. However, the reversal of this trend was first seen in the aggregation prone sequence α -synuclein, where diffusion was seen slowing down with temperature, and it seemed to be undergoing a reverse glass like transition [18]. $A\beta_{42}$ peptide under aggregating conditions was also seen to behave like α -synuclein. Both $A\beta_{42}$ and α -synuclein are extremely hydrophobic sequences and hydrophobic interactions can dominate at higher temperatures, thus slowing down diffusion. However, at higher pH, there is an increase in the net charge of the sequence and also overall charge distribution, which would increase

disorder in the sequence and prevent compaction. Our measurements are in agreement with that and show that size of the chain is increasing with increase in pH. Charge-charge repulsion can result in decrease of intra-molecular contacts, causing the sequence to change shape faster with time and thus intramolecular diffusion increases. The calculated reconfiguration at pH 10 is also faster than at pH7.5, which causes stable bimolecular association much more difficult and hence makes the protein less aggregation prone.

Figure 3.5f shows the raw data plot of $1/k_{obs}$ versus viscosity when inhibitor curcumin was added to A β_{42} peptide in equal concentrations. Curcumin is a polyphenolic compound, derived from common Indian spice turmeric, that is known to prevent aggregation of many proteins, including A β peptide [93][94]. Under aggregating conditions, Curcumin was observed to inhibit A β aggregation *in vitro* by preventing fibril and oligomer formation in a dose-dependent manner, and also blocked neurotoxicity. It was also able to cross the blood brain barrier in a transgenic mouse model, to prevent A β deposition in the brain of mice as confirmed by ELISA assay [94]. Our measurements show that curcumin was able to increase diffusion and open up A β_{42} peptide chain sequence, thus speeding up reconfiguration and preventing aggregation. Our results show that curcumin can be a potential drug candidate for treatment of AD as it is able to shift reconfiguration to a safe regime, where stable bimolecular association formation is unlikely, and hence it is able to arrest early aggregation. Curcumin has been reported to interact with the residues 12 and 17-21 [95] which possibly disrupts intra-molecular interactions of those residues with the hydrophobic patch far in sequence and leads to an increase in chain size along with diffusivity, just like we have measured.

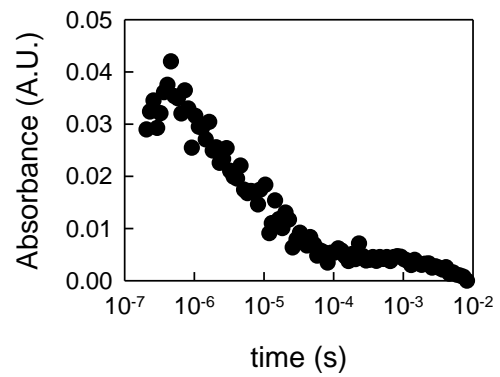


Figure 3.4 Decay of Trp triplet states W19C35 at pH 7.5, 0 C as monitored by the decay of absorption of 445 nm light and captured through oscilloscope.

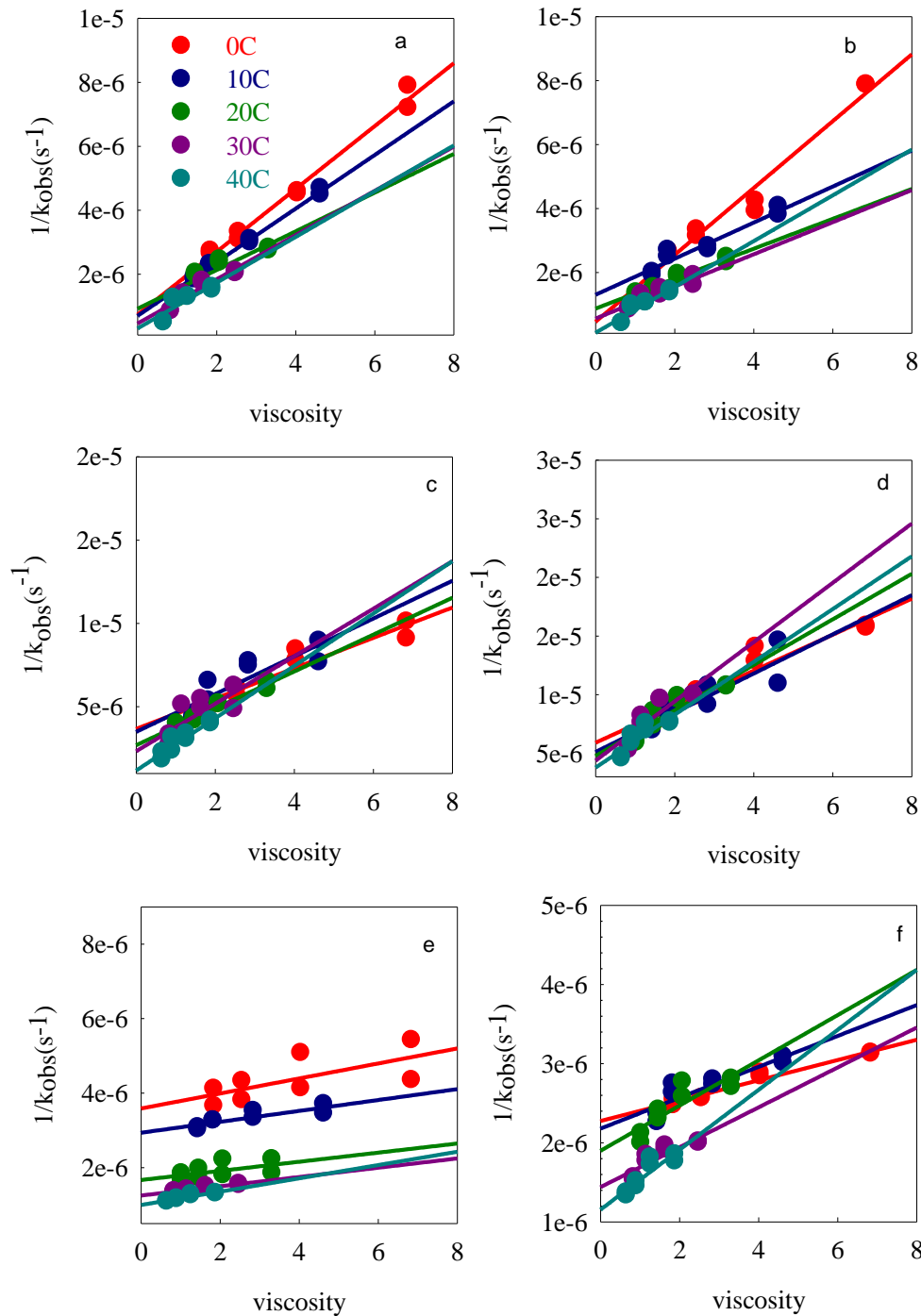


Figure 3.5 The fast lifetimes of Trp triplet at pH 7.5 for various viscosities and temperatures as marked. a) $A\beta_{42}$ M35C, F19W loop, pH 7.5 b) $A\beta_{42}$ F4C, F19W loop, pH 7.5 c) $A\beta_{40}$ M35C, F19W loop, pH 7.5 d) $A\beta_{40}$ F4C, F19W loop, pH 7.5 e) $A\beta_{42}$ M35C, F19W loop, pH 10 f) $A\beta_{42}$ M35C, F19W loop, pH 7.5: Curcumin

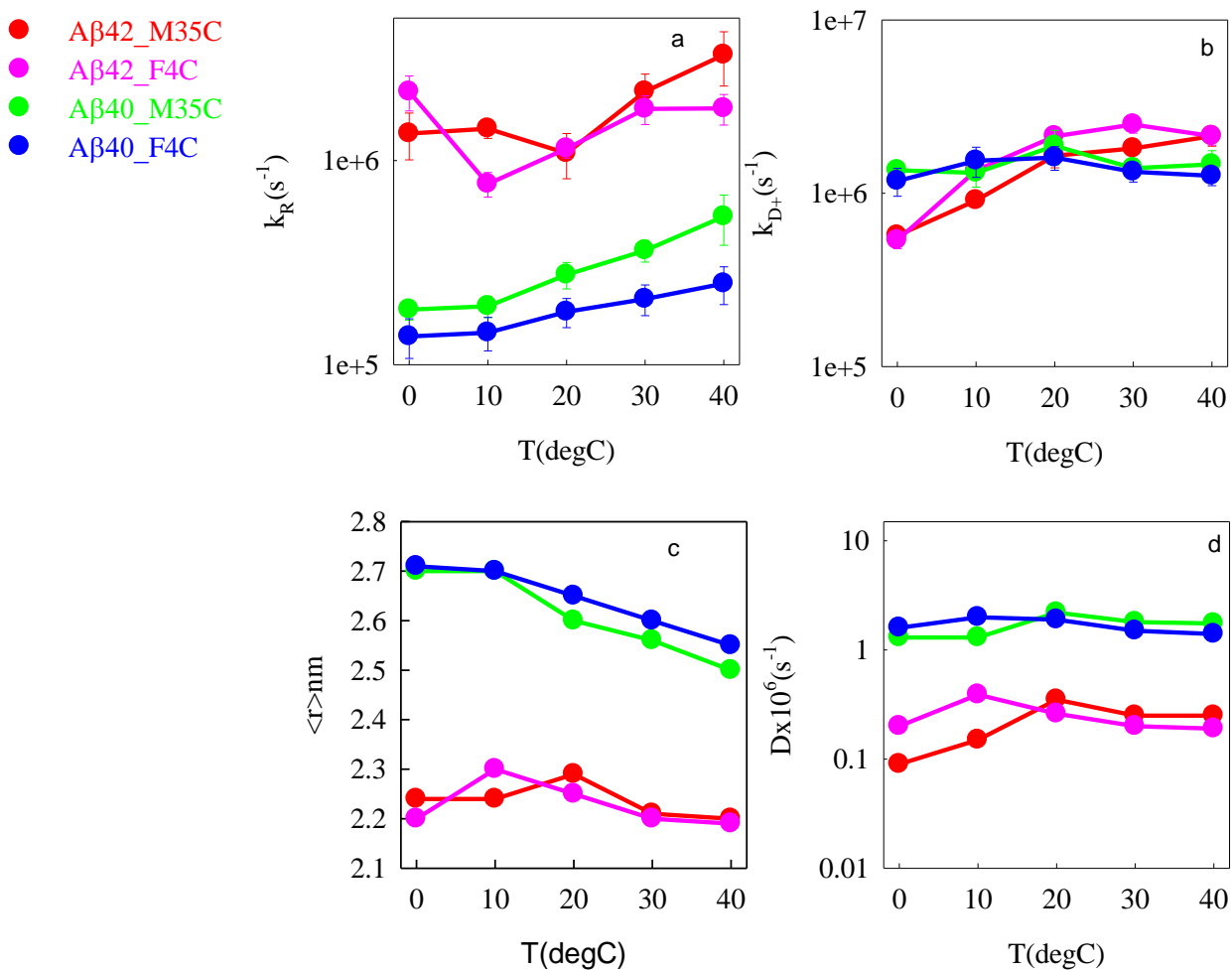


Figure 3.6 Comparison of intramolecular diffusion of the 2 loops of A β_{40} and A β_{42} (peptide concentration =30 μ M) a) Measured reaction-limited rates, as determined from the intercept of plots such as Fig. 9 (a, b, c, d) versus temperature b) Measured diffusion-limited rates as determined from the slope of plots such as Fig. 9 a, b, c, d normalized to the viscosity of water at each temperature. Errors from the linear fits are shown as error bars in (a) and (b). c) Average Trp-Cys distance calculated from the reweighted worm-like chain (WLC) model as described above d) Intramolecular diffusion coefficients determined using the WLC model.

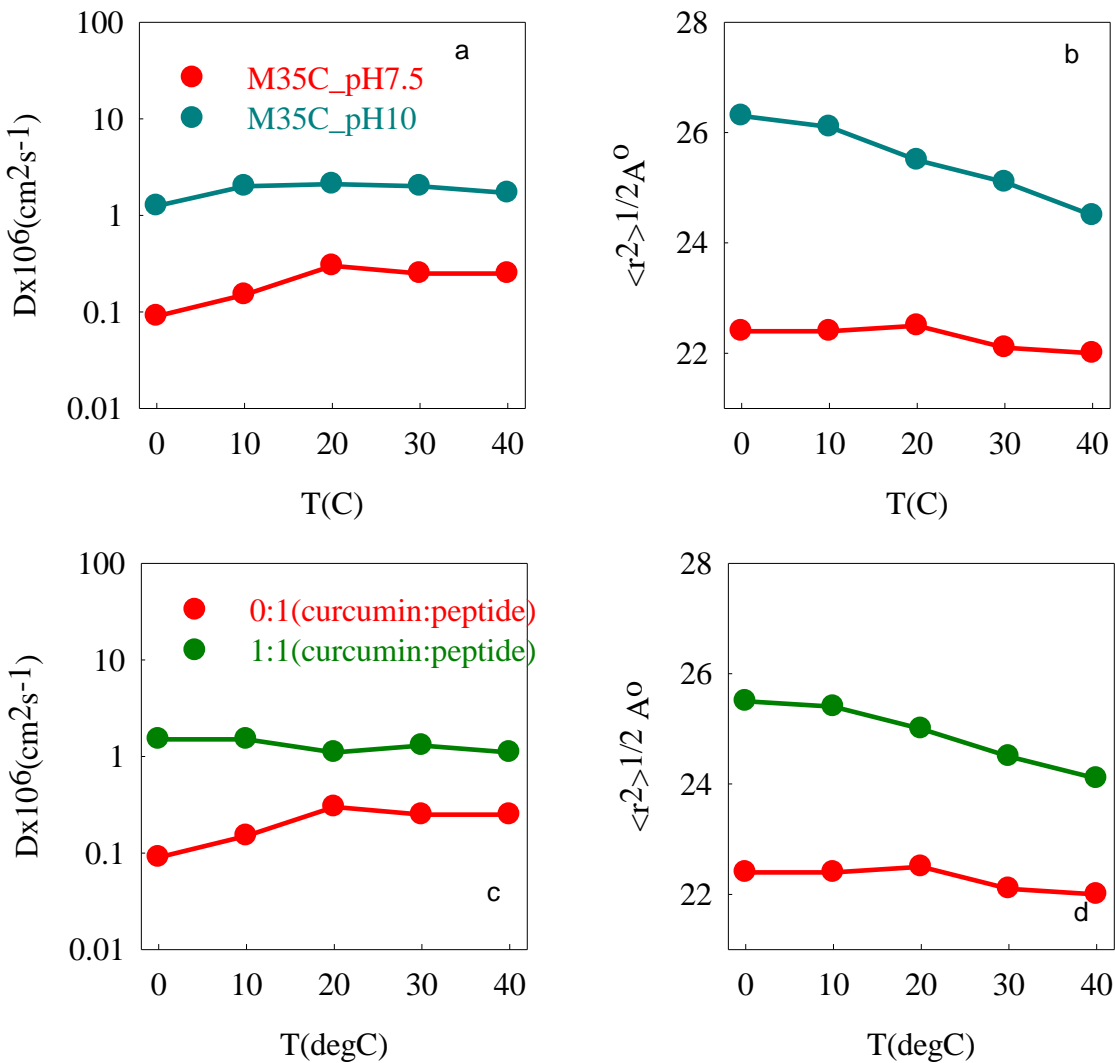


Figure 3.7 Modulation of reconfiguration of $A\beta_{42}$ by altering solution conditions and adding an inhibitor a) Measured intramolecular diffusion coefficients at pH 7.5 and pH 10 for $A\beta_{42}$ M35C, F19W loop b) Average Trp-Cys distance at pH 7.5 and pH 10 for $A\beta_{42}$ M35C, F19W loop determined using the WLC model from measured reaction and diffusion-limited rates obtained from plots shown in Fig. 9e c) Measured intramolecular diffusion coefficients for $A\beta_{42}$ M35C, F19W loop, with and without inhibitor Curcumin (peptide: Curcumin=1:1) d) Average Trp-Cys distance for $A\beta_{42}$ M35C, F19W loop, with and without curcumin, determined using the WLC model from measured reaction and diffusion-limited rates obtained from plots shown in Fig. 9f.

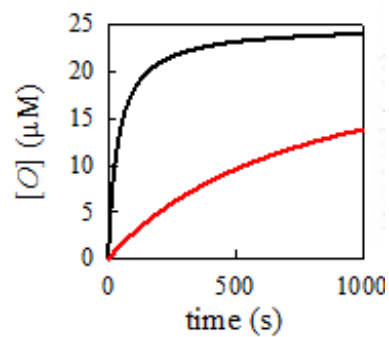


Figure 3.8 Formation of oligomer [O] versus time for Aβ₄₂ (black) and Aβ₄₀ (red) which was calculated using previously reported kinetic model that correlates reconfiguration with oligomer formation.

Table 3.1 Parameters for two different polymeric models that best fit the experimental data

Peptide	T (C)	Gaussian $\langle r^2 \rangle^{1/2}$ (Å)	Gaussian D (cm^2s^{-1})	WLC σ	WLC γ	WLC $\langle r \rangle$ (Å)	WLC D (cm^2s^{-1})
A β_{1-42} C4W19 pH 7.5	0	34.6	1.2×10^{-7}	1.85	0	21.0	2.0×10^{-7}
	10	50.0	8.8×10^{-7}	0.7	0	24.0	3.9×10^{-7}
	20	42	8.4×10^{-7}	1.1	0	22.5	2.6×10^{-7}
	30	37.4	6.5×10^{-7}	1.65	0	22.0	2.0×10^{-7}
	40	36.7	5.5×10^{-7}	1.7	0	21.9	1.9×10^{-7}
A β_{1-40} C4W19 pH 7.5	0	84	3.9×10^{-6}	-1.8	0	27.1	1.6×10^{-6}
	10	82	4.8×10^{-6}	-1.7	0	27.0	2.0×10^{-6}
	20	79	4.1×10^{-6}	-1.6	0	26.5	1.9×10^{-6}
	30	77.5	3.4×10^{-6}	-1.5	0	26.0	1.5×10^{-6}
	40	72.1	2.5×10^{-6}	-1.0	0	25.5	1.4×10^{-6}
A β_{1-42} W19C35 pH 7.5	0	39.4	1.7×10^{-7}	0.15	56	22.4	9.0×10^{-8}
	10	39.6	2.8×10^{-7}	0.2	55	22.4	1.5×10^{-7}
	20	44.0	7.4×10^{-7}	0.02	52	22.9	2.5×10^{-7}
	30	35.7	4.4×10^{-7}	0.55	52	22.1	2.5×10^{-7}
	40	32.2	3.9×10^{-7}	0.9	52	22.0	2.5×10^{-7}
A β_{1-42} W19C35 pH 10	0	69.3	4.5×10^{-6}	-0.1	57	26.3	1.2×10^{-6}
	10	62	6×10^{-6}	-0.02	55	26.1	1.3×10^{-6}
	20	48	4.6×10^{-6}	0.03	52	25.5	1.3×10^{-6}
	30	47	5×10^{-6}	0.2	54	25.1	1.2×10^{-6}
	40	42	3.7×10^{-6}	0.35	55	24.5	1.7×10^{-6}
A β_{1-42} W19C35 curcumin	0	60	4.1×10^{-6}	0.5	0	25.5	1.5×10^{-6}
	10	58	3.5×10^{-6}	0.2	0	25.4	1.5×10^{-6}
	20	55	3.3×10^{-6}	0.3	0	25.0	1.1×10^{-6}
	30	50	3×10^{-6}	0.5	0	24.5	1.3×10^{-6}
	40	46	2×10^{-6}	0.7	0	24.1	1.1×10^{-6}
A β_{1-40} W19C35 pH 7.5	0	80	3.5×10^{-6}	-0.8	0	27.0	1.3×10^{-6}
	10	78	3.3×10^{-6}	-0.5	0	27.0	1.3×10^{-6}
	20	69	3.1×10^{-6}	-0.4	0	26.0	2.2×10^{-6}
	30	62	1.8×10^{-6}	0.1	0	25.6	1.8×10^{-6}
	40	56	1.3×10^{-6}	0.6	0	25.0	1.7×10^{-6}

Chapter 4

Protein Aggregation in Parkinson's Disease

In this chapter, I will talk about α -synuclein protein in connection with Parkinson's disease and then show that its reconfiguration rates can be controlled by inhibitors or point mutations.

4.1 Introduction

Synucleins belong to a family of closely related presynaptic proteins encoded by three distinct genes SNCA, SNCB, SNCG found abundantly in the neuronal tissues of vertebrates, which express the proteins α , β and γ -synuclein respectively [96]. The first synuclein protein was discovered in the electric organ synapses of the electric ray *Torpedo californica*, where it was found in both nerve terminals (presynaptic membrane) and nuclear envelope (hence the name synuclein) [97]. α -synuclein is a 140-residue protein which has been estimated to account for 1% of the total protein in soluble cytosolic brain fractions. The protein is expressed widely across neurons, including the nucleus, and has also been found in the neuritis of mature neurons [98]. It has been detected in the cytosol, mitochondria, mitochondria-associated endoplasmic reticulum (ER) membrane (MAM) and vesicles found in cells[99]. Reportedly, it can be secreted from neuronal cells in small amounts by exocytosis under normal conditions and in the presence of stressors, may be released in large quantities into the surrounding extracellular space to be taken up by neighboring cells, by endocytosis [100]. Although it is extensively found in the brain, it has also been detected in other tissues, including red blood cells in humans [101].

Parkinson's disease (PD) was first described by Dr. James Parkinson in his essay "An Essay on the Shaking Palsy" in the year 1817, where he documented the medical cases of six

people who suffered from unusual symptoms such as involuntary tremulous motion, bending of trunk, and diminished muscle power, that worsened with time. Neuropathologically PD is characterized by progressive loss of neurons in the substantia nigra (midbrain) and other regions of the brain, and surviving neurons contain cytosolic filamentous inclusions known as Lewy bodies (LBs) and Lewy neurites (LNs). LBs are large intracytoplasmic proteinaceous inclusions, 5-25 μm in diameter, with a dense core of filamentous and granular materials, and LNs correspond to abnormal neurites that contain filaments (5-10nm in diameter) similar to those found in LB's [102]. Abundant LBs and LNs in the cerebral cortex are the neuropathological hallmarks of PD as well as dementia with Lewy bodies (DLBs) a common late life dementia clinically similar to Alzheimer's disease (AD). In general an average person undergoes regular nigral cell loss with age; but in PD the neuron loss is considerably accelerated. The symptoms of PD become evident after more than 70% of the dopaminergic neurons have already died. Sporadic forms of the disease sets in at an mean age of 70 and accounts for about 95% of the total cases, while multiple familial mutations associated with the disease causes an early-onset of the disease before the age of 50 and the hereditary forms account for about 4% of the PD cases [103].

Several evidence have suggested the possible role of α -synuclein in the pathogenesis of Parkinson's disease (PD) [96][104].

- 1) α -synuclein is the primary component of LBs and LNs in all PD patients. Antibodies which recognize the carboxyl-terminal region of α -synuclein, labeled whole filaments extracted out of such inclusions, indicating that α -synuclein is the major component. Also, α -synuclein can be purified and recovered in large amounts from LBs [103].

- 2) Autosomal dominant early-onset PD cases have been identified in people carrying missense mutations in the α -synuclein gene, corresponding to A30P, E46K and A53T substitutions in the α -synuclein protein sequence or as a result of over-expression of wild type α -synuclein due to the gene duplication or triplication [105][106][103].
- 3) The transgenic mice and *Drosophila* expressing human WT α -synuclein and or the mutants, have led to PD like symptoms like motor deficits and to the formation of neuronal inclusion bodies that resemble LBs [107][108].
- 4) Cells transfected with α -synuclein can develop LB-like inclusions under certain conditions [103].

4.2 Physiological Function

The function of α -synuclein remains controversial and poorly understood [97]. In transgenic mouse models that either over expressed wildtype human α -synuclein or A53T mutant in the brain, showed alterations in synaptic plasticity by modulations of signaling pathways. Such mice were reportedly prone to developing PD like symptoms, due to overexpressed α -synuclein, which caused dampening of its synaptic transmission and reduced movement [109]. However whether those alterations were arising out of neurodegenerative mechanisms linked to α -synuclein aggregation or due to α -synuclein dysfunctioning as a result of aggregation can be debated as the evidence found were indirect. Synaptic transmission is involved in ensuring healthy learning memory and normal amounts of α -synuclein expression was seen to be a key modulator of song learning in a zebra finch, which led to the conclusion that α -synuclein may be a critical regulator of neuronal plasticity [110]. Another study showed that mice normally expressing α -synuclein are viable, fertile, exhibit intact brain architecture (as demonstrated by

electro-physiological studies) and concluded that α -synuclein is an essential regulator of neurotransmission[111]. Such data have led to the notion that α -synuclein may have a role in synaptic transmission [112] [113]. Cysteine-string protein- α (CSP α) is another synaptic vesicle protein whose deletion have been linked to neurodegeneration and is believed to be essential for neuronal survival. Expression of α -synuclein in mice was able to counteract the lethality imposed by deletion of CSP α , and together with CSP α and other proteins, was able to protect nerve terminals against injury [114]. In primary hippocampal neuronal cell cultures, suppression of α -synuclein expression led to significant reduction in the size of the pre-synaptic vesicular pool, which led to the conclusion that α -synuclein may interact with and regulate specific pools of synaptic vesicles in neurons, thus modulating synaptic functions in the normal brain [115].

4.3 Effects of Oligomers on Neurotoxicity

One of the earliest pieces of evidence that suggested that protein inclusions do not invariably cause neurodegeneration was the observation of incidental LBs at autopsy of aged individuals without clinical features of PD or other neurodegenerative diseases [116]. Incidental LBs without degeneration in asymptomatic individuals were observed in 12% autopsy cases in another study[117]. Recent studies have revealed higher presence of soluble oligomers of α -synuclein in the CSF and human blood plasma in patients clinically diagnosed with PD, which further led to the conclusion that they may be involved with the disease [118] [119] .

Much evidence in the field suggests that early soluble oligomers and pre-fibrillar assemblies may be more neurotoxic and correlated with PD, compared to fibrils found in the inclusion bodies such as LBs [113][117][120][121]. In one such study, a striking correlation was found between the presence of prefibrillar aggregates in the cytoplasm of cell culture with Golgi

body fragmentation and decline of cell viability[122]. Interestingly, the increase in Golgi fragmentation occurred much before the appearance of fibrillar inclusions. There was no further spread of such destructive events and the cells were able to maintain Golgi structure once the fibrillar inclusion bodies formed. Rather, co-staining of fibrillar inclusions with α -synuclein, Golgi markers, and the presence of lysosomes and mitochondria near the juxtannuclear inclusion bodies, led to the conclusion that inclusions might be a consequence of the cell attempting to sequester protein aggregates and impair organelles from the cytoplasm.

Cells have various quality control mechanisms that ensure that the proteins are folded properly post translation, before being released; however when misfolded proteins accumulate in the cell, it triggers unfolded protein response (UPR) stress signaling, which may lead to increased expression of chaperone proteins that help to properly fold protein, or proteasomic degradation of such misfolded proteins [13]. The accumulation of toxic protein conformations in neurodegenerative diseases implies failure of such defense mechanisms. Another study identified a compound that promotes inclusion body formation that was able to prevent α -synuclein mediated toxicity [123] and led to the conclusion that fibrillar inclusion body formation may be protective mechanisms to counteract degeneration.

In another comparison study, α -synuclein mutants that promote oligomer formation led to an increased loss of nigral TH-positive neurons, compared to those mutants that causes increased fibril formation, in a murine model [124]. *In vivo*, following lentiviral injection into the substantia nigra region of the rat brain, the mutants that causes maximum oligomer formation *in vitro* induced increased dopaminergic loss and neuronal cell death. Dissection of the rat brain showed the increased occurrence of SDS-stable trimers corresponding to those bad mutations, which correlated very well with cell death. Typically, the decrease in the number of TH-positive

cells was at least three times or more higher for those mutations that caused increased relative trimer formation *in vivo*. Abnormal calcium homeostasis reportedly plays a crucial role in the pathogenesis of neurodegenerative disorders, and in another comparison study, the smallest oligomers (2-6 nm in height as observed by AFM) generated *in vitro* when injected into human cell cultures, were able to cause elevation of intracellular calcium levels and also seeded further aggregation of cytosolic α -synuclein in cells [125].

4.4 Structure

α -synuclein is a polypeptide chain sequence of molecular weight ~14kDa, whose amino acid sequence can be divided into three regions: residues 1-60 which contain four 11-amino acid imperfect repeats (that codes for amphipathic helices) with a conserved motif (KTKEGV); residues 61-95, containing mostly of hydrophobic residues, the highly amyloidogenic NAC region and two additional repeats; and residues 96-140 representing the highly charged C-terminal region. At physiological pH it has a net charge of -9 (24 negatively charged side chains, and 15 positively charged side chains).

At neutral pH α -synuclein shows far-UV CD and FTIR spectra typical of an unfolded polypeptide chain [126]. The CD spectrum is characterized by a minimum around 196 nm and absence of bands in the 210-230 nm region, and the FTIR spectrum shows a broad peak at 1650 cm^{-1} , suggesting that majority of molecules are disordered. The hydrodynamic properties of α -synuclein analyzed by size exclusion chromatography and small angle X ray scattering (SAXS) were all in agreement with the CD and FTIR studies. Surprisingly, the Stokes radius measured for α -synuclein by size exclusion chromatography was much lower than that of a completely unfolded peptide chain of the same molecular mass, which led to the conclusion that α -synuclein

is slightly more compact than a typical random coil [96]. The radius of gyration (R_g) for α -synuclein calculated at neutral pH from SAXS data (around 40Å) was also significantly smaller than that of a random coil polypeptide of the same length (52 Å) [126]. NMR studies subsequently demonstrated the presence of transient long-range contacts within the protein, that reportedly has a role to play in inhibiting aggregation of the protein [127] and disruption of such contacts may lead to a more disordered conformation which could initiate aggregation.

Thus α -synuclein is considered to belong to the family of intrinsically disordered proteins, characterized by a unique combination of low hydrophobicity and high net charge [128]. Any changes in local environment leading to increase in hydrophobicity and decrease in net charge can lead to partial folding of the intrinsically disordered protein structure leading to a pre-molten globule like conformation [103]. α -synuclein has a negative charge at neutral pH (pI 4.7) and at lower pH there would be a minimization of the high net charge of the protein leading to decreased intramolecular charge-charge repulsion and compaction. Similarly there is an increased hydrophobic effect at higher temperatures, leading to a stronger hydrophobic driving force for compaction. The pH and temperature induced structural transitions occurred simultaneously in a cooperative manner, when monitored by ANS fluorescence and CD [103].

Whether α -synuclein is natively unfolded has been a subject of much debate. Until very recently α -synuclein was known to exist as a random coil with some residual structures, which acquires α -helical secondary structure only upon binding to lipid vesicles[129]. However one recent study showed that α -synuclein isolated and analyzed under non-denaturing conditions from mammalian cells and red blood cells exist predominantly as a tetramer of molecular weight \sim 58kDa that is rich in α -helical structure [130]. This study also showed that cell-derived α -synuclein behaved very differently from the *in vitro* recombinantly expressed monomers. It

showed significantly increased affinity for lipid binding and also the aggregation behavior was vastly different, with the folded tetramers showing almost no fibril formation *in vitro*, as confirmed by ThT fluorescence studies. These observations led to the important question that whether the less aggregation-prone folded tetramer conformation was the native form of α -synuclein and if destabilization of such conformation into an unfolded disordered state precedes its misfolding and aggregation?

This study attributed the differences in conformations to the long established recombinant α -synuclein purification protocol which uses denaturing conditions like heating or denaturants. A subsequent study that used modified bacterial expression protocol using a fusion construct, avoiding heating or denaturants was able to reproduce the helical folded tetramer structure [131]. However whether or not this putative tetramer is the main physiological form of α -synuclein in the brain is still controversial. Almost all studies conducted later could not replicate this folded tetramer conformation of α -synuclein and confirmed that endogenous and overexpressed α -synuclein in human, mouse and rat brain predominantly exist in a monomeric state, and co-migrates with the unfolded recombinantly derived unfolded monomeric α -synuclein in native gels and gel filtration columns [132]. Similar behavior was observed in α -synuclein expressed in mammalian cell lines, and interestingly even the modified bacterial expression protocol using a fusion construct in absence of any denaturing conditions yielded the monomeric disordered conformation. The concept of a protein-chameleon has been proposed in literature, according to which the structure of α -synuclein depends on its environment and the choice between various conformations is determined by the peculiarities of the protein's surroundings [133].

4.5 Mutations Associated with PD

Three autosomal dominantly inherited forms of PD have been identified, all of which is caused by mutations in the α -synuclein sequence. α -synuclein contains seven repeat regions (KTKEGV), within which all the familial mutations have been found. The first mutation identified among Greek and Italian kindred was A53T which is located between the fourth and fifth repeats [134]. The second mutation A30P located between second and third repeat was identified among German kindred [135]. The third mutation E46K was identified in a Spanish kindred, located within the fourth repeat region [106]. Surprisingly, within the two repeat regions in the NAC region, no mutation has been detected to date. All the mutants are more aggregation prone than the wild type (WT), and causes early onset of PD in people carrying them. However, the aggregation pathways differ significantly. For example the lag time (from ThT fluorescence) of A53T is much lower than the WT, while the lag time of A30P is higher than WT, which means fibrillation of A53T>WT>A30P and the consumption of monomers of A53T is also the fastest [136]. However the process of oligomerization is much faster in the case of A30P compared with the WT and also the monomers are consumed faster than WT, forming insoluble aggregates that could be precipitated by ultracentrifugation and analyzed using AFM and EM [137]. The E46K mutant also increases the aggregation propensity of α -synuclein, but the effect is less dramatic than that of A53T mutant. The relative differences in aggregation is consistent with the reported age of onset of PD, with the mean age of onset of PD in people carrying A53T mutant being 45 years, while that of E46K being 60 years [138]. Therefore the general aggregation propensity of the mutants (fibrillar and non-fibrillar combined) has been observed to be much higher than the WT.

Surprisingly, like WT the mutant proteins are all largely unstructured in solution [139] but exhibit different fibrillar morphologies. The WT fibrils form twisted filaments with a diameter 10-15 nm, while A30P mutants form straight filaments with a diameter 11-16 nm, and A53T form larger twisted filaments with a diameter of 16-19 nm [140]. The mutants were also observed to affect the morphology and size distribution of α -synuclein oligomeric intermediates like protofibrils, as measured by ultracentrifugation and scanning transmission electron microscopy [104]. The A30P promotes formation of annular, pore-like protofibrils, while the A53T forms annular and tubular protofibrillar assemblies. The WT forms annular protofibrils, but only after extended incubation.

Previous studies have reported that native α -synuclein adopts an ensemble of conformations, stabilized by long range interactions, involving the N(residues 1-60) and C termini (residues 109-140) which shields the highly amyloidogenic non-A β component of Alzheimer disease amyloid (NAC) residues 61-95 from solvent and hence prevents the native conformation from aggregating [127]. NMR studies have revealed absence of such long range contacts in both A30P and A53T mutants, which leaves the hydrophobic NAC region free to form intermolecular contacts and hence aggregation can be easily initiated [135]. This study further reveals that the compaction of the N-terminal observed in the WT is reduced in the mutants, although the C-terminal compaction is comparable to the WT.

Interestingly, all atom replica exchange molecular dynamics simulations (REMD) in aqueous water, have predicted increased long range intramolecular protein interactions of the C-terminal with the N-terminal and NAC region of E46K mutant, compared to the WT [141]. Based on the reported data, the probability of finding structures with R_g values between 25.5 and 32.5 Å is higher for the E46K compared to WT, while the WT is more probable of populating

conformations of R_g values between 35.5 and 55 Å. This suggests that the E46K mutant is more compact than the WT. NMR paramagnetic relaxation enhancement (PRE) measurements have also detected increased interaction of the acidic C-terminal tail with NAC and N-terminal regions. Also, extra interactions between residues 40-50 with both C-terminal and NAC regions of the E46K mutant protein is observed, which leads to significant compaction, compared to the WT [142]. These results are in agreement with observation that the E46K mutant elutes later than WT α -synuclein, and is characterized by higher retention time in the size exclusion chromatography [143], suggesting that it is more compact. This study further performed PRE analysis on the A30P and A53T mutants, and found similar long range contacts as observed in the WT, refuting previous claims that these mutants could be less compact than the WT. The previous PRE reports have detected only minor decrease of long range contacts compared to WT, which was not larger than the range of experimental error. Residual dipolar coupling (RDC) measurements have further confirmed the presence of long range contacts in E46K, as well as in the other two mutants A30P and A53T.

Thus recent findings that PD linked mutations could be more compact than the WT, challenges previous conclusions that the long range contacts in α -synuclein has a protective role to play against protein aggregation [127]. A compact structure does not necessarily shield the NAC region from initiating intermolecular interactions. Evidence supporting this idea have been reported recently, in which phosphorylation of α -synuclein at Ser 129 is shown to release the C-terminus from interacting with the N-terminal region as detected by NMR, yet at the same time significantly inhibiting α -synuclein aggregation [144]. The hydrodynamic radius calculated from the measured diffusion coefficient of phosphorylated α -synuclein is seen to be much higher than

that of WT, suggesting that phosphorylation strongly disrupts the ordering of monomeric α -synuclein, thus making the chain more expanded and less aggregation prone.

There have been numerous attempts to study how the mutants affect the residual structure and other properties of the WT, but each mutant has been observed to affect it differently. NMR studies have reported that α -synuclein is largely unfolded in solution, though the N-terminal exhibits preference for a helical conformation while the C-terminal shows an unfolded structure [145]. CD analysis has revealed a similar random coil secondary structure for both E46K and the WT, when free in solution [143] and in the presence of phospholipid vesicles, both E46K and WT undergo a structural transition to a primarily α -helical state. On the other hand, NMR studies have revealed that the helical propensity of residues 18-31 found in the WT is absent in A30P, exhibiting zero average population for α -helical conformation. In contrast, the A53T mutation leaves the helical propensity of this region intact [146]. Also the A53T exhibits slightly enhanced local preference for extended β -sheet-like conformations around the site of the mutation. Atomic force microscopy-based single molecule experiments have revealed that the primary random-coil structure of α -synuclein shows a tendency towards forming β -like conformers (that resembles β -sheets) in around 7% of the cases in WT, while this tendency increases 38% upon A30P mutation [8].

Other physiochemical property analysis has also revealed differences in behavior of the mutants. For example, the hydration properties of A53T mutant compared to the WT using NMR, differential scanning calorimetry and MD simulations, have revealed that the mutant displays somewhat higher level of hydration, suggesting a bias towards more open structures [140]. MD simulation studies also predict that there is considerable differences in the way each of these mutants interact with membranes [147] suggesting that each would affect the biological

role of α -synuclein differently. Electrostatics alone is also insufficient to explain why the mutants make the protein more aggregation prone. One of the mutants E46K increases the positive charge of N-terminal lipid binding domain, which would be expected to enhance interactions with the negatively charged C-terminal domain, but the same does not hold for the other two mutants. Therefore the key factor that drives these mutants to be so much more aggregation prone and pathogenic in nature than the WT and causes early onset of PD is still unknown.

4.6 Expression and Purification Protocol

The α -synuclein plasmid was a kind gift from Gary Pielak (University of North Carolina, Chapel Hill, NC). α -synuclein is a 140 residue long polypeptide chain sequence that does not contain either Trp or Cys. First, two different Trp/Cys pair-containing α -synuclein mutants, namely Y39W/A69C and F94W/A69C, were created using the QuikChange site-directed mutagenesis kit (Stratagene). For mutation studies, a third mutation was then introduced in the Y39W/A69C loop and five such triple mutants were created, namely A30P, A53T, E46K, V74E and T72P. At each step the mutations were confirmed by DNA sequencing. The mutants were then expressed in *E. coli* BL21 (DE3) cells and purified by a procedure described previously [18]. After the cells were grown and harvested, pellets were resuspended in Lysis buffer (containing Tris EDTA) after which protease inhibitor, DNAase, RNAase, and Lysozyme were added to the cell suspension and stirred for 30 minutes. It was then sonicated for 4-5 minutes, boiled for 20 minutes and centrifuged at 13,000 rpm for 30 minutes. The supernatant was collected and the protein was precipitated by addition of 0.361 g/mL ammonium sulfate. The

pellet was resuspended in buffer A (20 mM Tris, 100mM NaCl, pH=8.5) and chromatographed by anion exchange on a Q-Sepharose Fast Flow column equilibrated with buffer A, and eluted with a linear NaCl gradient (100-1,000 mM). α -Synuclein containing fractions were collected and further purified by gel filtration on a Hi-Prep Sephacryl S200 column equilibrated with buffer A. The monomeric α -synuclein peak was found to be >95% pure as assessed by SDS-PAGE and Coomassie blue staining. The protein concentration was determined from the absorbance at 280 nm using extinction coefficient of $11,460 \text{ M}^{-1} \text{ cm}^{-1}$ and stored for later experiments at -20C in the presence of 20 mM Tris, 100mM NaCl, pH=7.5 along with 1mM tris(2-carboxyethyl)phosphine (TCEP) to prevent disulfide bond formation.

4.7 Contact Quenching Experiment

For this experiment, the respective α -synuclein mutant fractions were thawed and diluted in 25 mM sodium phosphate buffer (pH=7.5), 10 mM TCEP (to prevent disulfide bond formation), and various sucrose concentrations (0, 10, 20 and 30% w/w). The final concentration of the mutant proteins was kept fixed at 30 μ M for each set of temperature and viscosity measurement. The buffer, sucrose and TCEP solutions were bubbled with N₂O for one hour, to eliminate oxygen and scavenge solvated electrons created in the UV laser pulse. Triplet lifetime decay kinetics of tryptophan as a result of cysteine quenching, was then measured with an instrument described in Chapter 2.

4.8 Effect of Good and Bad Mutations on Reconfiguration

The Trp triplet decay trace, as it is being quenched by Cys in α -synuclein, is comprised of two decays; a rapid decay in the microsecond time scale, which corresponds to the excited state

of tryptophan being quenched by cysteine, much faster than the natural decay rate of Trp, in the absence of any quencher, and a very slow decay in the 100 μ s to 1ms time-scale due to other photo effects. The fastest rate corresponds to monomer reconfiguration, in which Trp is readily quenched by the Cys, and is reported as k_{obs} . Figure 4.1a represents the sample $1/k_{obs}$ versus viscosity at various temperatures for the Y39W-A69C loop of α -synuclein measured at pH7.5, where the decay times at each temperature is fit to a straight line. The reaction and diffusion limited rates can be extracted from the intercept and slope respectively, as described previously. The trend is drastically different from all sequences measured previously, where the intercept is seen decreasing with temperature and slope increases dramatically, and the straight lines cross each other [18]. The analysis from both Gaussian and worm like chain analysis reveals that α -synuclein diffuses quite fast ($\sim 10^{-6}$ cm²/s) at lower temperature and physiological pH. However, as soon as it is exposed to aggregating conditions such as higher temperature (40°C) and lower pH [103], the diffusion slows down ($\sim 10^{-8}$ cm²/s) and the chain compacts significantly, slowing down reconfiguration. As reported previously, the reaction and diffusion limited rates and the diffusion coefficients measured for 4 different loops spanning the 140 residue long peptide were remarkable similar at pH7.5 [18].

Figure 4.1b shows the $1/k_{obs}$ versus viscosity plot at pH 7.5 and various temperatures for the aggregation enhancing mutation A53T, in the Y39W/A69C loop. Compared to the wild-type Y39W/A69C loop, the slope changes much more drastically, and the intercepts at each temperature decreases significantly, reaching close to zero. The trend of the plots for all 3 aggregation enhancing familial mutations, namely A53T, A30P and E46K are quite similar. Figure 4.2a shows the comparison of reaction limited rates of wild type with that of the 3 aggregation enhancing mutations such that $k_R=1/\text{intercept}$. The measured values of k_R are

slightly higher for the A53T mutant, and highest for the E46K mutant, while the A30P mutant behaves oppositely, with k_R values slightly lower than the wild type at all temperatures. Figure 4.2b shows the comparison of measured diffusion limited rates at all temperatures where $k_{D+}=1/(\eta\text{slope})$ where the slopes were picked from the respective $1/k_{obs}$ versus viscosity graphs and η is the viscosity of water at that temperature. The reaction and diffusion limited rates were analyzed, using the SSS polymer theory, which has been described previously. The probability distribution of average Trp Cys distances was chosen such that Equation 10 predicts the measured k_R . Figure 4.2(c,d) shows the average distance r between Trp39 and Cys69 and intramolecular diffusion coefficients D calculated by choosing a simple Gaussian distribution as the $P(r)$.

At higher temperatures, wildtype α -synuclein becomes more aggregation prone, with the k_R rising drastically, and the chain compacting at least 3 fold compared to that at lower temperatures, as shown in Table 4.1 [18]. Figure 4.2c reveals that at all temperatures the E46K mutant compacts the chain further. At higher temperatures, even though the wild type α -synuclein has already undergone significant compaction, a further 5Å collapse is seen for the E46K mutant. The A53T mutant's effects on the chain volume are less drastic than the E46K as shown by Figure 4.2c, and it uniformly compacts the chain by 3Å at all temperatures. Interestingly, the average distances between 39W and 69C is slightly higher for the A30P mutant compared to the wild type at lower temperatures, and remains unchanged at higher temperatures. Based on our measurements, we conclude that the aggregation enhancing mutants all affect the chain volume differently. The most drastic effect is seen in the E46K mutant, and that could be attributed to the addition of a positive charge in the N-terminal domain, which decreases repulsion of the negatively charged C-terminal and strengthens attraction, thus compacting the

chain. The effect of A53T and A30P mutant maybe less pronounced because alanine has similar hydrophobicities to both threonine and proline. Since all three mutants make the protein aggregation prone, we can argue that maybe their effects on chain volume alone cannot determine whether or not it aggregates.

Figure 4.2d shows the comparison of diffusion coefficients D of all the 3 mutants with that of the Y39W/A69C loop. Interestingly, all the three familial mutations are seen consistently slowing down the diffusion of the wild type 39W-69C loop by at least 2 fold at all temperatures, thus facilitating aggregation. The reconfiguration rates k_r has been calculated using the measured diffusion coefficient D and average Trp-Cys distances r and reported in Table 4.1. We find that the reconfiguration of all the familial mutations is slower than the wildtype, at all temperatures. Using Smoluchowski model of diffusion, the bimolecular diffusion rate k_{bi} for a $30\mu\text{M}$ concentration of α -synuclein is $7 \times 10^4 \text{ s}^{-1}$. At lower temperatures, when α -synuclein is less aggregation prone, its reconfiguration rate is seen to atleast 50 times higher than the bimolecular association formation rate. However, under aggregating conditions such as higher temperatures, the reconfiguration of α -synuclein slows down and is seen approaching the bimolecular diffusion regime. Since $k_r \approx 7.8 \times 10^5 \text{ s}^{-1}$ for the Y39W/A69C loop at $T=40^\circ\text{C}$ the reconfiguration and bimolecular association rates are within a factor of 10. We find that for all the three mutants the reconfiguration slows down significantly at $T=40^\circ\text{C}$ such that it is within a factor of 5 of the bimolecular association formation rates (Table 4.1). This allows the bad conformations to spend more time in the aggregation prone states, thus the likelihood of formation of stable bimolecular association increases, before they can escape by reconfiguration to some innocuous conformation. Therefore slowing down of reconfiguration is one common factor that seem to be driving aggregation in the mutants of α -synuclein.

Previously some aggregation reducing mutations of α -synuclein have been reported [148]. V74E reportedly is a self fibrillization defective mutant, which was able to completely suppress the fibrillation of the wildtype α -synuclein, as measured by ThT fluorescence. The T72P mutant interestingly was able to prevent the fibrillation of wildtype, as well as the familial mutants of α -synuclein, namely A53T, A30P and E46K. Figure 4.1b shows the $1/k_{obs}$ versus viscosity plot at pH 7.5 and various temperatures for the aggregation reducing mutation V74E, in the Y39W/A69C loop. Compared to the wild-type Y39W/A69C loop, the change in slope with temperature is much more moderate, and the intercepts also increases. The trend of the plots for the 2 aggregation enhancing familial mutations, namely V74E and T72P are quite similar. Figure 4.3a shows the comparison of reaction limited rates of wild type with that of the 2 aggregation reducing mutations such that $k_R=1/\text{intercept}$. Under aggregating conditions (higher temperatures), the drastic increase in k_R that is seen in the wild type is completely suppressed for both the aggregation reducing mutations and k_R is just seen rising only slightly with temperature. Figure 4.3b shows the comparison of measured diffusion limited rates at all temperatures. Using Gaussian distribution as $P(r)$ in equation 10, the diffusion coefficient D and average Trp Cys distances r were calculated, which have been shown in Figure 4.3c, d.

The analysis shows that at like higher temperature ($T=40^\circ\text{C}$) the aggregation reducing mutations V74E and T72P expands the chain at least 2 fold, and the distance between Trp39 and Cys69 increases by more than 20 \AA . Also, the slowing down of diffusion with temperature which was seen in the wild type is completely prevented; instead compared to the Y39W/A69C loop, the diffusion at $T=40^\circ\text{C}$ increases by almost 50 times for the V74E mutant and 30 times for the T72P mutant. Proline is known to stiffen the chain and that may be attributed to the relatively slower diffusion measured for the T72P compared to V74E [19]. This huge increase in diffusion

seen in the aggregation reducing mutants, translates into 10 times higher reconfiguration at $T=40^{\circ}\text{C}$. Because the reconfiguration rate ($\sim 10^6\text{s}^{-1}$) is much higher than bimolecular diffusion rate ($\sim 10^4\text{s}^{-1}$), the formation of stable bimolecular association formation is unlikely and thus aggregation is prevented. This result further corroborates our hypothesis that aggregation results from kinetic competition between reconfiguration and bimolecular association.

Because E46K and V74E mutants showed the biggest differences in chain volume and both causes change of charge in the polypeptide chain, we generated probability distributions $Z(r)$ using a previously reported model that reweights ensembles of random worm like chains to favor or disfavor conformations based on charge attraction or repulsion [28]. We started with a set of 10 million worm-like chains generated with a persistence length 4\AA and an excluded volume of 4\AA . Each chain was analyzed for non-local pair-wise interactions and assigned charge energy E_c as shown in equation 22. From these new distributions we created a contact map of average intramolecular distances between all pairs of residues. Figure 4.11 shows the difference between the maps for mutants E46K and V74E and the wildtype sequence. E46K shows significant compaction between residues 20-60 and residues 80-120 and a small expansion between the two termini of the chain. V74E shows some compaction between residues 20-60 and 100-120, though much less than for E46K and significant expansion between residues 20-80 and the C-terminus as well as expansion between residues 60-80 and 110-130. Thus the charge model predicts an overall compaction for the E46K and expansion for the V74E mutant. The extra positive charge induced by Lys46 would encourage increased intramolecular contacts with the negatively charged residues in C-terminus of α -synuclein, which could lead to compaction, while in the wildtype Glu46 is likely to repel the C-terminus. Similarly, Glu74 instead of uncharged Val in the NAC region would strongly disfavor contacts between the NAC region and

the negatively charged C-terminus region, which could open up the chain as we have measured. However, electrostatics alone may be insufficient to explain the chain dynamics, because the measured chain compaction or expansion clearly varies with temperature, which cannot be explained by charge effects. That's where hydrophobic effects come into play, and because Val74 to Glu74 transition involves replacement of a hydrophobic residue by a polar one, it could further expand chain by decreasing intramolecular contacts between hydrophobic residues of the NAC region with those in other parts of the chain.

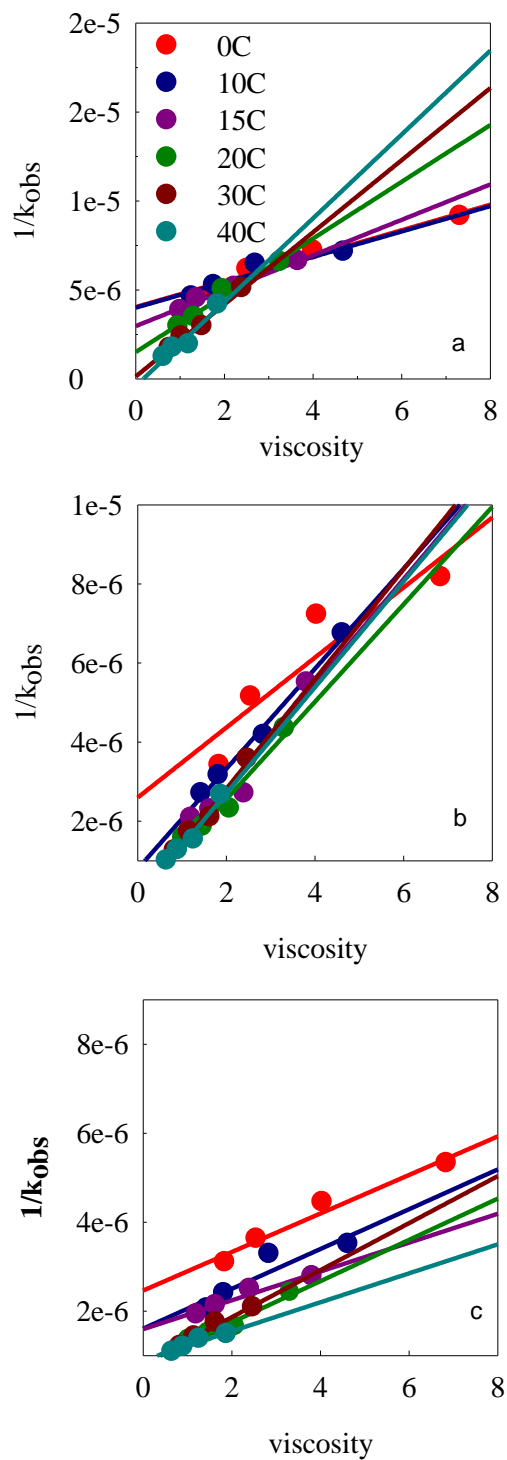


Figure 4.1 ($1/k_{obs}$) versus viscosity at pH 7.5, at various temperatures as marked, for α -synuclein a) Y39W-A69C loop in the wild type sequence b) A53T mutant c) V74E mutant. Protein concentration=30 μ M.

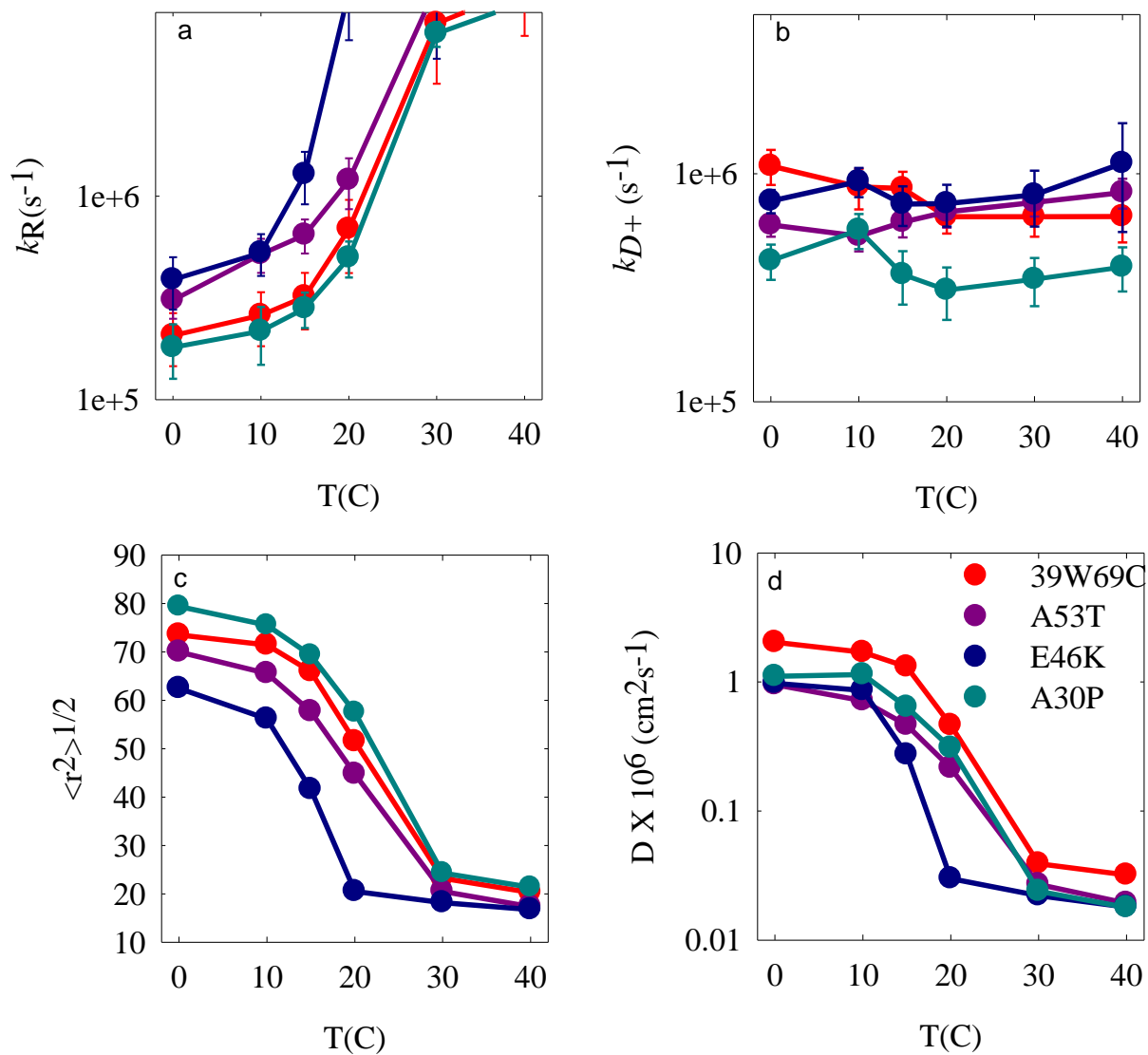


Figure 4.2 Effects of Aggregation-Enhancing, PD-Causing, Familial Mutations (A53T, E46K, and A30P). a) Reaction-limited rates. b) Diffusion-limited rates, normalized to the viscosity at water at that temperature. c) Average root mean square distance between W39 and C69 determined from reaction-limited rates d) Intramolecular diffusion coefficients determined for each diffusion-limited rate.

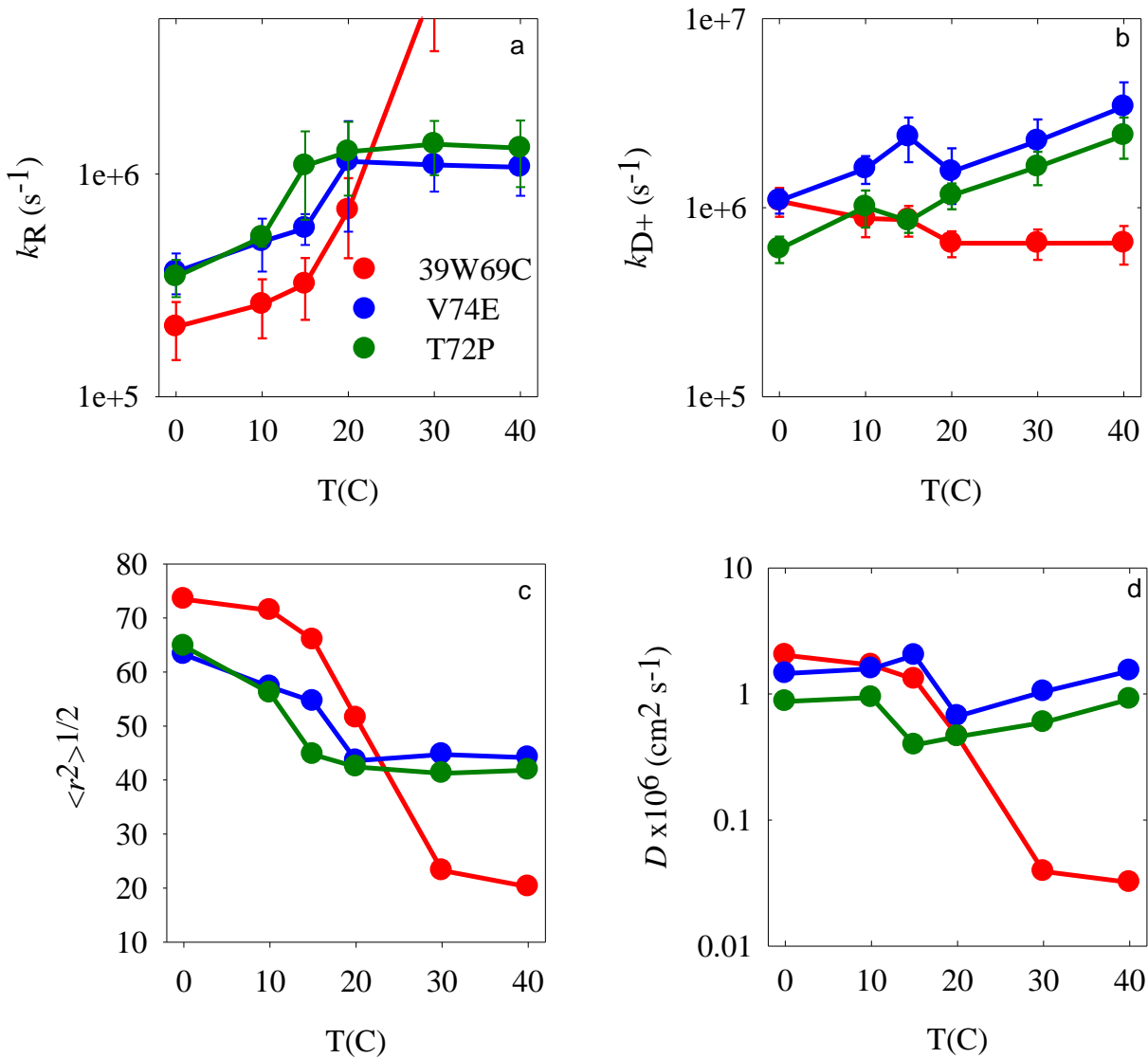


Figure 4.3 Effects of Aggregation Reducing Mutations (V74E and T72P). a) Reaction-limited rates. b) Diffusion-limited rates, normalized to the viscosity of water at that temperature. c) Average root mean square distance between W39 and C69 determined for each reaction-limited rate d) Intramolecular diffusion coefficients determined for each diffusion-limited rate.

4.9 Effect of Inhibitors on Reconfiguration

Several natural inhibitors of α -synuclein aggregation have been reported previously. The most common class of compounds that have exhibited neuroprotective effects belong to the class of polyphenolic compounds called flavonoids. They are found abundantly in a wide range of fruits, vegetables, and beverages like tea, red wine, etc. In humans the daily intake of such flavonoids can range from 50 to 800 mg depending on diet, and may well exceed that of other dietary antioxidants like vitamin C, E and carotenoids [149]. Therefore their role in prevention of neurodegeneration has been a subject of much interest.

One such compound is quercetin derived from different kinds of berries, red and yellow onions, tea, wine, apples, buckwheat and beans [150]. It has been studied extensively for its beneficial antioxidant properties. Oxidative stress has been reported to be a major risk factor for dopamine cell degeneration in PD and reportedly causes increased aggregation of α -synuclein *in vitro* [151]. Dopamine which is a principal neurotransmitter in the substantia nigra, generates free radicals during normal metabolism. Excessive accumulation of reactive oxygen species (ROS) produced in the brain is considered as an important factor that drives neuronal losses and dysfunction, leading to neurodegeneration. Natural antioxidants have been widely recognized as free radical scavenger, which can destroy ROS and prevent the progression of neurodegenerative diseases. However, the recent studies have shown that the covalent binding of quercetin to monomeric α -synuclein and not its redox properties is what makes it a strong candidate for fight against neurodegeneration [149]. One such study revealed that pre-incubated, oxidized quercetin caused stronger inhibition of α -synuclein fibrillation, compared to freshly prepared quercetin. Therefore the antioxidant activity which is the strongest in the freshly prepared quercetin is not the main cause for inhibition of α -synuclein aggregation. Similarly, another flavonoid baicalein,

derived from Chinese herbal medicine *Scutellaria baicalensis*, inhibits α -synuclein fibril formation and disaggregates existing fibrils more efficiently in its oxidized form [152]. Binding studies have revealed that baicalein binds strongly to α -synuclein with a $K_d \sim 500\text{nM}$, and covalently modifies the protein molecules, possibly modulating the aggregation pathway. However the molecular mechanism of how they were able to prevent α -synuclein aggregation is not known. And the more important question is, are they able to prevent aggregation early enough? Existing studies have reported their ability to prevent late stage aggregation, but there is no information if they are able to prevent the smallest aggregates, such as dimers or trimers.

Figure 4.4b shows the $1/k_{obs}$ versus viscosity plot at various temperatures when equimolar concentration of inhibitor baicalein (oxidized) was added to the F94W/A69C loop of α -synuclein. Quercetin (oxidized) also shows similar trend (raw data not shown). Compared to the protein in absence of any inhibitor, the change in slope with temperature is much more moderate. The intercepts also increase and don't change as much, when inhibitors were added. Figure 5a shows the comparison of reaction limited rates of protein alone with that of inhibitors quercetin and baicalein added. Under aggregating conditions, that is higher temperatures, the drastic increase in k_R which is normally seen in α -synuclein, is completely suppressed by the inhibitors, instead the k_R values becomes much smaller as a result of adding the inhibitors. Figure 4.5b shows the comparison of measured diffusion limited rates at all temperatures. Using Gaussian distribution as $P(r)$ in equation 10, the diffusion coefficient D and average Trp Cys distances r were calculated, which have been shown in Figure 4.5c, d.

The analysis shows that at all temperatures, the inhibitors expand the chain and increase diffusion of the polypeptide chain. The effect is especially pronounced under aggregation condition such as high temperature, when α -synuclein enters the dangerous regime of diffusion,

and the likelihood of aggregation increases. At $T=40^{\circ}\text{C}$, addition of inhibitor baicalein increases diffusion of α -synuclein by almost 40 times and the chain expands more than 2 fold, with a 30\AA expansion. Quercetin on the other hand increases diffusion 30 times at $T=40^{\circ}\text{C}$ and expands the chain as much as baicalein. The oxidized products of these inhibitors, reduce their antioxidant activities, but increase their polarity and hydrogen binding capacity [149]. When bound to monomeric α -synuclein, the inhibitor increases hydrophilicity of the chain, making it more hydrated and thus expanding the chain. Also increased hydrogen bonding capacity of the oxidized form may encourage the formation of local hydrogen bonds with α -synuclein, thus disrupting long range interactions, and making the chain bigger and more flexible. The reconfiguration of inhibitor baicalein is $3.4 \times 10^6 \text{s}^{-1}$ and that of quercetin is $2.8 \times 10^6 \text{s}^{-1}$ at $T=40^{\circ}\text{C}$. Since the reconfiguration rate is greater than the bimolecular diffusion rate, bimolecular association is highly unlikely. Even if the encounter complex forms out of two aggregation competent conformations, fast reconfiguration would allow one or both the conformations to reconfigure back to an innocuous conformation, thus preventing stable bimolecular association formation.

4.10 Molecule that Slows Down Reconfiguration

Figure 4.4c shows the $1/k_{obs}$ versus viscosity plot at various temperatures when polyphenol epigallocatechin galleate (EGCG) was added to the F94W/A69C loop of α -synuclein. Surprisingly, compared to the wild-type, the slope changes much more drastically, and the intercepts at each temperature decreases significantly, reaching close to zero, like it was observed in the case of the aggregation enhancing familial mutations. Figure 4.6(a,b) shows the

reaction and diffusion limited rates of the polypeptide chain respectively, at different concentrations of EGCG added. Figure 4.6(c,d) shows the average distances between Cys69 and Trp94 and the diffusion coefficients respectively, obtained using Gaussian analysis, with and without the inhibitor. Interestingly, we find that when equimolar concentration of EGCG was added, the diffusion increases slightly, and the chain volume remains unchanged, especially at higher temperatures. But at 5-times higher concentration of EGCG, the effect is pronounced and k_R increases drastically, at all temperatures, compared to when no inhibitor was added. At $T=30^\circ\text{C}$ and 40°C , the intercept of $1/k_{obs}$ versus viscosity plot becomes 0 within error (shown in figure 4.4c). The k_R values at those temperatures approach infinity and cannot be reasonably determined. Therefore we report the lower end of the error values as k_R at those temperatures, and use that to calculate the chain volume and diffusion constant. At higher concentrations of EGCG, the chain volume is collapsed and diffusion slows down, which results in decreased reconfiguration, nearing that of bimolecular diffusion. Therefore our measurements predict that at equimolar concentrations of EGCG, the polypeptide chain behaves little better than the wildtype and reconfiguration is slightly faster, but at higher concentrations it slows down reconfiguration of α -synuclein into the dangerous regime where bimolecular association is more likely and thus making it more prone to aggregation.

Our measurements are in agreement with previously reported studies [153][154]. Reportedly EGCG prevents fibril formation of α -synuclein at equimolar concentrations, relative to the protein, as observed by decrease of ThT fluorescence signal to $\sim 10\%$ of that observed when no EGCG was added. This effect is also caught in our measurements, where we observe the reconfiguration becoming slightly faster than the protein without the inhibitor. However, this increase in reconfiguration is nothing drastic, unlike observed in the case of inhibitors quercetin

and baicalein, merely 2 times faster than when no inhibitor was added, so it's still not convincingly out of the dangerous regime. Previous studies have also reported that at higher concentrations of EGCG, structured aggregates like fibrils is largely prevented but there is the sudden appearance of unstructured spherical oligomers, which are caught by EM studies. Our measurements show that at higher concentrations, the reconfiguration of α -synuclein is slowing down, causing it to enter the dangerous regime where the chain can easily form stable bimolecular associations. This may be facilitating the formation of the new oligomers and hence EGCG is modulating the aggregation pathway from fibrils to oligomers. These studies have concluded that these oligomers are non-toxic in nature, and hence EGCG may be successful in combating the harmful effects of α -synuclein aggregation in association with PD. However, these detected non-toxic oligomers were mostly higher order aggregates, which leave open the more important question of whether EGCG can prevent the formation of the smaller hard-to - detect toxic aggregates like dimers. Our results predict that EGCG, which is slowing down reconfiguration and encouraging bimolecular associations, may not be an ideal aggregation inhibitor. It is however possible that it combats α -synuclein induced toxicity in cells, by some other mechanism and not by virtue of remodeling the aggregation pathway.

Of the polyphenolic inhibitors tested so far quercetin and baicalein have given positive results, but the problem with using them as inhibitors is that even though binding studies show that they bind to α -synuclein, it is not known exactly where they bind. However, specific binding is an important issue when it comes to choosing drug candidates, and that is what led to a very interesting molecule, called CLR01, also referred to as molecular tweezer (MT). Figure 4.8 shows the artificially generated molecular structure of MT, which displays an exceptionally high affinity for amino acid lysine (Dissociation constant~200 μ M in neutral phosphate buffer) [155].

It comprises of an electron-rich cavity with two anionic phosphonate groups, which facilitates strong binding of lysine by locking the amino acid side chain through the cavity and subsequent locking by formation of phosphonate-ammonium salt bridge, as predicted using NMR by and Monte Carlo simulations. Thus the Lys butene group (C_4H_8) group is strongly threaded into the cavity, stabilized by electrostatic and Vander Waals interactions. Lysine residues are attractive targets since they are often involved in stabilizing long-range electrostatic interactions, disruption of which may bring about changes in aggregation behavior of the amyloidogenic proteins. Lysine specific MTs have been reported to prevent aggregation of many proteins, including α -synuclein, but the molecular mechanisms behind such behavior was not known and also the question of whether it can prevent early aggregation was open.

4.11 Molecular Tweezer

Figure 4.4a shows the $1/k_{obs}$ versus viscosity plot at various temperatures when equimolar concentration of MT was added to the F94W/A69C loop of α -synuclein. It shows that the change in slope with temperature is almost completely wiped out, and also the intercepts increase considerably, which yields much smaller k_R values compared to when no inhibitor was added. Figure 4.7a shows that at all temperatures the reaction limited rates decrease in a concentration dependant manner with the increase in MT concentration, and at higher ratios there is an order of magnitude difference in k_R values of α -synuclein. Figure 4.7b shows the diffusion limited rates with and without the MT. Using Gaussian distribution as $P(r)$ in equation 10, the diffusion coefficient D and average Trp Cys distances r were calculated, which have been shown in Figure 4.7c, d. The analysis shows that MT increases the diffusion of α -synuclein and also

expands the chain volume in a concentration dependant manner, as seen by increase in measured diffusion coefficient and the average distances between Trp94 and Cys69 positions. At T=30 and 40°C, the chain expands more than 3 fold and increase of diffusion is almost 50 times when equimolar concentrations or higher MT was added to α -synuclein. That results in a reconfiguration rate which is 10 times higher than the bimolecular diffusion rate of α -synuclein, which would make stable bimolecular association formation highly unlikely and thus aggregation is prevented.

α -synuclein has 15 lysine residues, and CLR01 binding site is located in the region spanning residues 10-20, most likely at Lys10 and or Lys12 which was determined by mass spectrometry [92]. There is fairly strong binding observed between α -synuclein and the MT with K_D values ranging from 10^{-7} to 10^{-4} M, as determined by binding studies done by monitoring Trp94 fluorescence with increasing concentrations of MT added to a fixed concentration of protein ($\sim 1\mu\text{M}$). Binding of MT to α -synuclein causes blue-shift of Trp94 and also increases the total fluorescence, as shown in Figure 4.9. This suggests that the Trp is becoming more sequestered from surrounding molecules, but the fact that Trp is becoming less solvent exposed does not necessarily guarantee compaction, as we showed in our measurements of k_R .

However a still unanswered question is exactly how CLR01, when bound to one or two Lys in α -synuclein, increases the reconfiguration rate. While bound, CLR01 changes the charge on Lys from +1 to -1 because each CLR01 molecule has two charged phosphate groups, so the addition of each CLR01 further decreases the net charge of the protein, which under physiological conditions is -9. It has been reported previously that there is a possible phase transition from a disordered globule to a swollen coil as the fraction of positively or negatively charged residues increases while mean hydrophathy remains constant [156] and that the pattern of

charges in the sequence affects the size of the chain significantly [157]. The charged Lys residues located throughout the first 100 residues in the sequence of α -synuclein likely preferentially associate with the multiple negatively charged residues, mostly located in the C-terminus, thus creating many close associations between distant residues in the α -synuclein sequence. With CLR01 bound, -1 charged Lys may prefer association with positively charged Lys or Arg residues nearby, creating close associations among residues located closer to each other in the sequence. Presumably, these local associations lead to conformations that are less compact and more diffusive.

Since MT binds to Lys10 and Lys12 causing a charge reversal of +1 to -1, a mimic of MT binding to α -synuclein can be performed by simple reversal of charge in those two residues in the sequence, which can be used to study the effects of MT binding to α -synuclein. Therefore, we reversed the charge on these residues and calculated Ee to compare with unbound α -synuclein, assuming that the hydrophathy remains unchanged on CLR01 binding to α -synuclein. Fig. 4.10 shows the re-weighted probability distributions for α -synuclein alone or with CLR01 bound to Lys10 and Lys12. As each CLR01 molecule binds to one or both residues, interestingly the distribution shifts to larger r , thus predicting that the chain becomes bigger, which matches our measured decrease in k_R . Contact maps that plots average intramolecular distances have predicted significantly closer contacts between N-terminal and C-terminal regions of α -synuclein (residues 1-40 and 120-140) than random coil. These close contacts are inhibited upon binding of the first CLR01 molecule, and decreases further upon binding of the second CLR01 [92].

To achieve quantitative agreement between the model and experiment, the tuning parameters σ and γ were adjusted such that the measured reaction limited rate is correctly predicted by Equation 20. First, γ was determined by adjusting the ratio of the calculated

reaction-limited rates for 1 and 2 CLR01 bound to match the measured ratio. Then σ was adjusted to match the absolute rates for those sequences. The best fit for these parameters is given by $\gamma=20$ and $\sigma=0.25$ and the rates have been plotted in Figure 4.10.

This model suggests that α -synuclein behaves as a random chain restrained by both repulsive and attractive interactions (excluded volume repulsion, hydrophobic attraction, and charge repulsion and attraction). Disruption of this balance of interactions, in this case by reversing the charge on certain residues, substantially changes the ensemble properties and therefore the dynamics. A more expanded chain is more diffusive and therefore more likely to avoid bimolecular association and subsequent oligomerization. CLR01 binds to α -synuclein and prevents its aggregation by perturbing key hydrophobic and electrostatic interactions, resulting in a concentration dependant increase of reconfiguration rate of the protein.

Our results predict that MT can be a potential drug candidate for fighting neurodegenerative diseases like PD. Previous reports suggest that MT inhibits α -synuclein aggregation by inhibiting fibril formation and disaggregation of preformed fibrils. The compound also completely blocked α -synuclein toxicity in cell lines, when α -synuclein was either overexpressed or exogenously added. Also, in a zebrafish model MT successfully combated neurotoxicity induced by α -synuclein, reducing neuronal apoptosis, improving abnormal phenotype and extending survival [158]. Using radio-labeled version of the compound, it was found that MT crosses the blood brain barrier and 1-month treatment resulted in the decrease of protein aggregates in the brain of mice, protection of neurons and reversal of disease progression, suggesting that this compound may actually be a breakthrough find in the fight against neurodegenerative diseases [159].

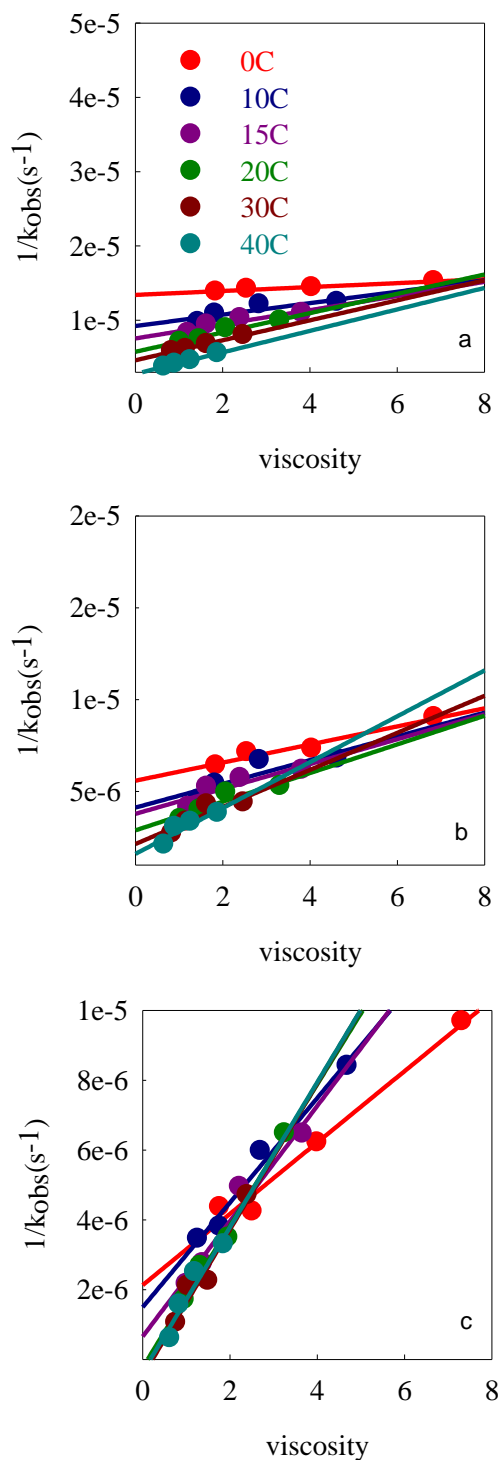


Figure 4.4 ($1/k_{obs}$) versus viscosity at pH 7.5, at various temperatures for inhibitor with α -synuclein Y39W-A69C loop a) Molecular tweezer, CLR01 b) inhibitor Baicalein c) inhibitor EGCG. Protein concentration= $30 \mu M$.

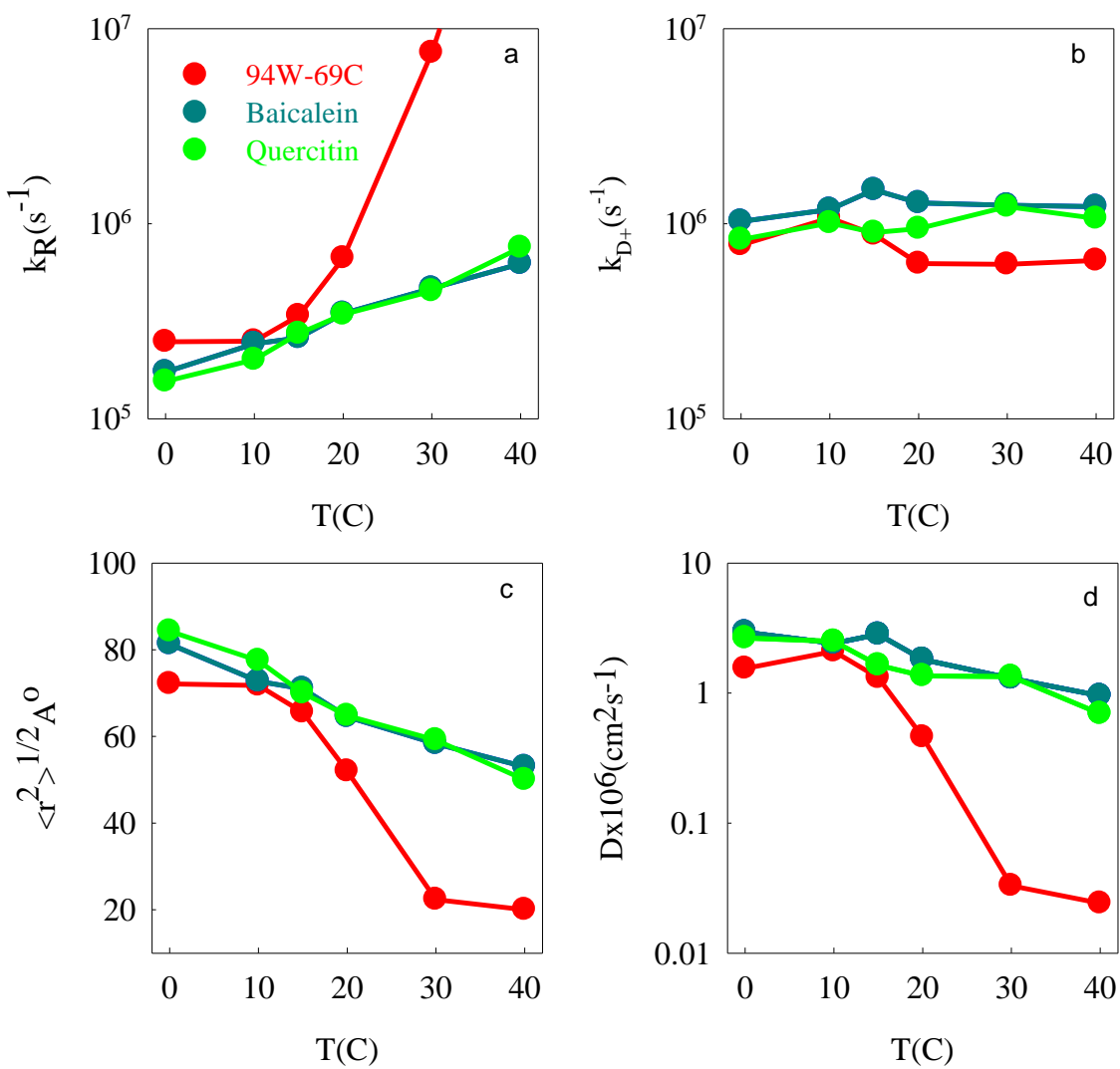


Figure 4.5 Effects of Natural Inhibitors on α -synuclein. a) Reaction-limited rates. b) Diffusion-limited rates, normalized to the viscosity of water at that temperature. c) Average root mean square distance between W94 and C69, determined from the reaction-limited rates d) Intramolecular diffusion coefficients determined from diffusion-limited rates.

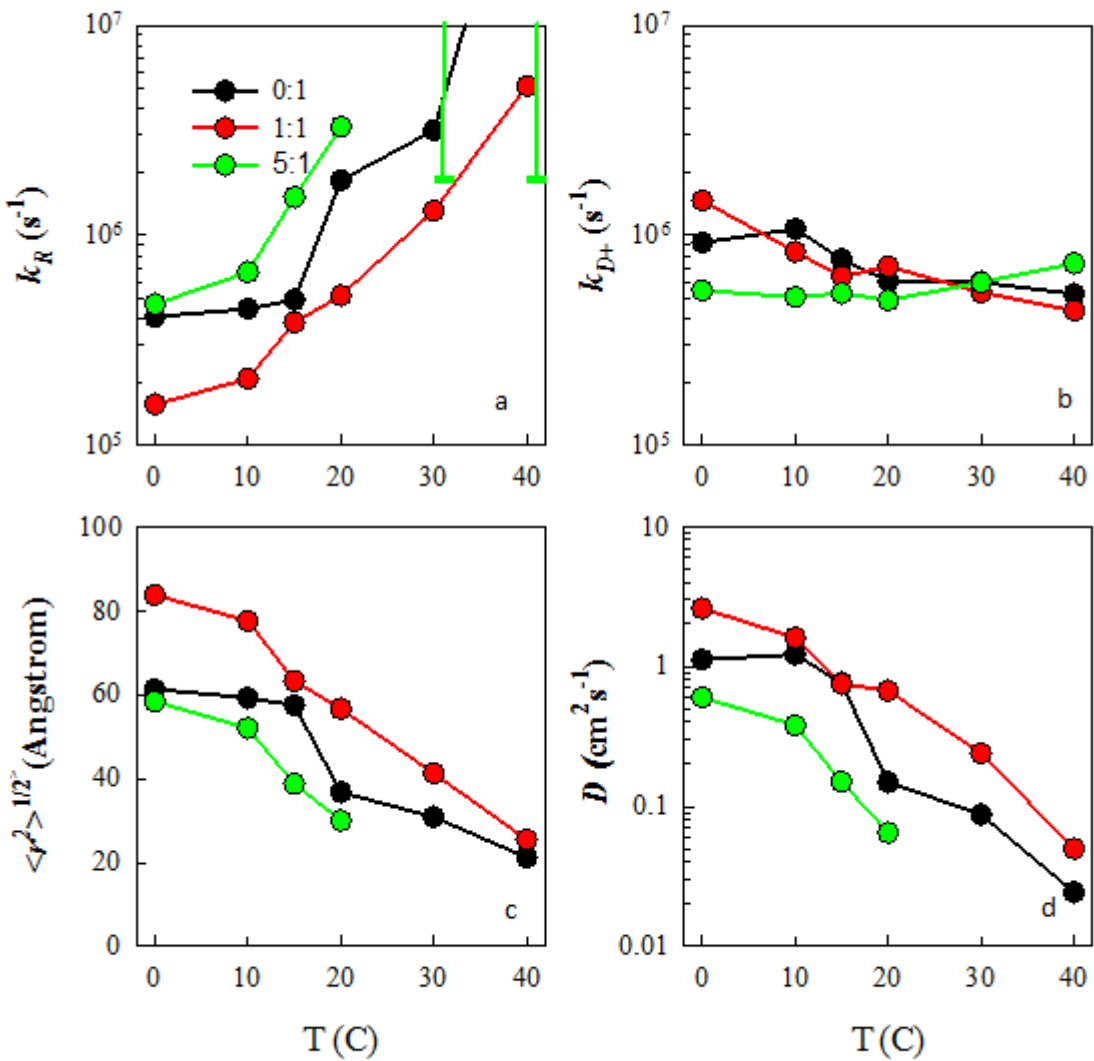


Figure 4.6 Effect of EGCG on α -synuclein. a) Reaction-limited rates. b) Diffusion-limited rates, normalized to the viscosity of water at that temperature. c) Average root mean square distance between W94 and C69, determined from the reaction-limited rates d) Intramolecular diffusion coefficients determined from diffusion-limited rates.

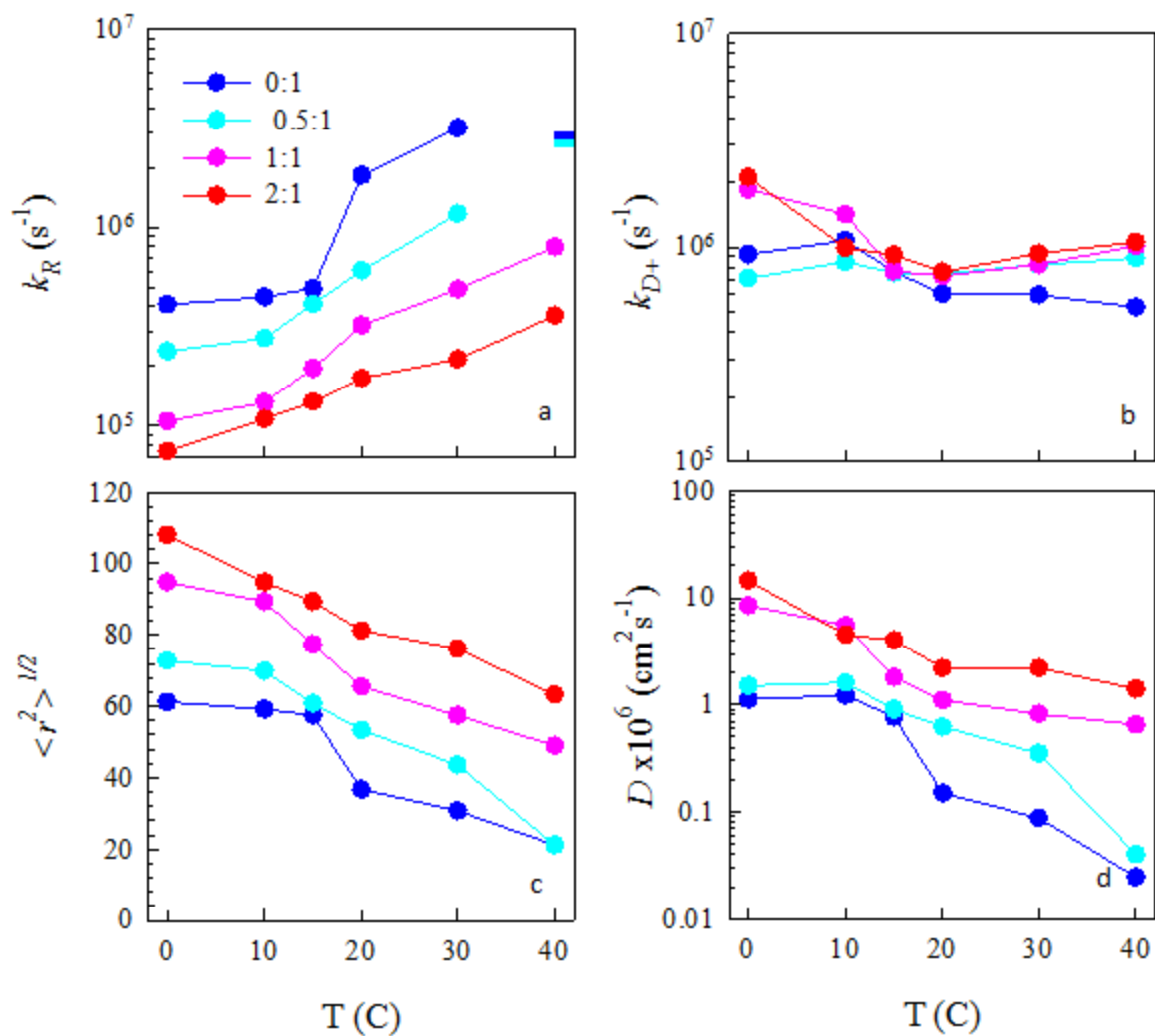


Figure 4.7 Concentration dependant effect of Molecular Tweezer on α -synuclein. a) Reaction-limited rates. b) Diffusion-limited rates, normalized to the viscosity of water at that temperature. c) Average root mean square distance between W94 and C69, determined from the reaction-limited rates d) Intramolecular diffusion coefficients determined from diffusion-limited rates.

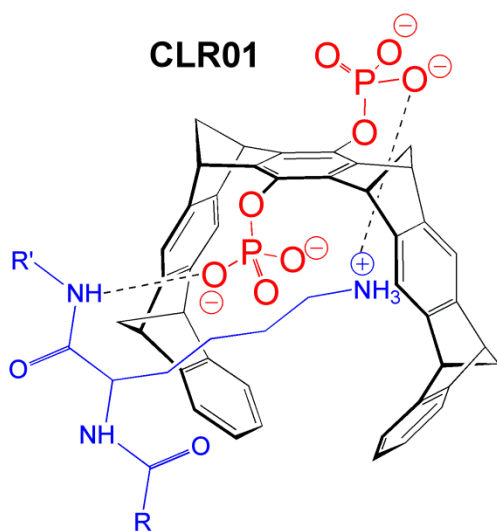


Figure 4.8 Molecular Tweezer CLR01 molecule

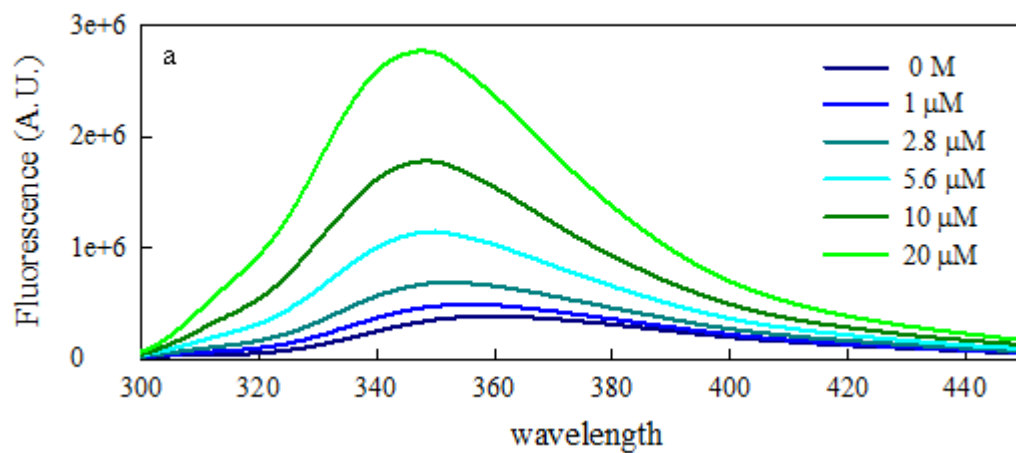


Figure 4.9 Effect of binding of CLR01 on Trp94 fluorescence of α -synuclein. Protein concentration was fixed at 1 μ M and the CLR01 concentration was gradually increased.

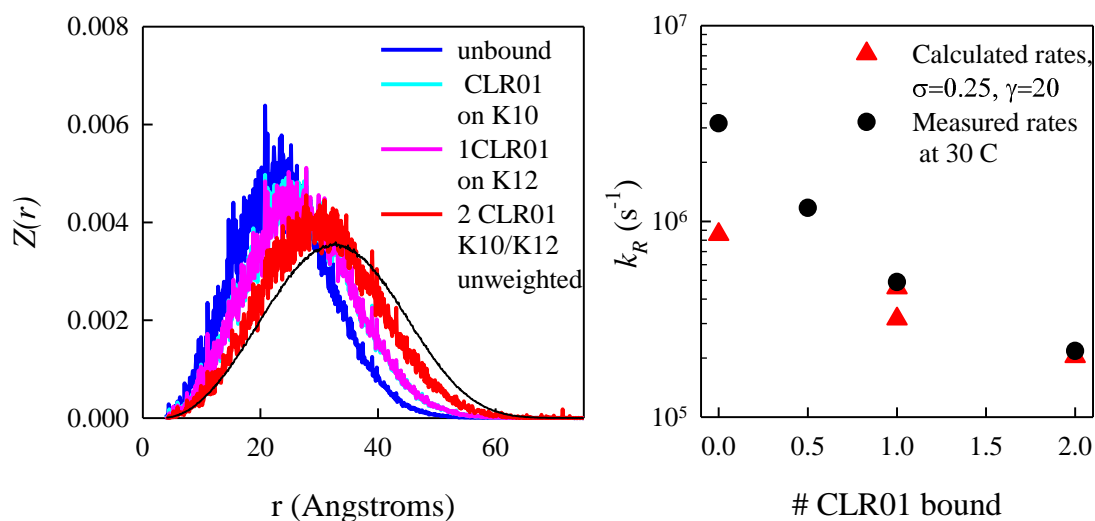


Figure 4.10 Calculated effect of CLR01 binding on α -synuclein conformation. a) Re-weighted probability distributions, $Z(r)$, for $\sigma = 0, \gamma = 20$ for α -synuclein alone (blue), α -synuclein with one CLR01 bound at Lys10 (cyan), one CLR01 bound at Lys12 (magenta), and α -synuclein bound to two CLR01 molecules in positions 10 and 12 (red). In each case, the bound CLR01 are approximated by Lys→Glu substitutions. b) Calculated (red triangles) reaction-limited rates using Eq. 9 and the probability distributions calculated in (a). The measured reaction-limited rates are plotted as black circles.

Table 4.1 Parameters obtained from Gaussian analysis for aggregation prone mutations

Peptide	Temperature °C	Diffusion Coefficient D (cm^2/s)	Average Trp-Cys distance (\AA)	Reconfiguration (s^{-1})
Y39W/A69C	0	2×10^{-6}	73	3.8×10^6
A53T	0	9.5×10^{-7}	70	1.9×10^6
E46K	0	9.6×10^{-7}	63	2.5×10^6
A30P	0	1×10^{-6}	79	1.75×10^6
Y39W/A69C	40	3.2×10^{-8}	21	7.8×10^5
A53T	40	1.5×10^{-8}	17	5×10^5
E46K	40	1.4×10^{-8}	16	5×10^5
A30P	40	1.8×10^{-8}	21	4×10^5

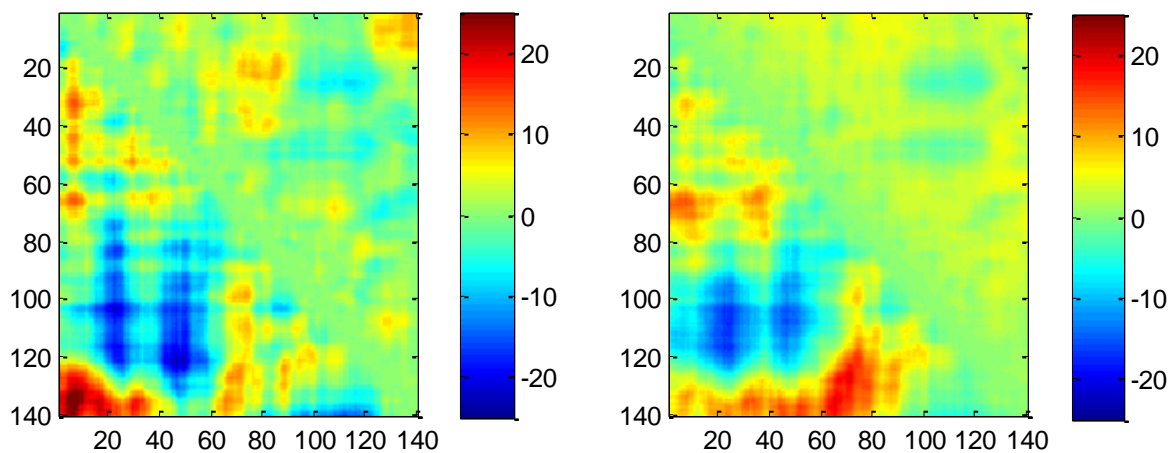


Figure 4.11 Intramolecular contact plots a) E46K and b) V74E. Each plot is the difference between the mutant and the wildtype sequence. The average distance is calculated from the reweighted ensembles using Eqs. 6 and 7 for $\gamma=9$.

Chapter 5

Conclusion

Protein aggregation is a complex process which has been linked to several neurodegenerative diseases like Alzheimer's and Parkinson's. The big challenge associated with treating these diseases is that by the time people go to the doctor the aggregation process has already spread all over their brain, killing a big chunk of the brain cells. It is almost impossible to control disease progression at this stage. The biochemical changes associated with the disease happen within the body at least a decade before actual symptoms occur. Therefore in order to treat these diseases it is really important to catch aggregation in its early stages. That was the primary motivation behind developing this novel biophysical technique, which can predict the early aggregation propensity of any sequence. Existing screening methods test inhibitors on their ability to prevent higher order aggregates, because most assays can detect aggregates only beyond a certain size. Since our technique probes the first stage in aggregation of proteins, it can be applied towards identifying inhibitors that prevent bimolecular association of proteins. Inhibitors that arrest early aggregation can be good drug candidates for neurodegenerative diseases.

Within the crowded cellular environment, the proteins are always colliding against each other, but not always do they end up sticking together. This model postulates that the speed at which they collide is very crucial and controls whether they make stable associations. Reconfiguration can be imagined as the measure of how fast a sequence is changing its shape with time and if a sequence changes shape faster than its ability to make bimolecular associations, it can escape making stable contact with another sequence. This escape by

reconfiguration is the salient feature of this model and gives it an edge over all other aggregation models proposed to date.

Based on my measurements, this model successfully predicts and explains why $A\beta_{42}$ is more aggregation prone than $A\beta_{40}$ peptide. The latter reconfigures much faster, and hence can easily escape making stable associations while the former ends up making stable intermolecular contacts more often. That would explain why senile plaques derived from postmortem Alzheimer's brain shows the presence of large amounts of $A\beta_{42}$ aggregates. Reconfiguration also emerges as a key factor that decides whether a mutation is good or bad. The familial mutant proteins that cause PD, reconfigure much slower compared to the wildtype, making escape by reconfiguration difficult and hence are much more likely to aggregate. On the other hand, mutations that prevent aggregation speed up reconfiguration thus making protein-protein interactions difficult. I further showed that reconfiguration can be moved around by varying solution conditions and also with the help of small molecule inhibitors that bind to proteins. Because reconfiguration controls early steps of aggregation of proteins, small molecule inhibitors that modulate reconfiguration to a safe regime, may be good therapeutic candidates for fighting neurodegenerative diseases like AD and PD.

However, this work leaves behind several questions unanswered, which could be the scope of future work. While this model gives a good insight into the aggregation from the dynamics point of view, the morphological aspect still remains unclear. Even though my measurements predict compact or expanded monomeric structures under different conditions, the exact structure is unknown. There is still the need to develop modern imaging techniques to observe live aggregation within cells and also to detect lowest order aggregate such as a dimer. Modern techniques such as super-resolution fluorescence imaging techniques have been

successful in capturing images of protein aggregates within the crowded cellular environment, but it was limited by resolution and could only observe fibrillar structures and higher order oligomers [160].

In the absence of structural information of lower order aggregates, we have to rely on the kinetic studies to detect protein aggregation in its early stages. That is where this aggregation model will be extremely useful. Using this model, I have successfully shown an excellent correlation between reconfiguration with that of the aggregation propensity of sequences. Therefore simply by measuring reconfiguration rate of sequences and using the aggregation model described in chapter 1, it is possible to predict the early aggregation propensity of sequences. This work further shows that it is possible to control the reconfiguration of sequences by changing the sequence length, conditions, addition of inhibitors or point mutations. By making the reconfiguration much higher than the dangerous bimolecular association regime, it is possible to rescue the protein from aggregation. This can be used as an effective strategy to screen inhibitors that can act in the beginning of the aggregation pathway, making bimolecular association difficult. Such inhibitors will be useful in fighting neurodegenerative diseases like Alzheimer's and Parkinson's disease.

BIBLIOGRAPHY

BIBLIOGRAPHY

- [1] C. B. Anfinsen, "Principles that Govern the Folding of Protein Chains," *Sci.*, vol. 181, no. 4096, pp. 223–230, Jul. 1973.
- [2] T. Mittag and J. D. Forman-Kay, "Atomic-level characterization of disordered protein ensembles," *Curr. Opin. Struct. Biol.*, vol. 17, no. 1, pp. 3–14, Feb. 2007.
- [3] S. A. Waldauer, O. Bakajin, T. Ball, Y. Chen, S. J. DeCamp, M. Kopka, M. Jäger, V. R. Singh, W. J. Wedemeyer, S. Weiss, S. Yao, and L. J. Lapidus, "Ruggedness in the folding landscape of protein L," *HFSP J.*, vol. 2, no. 6, pp. 388–395, Dec. 2008.
- [4] S. A. Waldauer, O. Bakajin, and L. J. Lapidus, "Extremely slow intramolecular diffusion in unfolded protein L," *Proc. Natl. Acad. Sci.*, vol. 107, no. 31, pp. 13713–13717, Aug. 2010.
- [5] V. A. Voelz, V. R. Singh, W. J. Wedemeyer, L. J. Lapidus, and V. S. Pande, "Unfolded-State Dynamics and Structure of Protein L Characterized by Simulation and Experiment," *J. Am. Chem. Soc.*, vol. 132, no. 13, pp. 4702–4709, Mar. 2010.
- [6] F. Chiti and C. M. Dobson, "Protein Misfolding, Functional Amyloid, and Human Disease," *Annu. Rev. Biochem.*, vol. 75, no. 1, pp. 333–366, Jun. 2006.
- [7] F. Bemporad and F. Chiti, "Protein Misfolded Oligomers: Experimental Approaches, Mechanism of Formation, and Structure-Toxicity Relationships," *Chem. Biol.*, vol. 19, no. 3, pp. 315–327, Mar. 2012.
- [8] M. Sandal, F. Valle, I. Tessari, S. Mammi, E. Bergantino, F. Musiani, M. Brucale, L. Bubacco, and B. Samorì, "Conformational Equilibria in Monomeric α -Synuclein at the Single-Molecule Level," *PLoS Biol.*, vol. 6, no. 1, p. e6, Jan. 2008.
- [9] L. F. Pease III, M. Sorci, S. Guha, D.-H. Tsai, M. R. Zachariah, M. J. Tarlov, and G. Belfort, "Probing the Nucleus Model for Oligomer Formation during Insulin Amyloid Fibrillogenesis," *Biophys. J.*, vol. 99, no. 12, pp. 3979–3985, Jul. 2014.
- [10] J. Lee, E. K. Culyba, E. T. Powers, and J. W. Kelly, "Amyloid- β forms fibrils by nucleated conformational conversion of oligomers," *Nat Chem Biol.*, vol. 7, no. 9, pp. 602–609, Sep. 2011.
- [11] T. R. Jahn and S. Radford, "Folding versus aggregation: Polypeptide conformations on competing pathways," *Arch. Biochem. Biophys.*, 2008.

- [12] C. M. Osowski and F. Urano, "Chapter Four - Measuring ER Stress and the Unfolded Protein Response Using Mammalian Tissue Culture System," in *The Unfolded Protein Response and Cellular Stress, Part B*, vol. Volume 490, P. M. C. B. T.-M. in Enzymology, Ed. Academic Press, 2011, pp. 71–92.
- [13] P. Walter and D. Ron, "The Unfolded Protein Response: From Stress Pathway to Homeostatic Regulation," *Sci.*, vol. 334, no. 6059, pp. 1081–1086, Nov. 2011.
- [14] V. N. Uversky, J. R. Gillespie, and A. L. Fink, "Why are 'natively unfolded' proteins unstructured under physiologic conditions?," *Proteins Struct. Funct. Bioinforma.*, vol. 41, no. 3, pp. 415–427, 2000.
- [15] V. N. et al Uversky, "Unfoldomics of human diseases: linking protein intrinsic disorder with diseases," 2008.
- [16] V. N. Uversky, "Intrinsically disordered proteins from A to Z," *Int. J. Biochem. Cell Biol.*, vol. 43, no. 8, pp. 1090–1103, Aug. 2011.
- [17] L. J. Lapidus, "Understanding protein aggregation from the view of monomer dynamics," *Mol. BioSyst.*, vol. 9, no. 1, pp. 29–35, 2013.
- [18] B. Ahmad, Y. Chen, and L. J. Lapidus, "Aggregation of α -synuclein is kinetically controlled by intramolecular diffusion," *Proc. Natl. Acad. Sci.*, vol. 109, no. 7, pp. 2336–2341, Feb. 2012.
- [19] L. J. Lapidus, W. A. Eaton, and J. Hofrichter, "Measuring the rate of intramolecular contact formation in polypeptides," *Proc. Natl. Acad. Sci.*, vol. 97, no. 13, pp. 7220–7225, Jun. 2000.
- [20] J. Vanderkooi, "Tryptophan Phosphorescence from Proteins at Room Temperature," in *Topics in Fluorescence Spectroscopy SE - 3*, vol. 3, J. Lakowicz, Ed. Springer US, 2002, pp. 113–136.
- [21] L. J. Lapidus, W. A. Eaton, and J. Hofrichter, "Dynamics of Intramolecular Contact Formation in Polypeptides: Distance Dependence of Quenching Rates in a Room-Temperature Glass," *Phys. Rev. Lett.*, vol. 87, no. 25, p. 258101, Nov. 2001.
- [22] R. R. Cheng, T. Uzawa, K. W. Plaxco, and D. E. Makarov, "The Rate of Intramolecular Loop Formation in DNA and Polypeptides: The Absence of the Diffusion-Controlled Limit and Fractional Power-Law Viscosity Dependence," *J. Phys. Chem. B*, vol. 113, no. 42, pp. 14026–14034, 2009.
- [23] E. Amouyal, A. Bernas, and D. Grand, "ON THE PHOTOIONIZATION ENERGY THRESHOLD OF TRYPTOPHAN IN AQUEOUS SOLUTIONS," *Photochem. Photobiol.*, vol. 29, no. 6, pp. 1071–1077, Jun. 1979.

- [24] A. Szabo, K. Schulten, and Z. Schulten, "1st Passage Time Approach to Diffusion Controlled Reactions," *J. Chem. Phys.*, vol. 72, no. 8, pp. 4350–4357, 1980.
- [25] L. J. Lapidus, P. J. Steinbach, W. A. Eaton, A. Szabo, and J. Hofrichter, "Effects of Chain Stiffness on the Dynamics of Loop Formation in Polypeptides. Appendix: Testing a 1-Dimensional Diffusion Model for Peptide Dynamics," *J. Phys. Chem. B*, vol. 106, no. 44, pp. 11628–11640, 2002.
- [26] V. R. Singh, M. Kopka, Y. Chen, W. J. Wedemeyer, and L. J. Lapidus, "Dynamic Similarity of the Unfolded States of Proteins L and G^{†,‡}," *Biochemistry*, vol. 46, no. 35, pp. 10046–10054, 2007.
- [27] J. E. Kohn, I. S. Millett, J. Jacob, B. Zagrovic, T. M. Dillon, N. Cingel, R. S. Dothager, S. Seifert, P. Thiyagarajan, T. R. Sosnick, M. Z. Hasan, V. S. Pande, I. Ruczinski, S. Doniach, and K. W. Plaxco, "Random-coil behavior and the dimensions of chemically unfolded proteins," *Proc. Natl. Acad. Sci. United States Am.*, vol. 101, no. 34, pp. 12491–12496, Aug. 2004.
- [28] Y. Chen, W. J. Wedemeyer, and L. J. Lapidus, "A General Polymer Model of Unfolded Proteins under Folding Conditions," *J. Phys. Chem. B*, vol. 114, no. 48, pp. 15969–15975, 2010.
- [29] M. M. Dedmon, K. Lindorff-Larsen, J. Christodoulou, M. Vendruscolo, and C. M. Dobson, "Mapping Long-Range Interactions in α -Synuclein using Spin-Label NMR and Ensemble Molecular Dynamics Simulations," *J. Am. Chem. Soc.*, vol. 127, no. 2, pp. 476–477, 2005.
- [30] T. W. Groemer, C. S. Thiel, M. Holt, D. Riedel, Y. Hua, J. Hüve, B. G. Wilhelm, and J. Klingauf, "Amyloid Precursor Protein Is Trafficked and Secreted via Synaptic Vesicles," *PLoS One*, vol. 6, no. 4, p. e18754, Apr. 2011.
- [31] D. J. Selkoe, "The cell biology of β -amyloid precursor protein and presenilin in Alzheimer's disease," *Trends Cell Biol.*, vol. 8, no. 11, pp. 447–453, Apr. 1998.
- [32] T. Okamoto, S. Takeda, Y. Murayama, E. Ogata, and I. Nishimoto, "Ligand-dependent G Protein Coupling Function of Amyloid Transmembrane Precursor," *J. Biol. Chem.*, vol. 270, no. 9, pp. 4205–4208, Mar. 1995.
- [33] S. L. Sabo, A. F. Ikin, J. D. Buxbaum, and P. Greengard, "The Alzheimer Amyloid Precursor Protein (APP) and Fe65, an APP-Binding Protein, Regulate Cell Movement," *J. Cell Biol.*, vol. 153, no. 7, pp. 1403–1414, Jun. 2001.
- [34] C. J. Maynard, A. I. Bush, C. L. Masters, R. Cappai, and Q.-X. Li, "Metals and amyloid- β in Alzheimer's disease," *Int. J. Exp. Pathol.*, vol. 86, no. 3, pp. 147–159, 2005.

- [35] J. Hardy and D. J. Selkoe, "The Amyloid Hypothesis of Alzheimer's Disease: Progress and Problems on the Road to Therapeutics," *Sci.*, vol. 297, no. 5580, pp. 353–356, Jul. 2002.
- [36] F. M. LaFerla, K. N. Green, and S. Oddo, "Intracellular amyloid-beta in Alzheimer's disease," *Nat Rev Neurosci*, vol. 8, pp. 499–509, 2007.
- [37] C. L. Masters, G. Simms, N. A. Weinman, G. Multhaup, B. L. McDonald, and K. Beyreuther, "Amyloid plaque core protein in Alzheimer disease and Down syndrome," *Proc. Natl Acad. Sci. USA*, vol. 82, pp. 4245–4249, 1985.
- [38] G. K. Gouras, C. G. Almeida, and R. H. Takahashi, "Intraneuronal A β accumulation and origin of plaques in Alzheimer's disease," *Neurobiology of aging*, vol. 26, no. 9. Elsevier, pp. 1235–1244, 01-Oct-2005.
- [39] M. Li, L. Chen, D. H. S. Lee, L.-C. Yu, and Y. Zhang, "The role of intracellular amyloid β in Alzheimer's disease," *Prog. Neurobiol.*, vol. 83, no. 3, pp. 131–139, Oct. 2007.
- [40] H. YAZAWA, Z.-X. YU, TAKEDA, Y. LE, W. GONG, V. J. FERRANS, J. J. OPPENHEIM, C. C. H. I. H. LI, and J. I. M. WANG, " β Amyloid peptide (A β 42) is internalized via the G-protein-coupled receptor FPRL1 and forms fibrillar aggregates in macrophages," *FASEB J.*, vol. 15, no. 13, pp. 2454–2462, Nov. 2001.
- [41] P. M. Clifford, S. Zarrabi, G. Siu, K. J. Kinsler, M. C. Kosciuk, V. Venkataraman, M. R. D'Andrea, S. Dinsmore, and R. G. Nagele, "A β peptides can enter the brain through a defective blood–brain barrier and bind selectively to neurons," *Brain Res.*, vol. 1142, no. 0, pp. 223–236, Apr. 2007.
- [42] R. E. Tanzi, R. D. Moir, and S. L. Wagner, "Clearance of Alzheimer's A β Peptide: The Many Roads to Perdition," *Neuron*, vol. 43, no. 5, pp. 605–608, Sep. 2004.
- [43] J. D. Harper and P. T. Lansbury, "MODELS OF AMYLOID SEEDING IN ALZHEIMER'S DISEASE AND SCRAPIE: Mechanistic Truths and Physiological Consequences of the Time-Dependent Solubility of Amyloid Proteins," *Annu. Rev. Biochem.*, vol. 66, no. 1, pp. 385–407, Jun. 1997.
- [44] R. Deane, R. . Bell, A. Sagare, and B. . Zlokovic, "Clearance of amyloid-beta peptide across the blood–brain barrier: implication for therapies in Alzheimer's disease," *CNS Neurol. Disord. Drug Targets*, vol. 8, pp. 16–30, 2009.
- [45] I. Grundke-Iqbal, K. Iqbal, Y. C. Tung, M. Quinlan, H. M. Wisniewski, and L. I. Binder, "Abnormal phosphorylation of the microtubule-associated protein tau (tau) in Alzheimer cytoskeletal pathology," *Proc. Natl. Acad. Sci.*, vol. 83, no. 13, pp. 4913–4917, Jul. 1986.

- [46] D. J. Selkoe, "Amyloid β -Protein and the Genetics of Alzheimer's Disease," *J. Biol. Chem.*, vol. 271, no. 31, pp. 18295–18298, Aug. 1996.
- [47] C. Haass, C. A. Lemere, A. Capell, M. Citron, P. Seubert, D. Schenk, L. Lannfelt, and D. J. Selkoe, "The Swedish mutation causes early-onset Alzheimer's disease by [beta]-secretase cleavage within the secretory pathway," *Nat Med*, vol. 1, pp. 1291–1296, 1995.
- [48] D. J. Selkoe, "The molecular pathology of Alzheimer's disease," *Neuron*, vol. 6, no. 4, pp. 487–498, Apr. 1991.
- [49] F. M. LaFerla and S. Oddo, "Alzheimer's disease: A β , tau and synaptic dysfunction," *Trends Mol. Med.*, vol. 11, no. 4, pp. 170–176, Apr. 2005.
- [50] N. B. Chauhan and G. J. Siegel, "Reversal of amyloid β toxicity in Alzheimer's disease model Tg2576 by intraventricular anti-amyloid β antibody," *J. Neurosci. Res.*, vol. 69, no. 1, pp. 10–23, 2002.
- [51] W. A. Banks, S. A. Farr, J. E. Morley, K. M. Wolf, V. Geylis, and M. Steinitz, "Anti-amyloid beta protein antibody passage across the blood–brain barrier in the SAMP8 mouse model of Alzheimer's disease: An age-related selective uptake with reversal of learning impairment," *Exp. Neurol.*, vol. 206, no. 2, pp. 248–256, Aug. 2007.
- [52] T. Nakagawa, H. Zhu, N. Morishima, E. Li, J. Xu, B. A. Yankner, and J. Yuan, "Caspase-12 mediates endoplasmic-reticulum-specific apoptosis and cytotoxicity by amyloid-[beta]," *Nature*, vol. 403, no. 6765, pp. 98–103, 2000.
- [53] V. H. FINDER and R. GLOCKSHUBER, "Amyloid- β Aggregation," *Neurodegener. Dis.*, vol. 4, no. 1, pp. 13–27, 2007.
- [54] S. T. Ferreira and W. L. Klein, "The A β oligomer hypothesis for synapse failure and memory loss in Alzheimer's disease," *Neurobiol. Learn. Mem.*, vol. 96, no. 4, pp. 529–543, Nov. 2011.
- [55] D. J. Selkoe, "Alzheimer's Disease Is a Synaptic Failure," *Sci.*, vol. 298, no. 5594, pp. 789–791, Oct. 2002.
- [56] L.-F. Lue, Y.-M. Kuo, A. E. Roher, L. Brachova, Y. Shen, L. Sue, T. Beach, J. H. Kurth, R. E. Rydel, and J. Rogers, "Soluble Amyloid β Peptide Concentration as a Predictor of Synaptic Change in Alzheimer's Disease," *The American journal of pathology*, vol. 155, no. 3. American Society for Investigative Pathology, pp. 853–862, 01-Sep-1999.
- [57] D. M. Walsh, I. Klyubin, J. V. Fadeeva, W. K. Cullen, R. Anwyl, M. S. Wolfe, M. J. Rowan, and D. J. Selkoe, "Naturally secreted oligomers of amyloid [beta] protein potently inhibit hippocampal long-term potentiation in vivo," *Nature*, vol. 416, no. 6880, pp. 535–539, 2002.

- [58] C. A. Lemere, J. K. Blusztajn, H. Yamaguchi, T. Wisniewski, T. C. Saido, and D. J. Selkoe, "Sequence of Deposition of Heterogeneous Amyloid β -Peptides and APO E in Down Syndrome: Implications for Initial Events in Amyloid Plaque Formation," *Neurobiol. Dis.*, vol. 3, no. 1, pp. 16–32, Feb. 1996.
- [59] C. A. McLean, R. A. Cherny, F. W. Fraser, S. J. Fuller, M. J. Smith, K. Vbeyreuther, A. I. Bush, and C. L. Masters, "Soluble pool of A β amyloid as a determinant of severity of neurodegeneration in Alzheimer's disease," *Ann. Neurol.*, vol. 46, no. 6, pp. 860–866, 1999.
- [60] G. M. Shankar, B. L. Bloodgood, M. Townsend, D. M. Walsh, D. J. Selkoe, and B. L. Sabatini, "Natural Oligomers of the Alzheimer Amyloid- β Protein Induce Reversible Synapse Loss by Modulating an NMDA-Type Glutamate Receptor-Dependent Signaling Pathway," *J. Neurosci.*, vol. 27, no. 11, pp. 2866–2875, Mar. 2007.
- [61] J. P. Cleary, D. M. Walsh, J. J. Hofmeister, G. M. Shankar, M. A. Kuskowski, D. J. Selkoe, and K. H. Ashe, "Natural oligomers of the amyloid- β protein specifically disrupt cognitive function," *Nat Neurosci.*, vol. 8, no. 1, pp. 79–84, 2005.
- [62] S. Lesne, M. T. AU - Koh, L. AU - Kotilinek, R. AU - Kaye, C. G. AU - Glabe, A. AU - Yang, M. AU - Gallagher, and K. H. AU - Ashe, "A specific amyloid- β protein assembly in the brain impairs memory," *Nature*, vol. 440, no. 7082, pp. 352–357, 2006.
- [63] Y. Zhang, R. McLaughlin, C. Goodyer, and A. LeBlanc, "Selective cytotoxicity of intracellular amyloid β peptide1–42 through p53 and Bax in cultured primary human neurons," *J. Cell Biol.*, vol. 156, no. 3, pp. 519–529, Feb. 2002.
- [64] S. Zhang, K. Iwata, M. J. Lachenmann, J. W. Peng, S. Li, E. R. Stimson, Y. -a. Lu, A. M. Felix, J. E. Maggio, and J. P. Lee, "The Alzheimer's Peptide A β Adopts a Collapsed Coil Structure in Water," *J. Struct. Biol.*, vol. 130, no. 2–3, pp. 130–141, Jun. 2000.
- [65] A. E. Roher, M. O. Chaney, Y.-M. Kuo, S. D. Webster, W. B. Stine, L. J. Haverkamp, A. S. Woods, R. J. Cotter, J. M. Tuohy, G. A. Krafft, B. S. Bonnell, and M. R. Emmerling, "Morphology and Toxicity of A β -(1-42) Dimer Derived from Neuritic and Vascular Amyloid Deposits of Alzheimer's Disease," *J. Biol. Chem.*, vol. 271, no. 34, pp. 20631–20635, Aug. 1996.
- [66] D. M. Walsh, B. P. Tseng, R. E. Rydel, M. B. Podlisny, and D. J. Selkoe, "The Oligomerization of Amyloid β -Protein Begins Intracellularly in Cells Derived from Human Brain†," *Biochemistry*, vol. 39, no. 35, pp. 10831–10839, Aug. 2000.
- [67] G. M. Shankar, S. Li, T. H. Mehta, A. Garcia-Munoz, N. E. Shepardson, I. Smith, F. M. Brett, M. A. Farrell, M. J. Rowan, C. A. Lemere, C. M. Regan, D. M. Walsh, B. L. Sabatini, and D. J. Selkoe, "Amyloid- β protein dimers isolated directly from Alzheimer's brains impair synaptic plasticity and memory," *Nat Med*, vol. 14, no. 8, pp. 837–842, 2008.

- [68] M. Townsend, G. Shankar, T. Mehta, D. Walsh, and D. Selkoe, “Effects of secreted oligomers of amyloid β -protein on hippocampal synaptic plasticity: a potent role for trimers,” *J Physiol*, vol. 477–492, 2006.
- [69] G. Shankar and D. Walsh, “Alzheimer’s disease: synaptic dysfunction and A β ,” *Mol. Neurodegener.*, vol. 4, no. 1, pp. 1–13, 2009.
- [70] M. Kawahara, M. Negishi-Kato, and Y. Sadakane, “Calcium dyshomeostasis and neurotoxicity of Alzheimer’s β -amyloid protein,” *Expert Rev. Neurother.*, vol. 9, no. 5, pp. 681–693, May 2009.
- [71] D. H. Small, R. Gasperini, A. J. Vincent, A. C. Hung, and L. Foa, “The Role of A β -Induced Calcium Dysregulation in the Pathogenesis of Alzheimer’s Disease,” *J. Alzheimer’s Dis.*, vol. 16, no. 2, pp. 225–233, Jan. 2009.
- [72] D. G. Georganopoulou, L. Chang, J.-M. Nam, C. S. Thaxton, E. J. Mufson, W. L. Klein, and C. A. Mirkin, “Nanoparticle-based detection in cerebral spinal fluid of a soluble pathogenic biomarker for Alzheimer’s disease,” *Proc. Natl. Acad. Sci. United States Am.* , vol. 102 , no. 7 , pp. 2273–2276, Feb. 2005.
- [73] K. E. Marshall and L. C. Serpell, “Insights into the Structure of Amyloid Fibrils,” *Open Biol. J.*, vol. 2, pp. 185–192, 2009.
- [74] T. Lührs, C. Ritter, M. Adrian, D. Riek-Loher, B. Bohrmann, H. Döbeli, D. Schubert, and R. Riek, “3D structure of Alzheimer’s amyloid- β (1–42) fibrils,” *Proc. Natl. Acad. Sci. United States Am.* , vol. 102 , no. 48 , pp. 17342–17347, Nov. 2005.
- [75] K. Irie, K. Murakami, Y. Masuda, A. Morimoto, H. Ohigashi, R. Ohashi, K. Takegoshi, M. Nagao, T. Shimizu, and T. Shirasawa, “Structure of β -amyloid fibrils and its relevance to their neurotoxicity: Implications for the pathogenesis of Alzheimer’s disease,” *J. Biosci. Bioeng.*, vol. 99, no. 5, pp. 437–447, May 2005.
- [76] T. R. Jahn, O. S. Makin, K. L. Morris, K. E. Marshall, P. Tian, P. Sikorski, and L. C. Serpell, “The Common Architecture of Cross- β Amyloid,” *J. Mol. Biol.*, vol. 395, no. 4, pp. 717–727, Jan. 2010.
- [77] K. Pauwels, T. L. Williams, K. L. Morris, W. Jonckheere, A. Vandersteen, G. Kelly, J. Schymkowitz, F. Rousseau, A. Pastore, L. C. Serpell, and K. Broersen, “Structural Basis for Increased Toxicity of Pathological A β 42:A β 40 Ratios in Alzheimer Disease,” *J. Biol. Chem.* , vol. 287 , no. 8 , pp. 5650–5660, Feb. 2012.
- [78] I. Kuperstein, K. Broersen, I. Benilova, J. Rozenski, W. Jonckheere, M. Debulpaep, A. Vandersteen, I. Segers-Nolten, K. Van Der Werf, V. Subramaniam, D. Braeken, G. Callewaert, C. Bartic, R. D’Hooge, I. C. Martins, F. Rousseau, J. Schymkowitz, and B. De Strooper, “Neurotoxicity of Alzheimer’s disease A β peptides is induced

- by small changes in the A β 42 to A β 40 ratio,” *EMBO J.*, vol. 29, no. 19, pp. 3408–3420, Sep. 2010.
- [79] J. C. Stroud, C. Liu, P. K. Teng, and D. Eisenberg, “Toxic fibrillar oligomers of amyloid- β have cross- β structure,” *Proc. Natl. Acad. Sci.*, Apr. 2012.
- [80] V. H. FINDER, I. Vodopivec, R. M. Nitsch, and R. Glockshuber, “The Recombinant Amyloid- β Peptide A β 1–42 Aggregates Faster and Is More Neurotoxic than Synthetic A β 1–42,” *J. Mol. Biol.*, vol. 396, no. 1, pp. 9–18, Feb. 2010.
- [81] R. B. Kapust, J. Tözsér, T. D. Copeland, and D. S. Waugh, “The P1' specificity of tobacco etch virus protease,” *Biochem. Biophys. Res. Commun.*, vol. 294, no. 5, pp. 949–955, 2002.
- [82] D. B. Teplow, “Preparation of Amyloid β -Protein for Structural and Functional Studies,” in *Amyloid, Prions, and Other Protein Aggregates, Part C*, vol. Volume 413, I. K. and R. W. B. T.-M. in *Enzymology*, Ed. Academic Press, 2006, pp. 20–33.
- [83] A.-M. Fernandez-Escamilla, F. Rousseau, J. Schymkowitz, and L. Serrano, “Prediction of sequence-dependent and mutational effects on the aggregation of peptides and proteins,” *Nat Biotech*, vol. 22, no. 10, pp. 1302–1306, 2004.
- [84] G. G. Tartaglia and M. Vendruscolo, “The Zyggregator method for predicting protein aggregation propensities,” *Chem. Soc. Rev.*, vol. 37, no. 7, pp. 1395–1401, 2008.
- [85] H. Levine, “Thioflavine T interaction with synthetic Alzheimer’s disease β -amyloid peptides: Detection of amyloid aggregation in solution,” *Protein Sci.*, vol. 2, no. 3, pp. 404–410, 1993.
- [86] H. Levine III, “Stopped-Flow Kinetics Reveal Multiple Phases of Thioflavin T Binding to Alzheimer β (1-40) Amyloid Fibrils,” *Arch. Biochem. Biophys.*, vol. 342, no. 2, pp. 306–316, Jun. 1997.
- [87] M. Yang and D. B. Teplow, “Amyloid β -Protein Monomer Folding: Free-Energy Surfaces Reveal Alloform-Specific Differences,” *J. Mol. Biol.*, vol. 384, no. 2, pp. 450–464, Dec. 2008.
- [88] R. P. Bora and R. Prabhakar, “Translational, rotational and internal dynamics of amyloid β -peptides (A β 40 and A β 42) from molecular dynamics simulations,” *J. Chem. Phys.*, vol. 131, no. 15, p. -, 2009.
- [89] C. Lee and S. Ham, “Characterizing amyloid-beta protein misfolding from molecular dynamics simulations with explicit water,” *J. Comput. Chem.*, vol. 32, no. 2, pp. 349–355, 2011.

- [90] A. E. Sgourakis, N. G., Yan, Y. L., McCallum, S. A., Wang, C. Y. & Garcia, “The Alzheimer’s peptides A beta 40 and 42 adopt distinct conformations in water: A combined MD/NMR study,” *J. Mol. Biol.*, vol. 368, pp. 1448–1457, 2007.
- [91] Y. Yan and C. Wang, “A β 42 is More Rigid than A β 40 at the C Terminus: Implications for A β Aggregation and Toxicity,” *J. Mol. Biol.*, vol. 364, no. 5, pp. 853–862, Dec. 2006.
- [92] S. Acharya, B. M. Safaie, P. Wongkongkathep, M. I. Ivanova, A. Attar, F.-G. Klärner, T. Schrader, J. A. Loo, G. Bitan, and L. J. Lapidus, “Molecular Basis for Preventing α -Synuclein Aggregation by a Molecular Tweezer,” *J. Biol. Chem.*, Feb. 2014.
- [93] B. Ahmad and L. J. Lapidus, “Curcumin Prevents Aggregation in α -Synuclein by Increasing Reconfiguration Rate,” *J. Biol. Chem.*, vol. 287, no. 12, pp. 9193–9199, Mar. 2012.
- [94] F. Yang, G. P. Lim, A. N. Begum, O. J. Ubeda, M. R. Simmons, S. S. Ambegaokar, P. P. Chen, R. Kaye, C. G. Glabe, S. A. Frautschy, and G. M. Cole, “Curcumin Inhibits Formation of Amyloid β Oligomers and Fibrils, Binds Plaques, and Reduces Amyloid in Vivo,” *J. Biol. Chem.*, vol. 280, no. 7, pp. 5892–5901, Feb. 2005.
- [95] Y. Masuda, M. Fukuchi, T. Yatagawa, M. Tada, K. Takeda, K. Irie, K. Akagi, Y. Monobe, T. Imazawa, and K. Takegoshi, “Solid-state NMR analysis of interaction sites of curcumin and 42-residue amyloid β -protein fibrils,” *Bioorg. Med. Chem.*, vol. 19, no. 20, pp. 5967–5974, Oct. 2011.
- [96] V. N. Uversky, J. Li, P. Souillac, I. S. Millett, S. Doniach, R. Jakes, M. Goedert, and A. L. Fink, “Biophysical Properties of the Synucleins and Their Propensities to Fibrillate: INHIBITION OF α -SYNUCLEIN ASSEMBLY BY β - AND γ -SYNUCLEINS,” *J. Biol. Chem.*, vol. 277, no. 14, pp. 11970–11978, Apr. 2002.
- [97] I. Dikiy and D. Eliezer, “Folding and misfolding of alpha-synuclein on membranes,” *Biochim. Biophys. Acta - Biomembr.*, vol. 1818, no. 4, pp. 1013–1018, Apr. 2012.
- [98] P. J. McLean, S. Ribich, and B. T. Hyman, “Subcellular localization of α -synuclein in primary neuronal cultures: effect of missense mutations,” in *Advances in Research on Neurodegeneration SE - 5*, Y. Mizuno, D. B. Calne, R. Horowski, W. Poewe, P. Riederer, and M. B. H. Youdim, Eds. Springer Vienna, 2000, pp. 53–63.
- [99] C. Guardia-Laguarta, E. Area-Gomez, C. Rüb, Y. Liu, J. Magrané, D. Becker, W. Voos, E. A. Schon, and S. Przedborski, “ α -Synuclein Is Localized to Mitochondria-Associated ER Membranes,” *J. Neurosci.*, vol. 34, no. 1, pp. 249–259, Jan. 2014.
- [100] N. Braidy, W.-P. Gai, Y. Xu, P. Sachdev, G. Guillemin, X.-M. Jiang, J. W. Ballard, M. Horan, Z. Fang, B. Chong, and D. K. Chan, “Uptake and mitochondrial dysfunction of alpha-synuclein in human astrocytes, cortical neurons and fibroblasts,” *Transl. Neurodegener.*, vol. 2, no. 1, p. 20, 2013.

- [101] O. Marques and T. F. Outeiro, “Alpha-synuclein: from secretion to dysfunction and death,” *Cell Death Dis*, vol. 3, 2012.
- [102] M. G. Spillantini, R. A. Crowther, R. Jakes, M. Hasegawa, and M. Goedert, “ α -Synuclein in filamentous inclusions of Lewy bodies from Parkinson’s disease and dementia with Lewy bodies,” *Proc. Natl. Acad. Sci.*, vol. 95, no. 11, pp. 6469–6473, May 1998.
- [103] V. N. Uversky and D. Eliezer, “Biophysics of Parkinson’s disease: structure and aggregation of alpha-synuclein,” *Curr Protein Pept Sci*, vol. 10, no. 5, pp. 483–499, 2009.
- [104] H. A. Lashuel, B. M. Petre, J. Wall, M. Simon, R. J. Nowak, T. Walz, and P. T. Lansbury Jr, “ α -Synuclein, Especially the Parkinson’s Disease-associated Mutants, Forms Pore-like Annular and Tubular Protofibrils,” *J. Mol. Biol.*, vol. 322, no. 5, pp. 1089–1102, Oct. 2002.
- [105] K. A. Conway, J. D. Harper, and P. T. Lansbury, “Accelerated in vitro fibril formation by a mutant [alpha]-synuclein linked to early-onset Parkinson disease,” *Nat Med*, vol. 4, no. 11, pp. 1318–1320, 1998.
- [106] J. J. Zarranz, J. Alegre, J. C. Gómez-Esteban, E. Lezcano, R. Ros, I. Ampuero, L. Vidal, J. Hoenicka, O. Rodriguez, B. Atarés, V. Llorens, E. G. Tortosa, T. del Ser, D. G. Muñoz, and J. G. de Yebenes, “The new mutation, E46K, of α -synuclein causes parkinson and Lewy body dementia,” *Ann. Neurol.*, vol. 55, no. 2, pp. 164–173, 2004.
- [107] E. Masliah, E. Rockenstein, I. Veinbergs, M. Mallory, M. Hashimoto, A. Takeda, Y. Sagara, A. Sisk, and L. Mucke, “Dopaminergic Loss and Inclusion Body Formation in α -Synuclein Mice: Implications for Neurodegenerative Disorders,” *Sci.*, vol. 287, no. 5456, pp. 1265–1269, Feb. 2000.
- [108] M. B. Feany and W. W. Bender, “A Drosophila model of Parkinson’s disease,” *Nature*, vol. 404, no. 6776, pp. 394–398, 2000.
- [109] J. B. Watson, A. Hatami, H. David, E. Masliah, K. Roberts, C. E. Evans, and M. S. Levine, “Alterations in corticostriatal synaptic plasticity in mice overexpressing human α -synuclein,” *Neuroscience*, vol. 159, no. 2, pp. 501–513, Mar. 2009.
- [110] J. M. George, H. Jin, W. S. Woods, and D. F. Clayton, “Characterization of a novel protein regulated during the critical period for song learning in the zebra finch,” *Neuron*, vol. 15, no. 2, pp. 361–372, Jul. 2014.
- [111] A. Abeliovich, Y. Schmitz, I. Fariñas, D. Choi-Lundberg, W.-H. Ho, P. E. Castillo, N. Shinsky, J. M. G. Verdugo, M. Armanini, A. Ryan, M. Hynes, H. Phillips, D. Sulzer, and A. Rosenthal, “Mice Lacking α -Synuclein Display Functional Deficits in the Nigrostriatal Dopamine System,” *Neuron*, vol. 25, no. 1, pp. 239–252, Jul. 2014.

- [112] N. G. Kholodilov, M. Neystat, F. O. Tinmarla, E. Lo Steven, K. E. Larsen, D. Sulzer, and R. E. Burke, "Increased Expression of Rat Synuclein in the Substantia Nigra Pars Compacta Identified by mRNA Differential Display in a Model of Developmental Target Injury," *J. Neurochem.*, vol. 73, no. 6, pp. 2586–2599, Dec. 1999.
- [113] L. Stefanis, "α-Synuclein in Parkinson's Disease," *Cold Spring Harb Perspect Med*, 2012.
- [114] S. Chandra, G. Gallardo, R. Fernández-Chacón, O. M. Schlüter, and T. C. Südhof, "α-Synuclein Cooperates with CSPα in Preventing Neurodegeneration," *Cell*, vol. 123, no. 3, pp. 383–396, Jul. 2014.
- [115] D. D. Murphy, S. M. Rueter, J. Q. Trojanowski, and V. M.-Y. Lee, "Synucleins Are Developmentally Expressed, and α-Synuclein Regulates the Size of the Presynaptic Vesicular Pool in Primary Hippocampal Neurons," *J. Neurosci.*, vol. 20, no. 9, pp. 3214–3220, May 2000.
- [116] F. LS, "Concentric hyalin intraneuronal inclusions of Lewy type in the brains of elderly persons (50 incidental cases): relationship to parkinsonism," *J. Am. Geriatr. Soc.*, 1969.
- [117] L. V Kalia, S. K. Kalia, P. J. McLean, A. M. Lozano, and A. E. Lang, "α-Synuclein oligomers and clinical implications for Parkinson disease," *Ann. Neurol.*, vol. 73, no. 2, pp. 155–169, Feb. 2013.
- [118] O. M. A. El-Agnaf, S. A. Salem, K. E. Paleologou, M. D. Curran, M. J. Gibson, J. A. Court, M. G. Schlossmacher, and D. Allsop, "Detection of oligomeric forms of α-synuclein protein in human plasma as a potential biomarker for Parkinson's disease," *FASEB J.*, vol. 20, no. 3, pp. 419–425, Mar. 2006.
- [119] T. et al Tokuda, "Detection of elevated levels of α-synuclein oligomers in CSF from patients with Parkinson disease.," *Neurology*, 2010.
- [120] D. P. B. Karpinar Madhu Babu Gajula Kügler, Sebastian Opazo, Felipe Rezaei-Ghaleh, Nasrollah Wender, Nora Kim, Hai-Young Taschenberger, Grit Falkenburger, Björn H Heise, Henrike Kumar, Ashutosh Riedel, Dietmar Fichtner, Lars Voigt, Aaron Braus, Gerhard H Giller, "Pre-fibrillar α-synuclein variants with impaired β-structure increase neurotoxicity in Parkinson's disease models," *EMBO J.*, vol. 28, no. 20, pp. 3256–3268, Sep. 2009.
- [121] O. W. Wan and K. K. K. Chung, "The Role of Alpha-Synuclein Oligomerization and Aggregation in Cellular and Animal Models of Parkinson's Disease," *PLoS One*, vol. 7, no. 6, p. e38545, 2012.
- [122] N. Gosavi, H.-J. Lee, J. S. Lee, S. Patel, and S.-J. Lee, "Golgi Fragmentation Occurs in the Cells with Prefibrillar α-Synuclein Aggregates and Precedes the Formation of Fibrillar Inclusion," *J. Biol. Chem.*, vol. 277, no. 50, pp. 48984–48992, Dec. 2002.

- [123] R. A. Bodner, T. F. Outeiro, S. Altmann, M. M. Maxwell, S. H. Cho, B. T. Hyman, P. J. McLean, A. B. Young, D. E. Housman, and A. G. Kazantsev, "Pharmacological promotion of inclusion formation: A therapeutic approach for Huntington's and Parkinson's diseases," *Proc. Natl. Acad. Sci. United States Am.* , vol. 103 , no. 11 , pp. 4246–4251, Mar. 2006.
- [124] B. Winner, R. Jappelli, S. K. Maji, P. A. Desplats, L. Boyer, S. Aigner, C. Hetzer, T. Loher, M. Vilar, S. Campioni, C. Tzitzilonis, A. Soragni, S. Jessberger, H. Mira, A. Consiglio, E. Pham, E. Masliah, F. H. Gage, and R. Riek, "In vivo demonstration that α -synuclein oligomers are toxic," *Proc. Natl. Acad. Sci.* , vol. 108 , no. 10 , pp. 4194–4199, Mar. 2011.
- [125] K. M. Danzer, D. Haasen, A. R. Karow, S. Moussaud, M. Habeck, A. Giese, H. Kretschmar, B. Hengerer, and M. Kostka, "Different Species of α -Synuclein Oligomers Induce Calcium Influx and Seeding," *J. Neurosci.* , vol. 27 , no. 34 , pp. 9220–9232, Aug. 2007.
- [126] V. N. Uversky, J. Li, and A. L. Fink, "Evidence for a partially folded intermediate in alpha-synuclein fibril formation.," *J. Biol. Chem.*, 2001.
- [127] C. W. Bertoncini, Y.-S. Jung, C. O. Fernandez, W. Hoyer, C. Griesinger, T. M. Jovin, and M. Zweckstetter, "Release of long-range tertiary interactions potentiates aggregation of natively unstructured α -synuclein," *Proc. Natl. Acad. Sci. United States Am.* , vol. 102 , no. 5 , pp. 1430–1435, Feb. 2005.
- [128] V. N. Uversky, "What does it mean to be natively unfolded?," *Eur. J. Biochem.*, vol. 269, no. 1, pp. 2–12, Jan. 2002.
- [129] W. S. Davidson, A. Jonas, D. F. Clayton, and J. M. George, "Stabilization of α -Synuclein Secondary Structure upon Binding to Synthetic Membranes," *J. Biol. Chem.* , vol. 273 , no. 16 , pp. 9443–9449, Apr. 1998.
- [130] T. Bartels, J. G. Choi, and D. J. Selkoe, "[agr]-Synuclein occurs physiologically as a helically folded tetramer that resists aggregation," *Nature*, vol. 477, no. 7362, pp. 107–110, Sep. 2011.
- [131] W. Wang, I. Perovic, J. Chittuluru, A. Kaganovich, L. T. T. Nguyen, J. Liao, J. R. Auclair, D. Johnson, A. Landru, A. K. Simorellis, S. Ju, M. R. Cookson, F. J. Asturias, J. N. Agar, B. N. Webb, C. Kang, D. Ringe, G. A. Petsko, T. C. Pochapsky, and Q. Q. Hoang, "A soluble α -synuclein construct forms a dynamic tetramer," *Proc. Natl. Acad. Sci.* , vol. 108 , no. 43 , pp. 17797–17802, Oct. 2011.
- [132] B. Fauvet, M. K. Mbefo, M.-B. Fares, C. Desobry, S. Michael, M. T. Ardah, E. Tsika, P. Coune, M. Prudent, N. Lion, D. Eliezer, D. J. Moore, B. Schneider, P. Aebischer, O. M. El-Agnaf, E. Masliah, and H. A. Lashuel, " α -Synuclein in Central Nervous System and

- from Erythrocytes, Mammalian Cells, and Escherichia coli Exists Predominantly as Disordered Monomer,” *J. Biol. Chem.* , vol. 287 , no. 19 , pp. 15345–15364, May 2012.
- [133] V. N. Uversky, “A Protein-Chameleon: Conformational Plasticity of α -Synuclein, a Disordered Protein Involved in Neurodegenerative Disorders,” *J. Biomol. Struct. Dyn.*, vol. 21, no. 2, 2003.
- [134] M. H. Polymeropoulos, C. Lavedan, E. Leroy, S. E. Ide, A. Dehejia, A. Dutra, B. Pike, H. Root, J. Rubenstein, R. Boyer, E. S. Stenroos, S. Chandrasekharappa, A. Athanassiadou, T. Papapetropoulos, W. G. Johnson, A. M. Lazzarini, R. C. Duvoisin, G. Di Iorio, L. I. Golbe, and R. L. Nussbaum, “Mutation in the α -Synuclein Gene Identified in Families with Parkinson’s Disease,” *Sci.* , vol. 276 , no. 5321 , pp. 2045–2047, Jun. 1997.
- [135] C. W. Bertoncini, C. O. Fernandez, C. Griesinger, T. M. Jovin, and M. Zweckstetter, “Familial Mutants of α -Synuclein with Increased Neurotoxicity Have a Destabilized Conformation,” *J. Biol. Chem.* , vol. 280 , no. 35 , pp. 30649–30652, Sep. 2005.
- [136] K. A. Conway, S.-J. Lee, J.-C. Rochet, T. T. Ding, R. E. Williamson, and P. T. Lansbury, “Acceleration of oligomerization, not fibrillization, is a shared property of both α -synuclein mutations linked to early-onset Parkinson’s disease: Implications for pathogenesis and therapy,” *Proc. Natl. Acad. Sci.* , vol. 97 , no. 2 , pp. 571–576, Jan. 2000.
- [137] L. Narhi, S. J. Wood, S. Steavenson, Y. Jiang, G. M. Wu, D. Anafi, S. A. Kaufman, F. Martin, K. Sitney, P. Denis, J.-C. Louis, J. Wypych, A. L. Biere, and M. Citron, “Both Familial Parkinson’s Disease Mutations Accelerate α -Synuclein Aggregation,” *J. Biol. Chem.* , vol. 274 , no. 14 , pp. 9843–9846, Apr. 1999.
- [138] E. A. Greenbaum, C. L. Graves, A. J. Mishizen-Eberz, M. A. Lupoli, D. R. Lynch, S. W. Englander, P. H. Axelsen, and B. I. Giasson, “The E46K Mutation in α -Synuclein Increases Amyloid Fibril Formation,” *J. Biol. Chem.* , vol. 280 , no. 9 , pp. 7800–7807, Mar. 2005.
- [139] L. R. Lemkau, G. Comellas, S. W. Lee, L. K. Rikardsen, W. S. Woods, J. M. George, and C. M. Rienstra, “Site-Specific Perturbations of Alpha-Synuclein Fibril Structure by the Parkinson’s Disease Associated Mutations A53T and E46K,” *PLoS One*, vol. 8, no. 3, p. e49750, Mar. 2013.
- [140] E. Hazy, M. Bokor, L. Kalmar, A. Gelencser, P. Kamasa, K.-H. Han, K. Tompa, and P. Tompa, “Distinct Hydration Properties of Wild-Type and Familial Point Mutant A53T of α -Synuclein Associated with Parkinson’s Disease,” *Biophys. J.*, vol. 101, no. 9, pp. 2260–2266, Jul. 2014.
- [141] O. Wise-Scira, A. Dunn, A. K. Aloglu, I. T. Sakallioglu, and O. Coskuner, “Structures of the E46K Mutant-Type α -Synuclein Protein and Impact of E46K Mutation on the

- Structures of the Wild-Type α -Synuclein Protein,” *ACS Chem. Neurosci.*, vol. 4, no. 3, pp. 498–508, Jan. 2013.
- [142] C. C. Rospigliosi, S. McClendon, A. W. Schmid, T. F. Ramlall, P. Barré, H. A. Lashuel, and D. Eliezer, “E46K Parkinson’s-Linked Mutation Enhances C-Terminal-to-N-Terminal Contacts in α -Synuclein,” *J. Mol. Biol.*, vol. 388, no. 5, pp. 1022–1032, May 2009.
- [143] R. A. Fredenburg, C. Rospigliosi, R. K. Meray, J. C. Kessler, H. A. Lashuel, D. Eliezer, and P. T. Lansbury, “The Impact of the E46K Mutation on the Properties of α -Synuclein in Its Monomeric and Oligomeric States†,” *Biochemistry*, vol. 46, no. 24, pp. 7107–7118, May 2007.
- [144] K. E. Paleologou, A. W. Schmid, C. C. Rospigliosi, H.-Y. Kim, G. R. Lamberto, R. A. Fredenburg, P. T. Lansbury, C. O. Fernandez, D. Eliezer, M. Zweckstetter, and H. A. Lashuel, “Phosphorylation at Ser-129 but Not the Phosphomimics S129E/D Inhibits the Fibrillation of α -Synuclein,” *J. Biol. Chem.*, vol. 283, no. 24, pp. 16895–16905, Jun. 2008.
- [145] D. Eliezer, E. Kutluay, R. Bussell Jr, and G. Browne, “Conformational properties of α -synuclein in its free and lipid-associated states,” *J. Mol. Biol.*, vol. 307, no. 4, pp. 1061–1073, Apr. 2001.
- [146] R. Bussell and D. Eliezer, “Residual Structure and Dynamics in Parkinson’s Disease-associated Mutants of α -Synuclein,” *J. Biol. Chem.*, vol. 276, no. 49, pp. 45996–46003, Dec. 2001.
- [147] J. D. Perlmutter, A. R. Braun, and J. N. Sachs, “Curvature Dynamics of α -Synuclein Familial Parkinson Disease Mutants: MOLECULAR SIMULATIONS OF THE MICELLE- AND BILAYER-BOUND FORMS,” *J. Biol. Chem.*, vol. 284, no. 11, pp. 7177–7189, Mar. 2009.
- [148] H.-J. Koo, M. Y. Choi, and H. Im, “Aggregation-defective α -synuclein mutants inhibit the fibrillation of Parkinson’s disease-linked α -synuclein variants,” *Biochem. Biophys. Res. Commun.*, vol. 386, no. 1, pp. 165–169, Aug. 2009.
- [149] M. Zhu, S. Han, and A. L. Fink, “Oxidized quercetin inhibits α -synuclein fibrillization,” *Biochim. Biophys. Acta - Gen. Subj.*, vol. 1830, no. 4, pp. 2872–2881, Apr. 2013.
- [150] M. Caruana, T. Högen, J. Levin, A. Hillmer, A. Giese, and N. Vassallo, “Inhibition and disaggregation of α -synuclein oligomers by natural polyphenolic compounds,” *FEBS letters*, vol. 585, no. 8, Elsevier Science B.V., pp. 1113–1120, 20-Apr-2011.
- [151] N. Ostrerova-Golts, L. Petrucelli, J. Hardy, J. M. Lee, M. Farer, and B. Wolozin, “The A53T α -Synuclein Mutation Increases Iron-Dependent Aggregation and Toxicity,” *J. Neurosci.*, vol. 20, no. 16, pp. 6048–6054, Aug. 2000.

- [152] M. Zhu, S. Rajamani, J. Kaylor, S. Han, F. Zhou, and A. L. Fink, "The Flavonoid Baicalein Inhibits Fibrillation of α -Synuclein and Disaggregates Existing Fibrils," *J. Biol. Chem.* , vol. 279 , no. 26 , pp. 26846–26857, Jun. 2004.
- [153] D. E. Ehrnhoefer, J. Bieschke, A. Boeddrich, M. Herbst, L. Masino, R. Lurz, S. Engemann, A. Pastore, and E. E. Wanker, "EGCG redirects amyloidogenic polypeptides into unstructured, off-pathway oligomers," *Nat Struct Mol Biol*, vol. 15, no. 6, pp. 558–566, Jun. 2008.
- [154] J. Bieschke, J. Russ, R. P. Friedrich, D. E. Ehrnhoefer, H. Wobst, K. Neugebauer, and E. E. Wanker, "EGCG remodels mature α -synuclein and amyloid- β fibrils and reduces cellular toxicity," *Proc. Natl. Acad. Sci.* , vol. 107 , no. 17 , pp. 7710–7715, Apr. 2010.
- [155] M. Fokkens, T. Schrader, and F.-G. Klärner, "A Molecular Tweezer for Lysine and Arginine," *J. Am. Chem. Soc.*, vol. 127, no. 41, pp. 14415–14421, Sep. 2005.
- [156] A. H. Mao, S. L. Crick, A. Vitalis, C. L. Chicoine, and R. V Pappu, "Net charge per residue modulates conformational ensembles of intrinsically disordered proteins," *Proc. Natl. Acad. Sci.* , vol. 107 , no. 18 , pp. 8183–8188, May 2010.
- [157] R. K. Das and R. V Pappu, "Conformations of intrinsically disordered proteins are influenced by linear sequence distributions of oppositely charged residues," *Proc. Natl. Acad. Sci.* , Jul. 2013.
- [158] S. Prabhudesai, S. Sinha, A. Attar, A. Kotagiri, A. Fitzmaurice, R. Lakshmanan, M. Ivanova, J. Loo, F.-G. Klärner, T. Schrader, M. Stahl, G. Bitan, and J. Bronstein, "A Novel 'Molecular Tweezer' Inhibitor of α -Synuclein Neurotoxicity in Vitro and in Vivo," *Neurotherapeutics*, vol. 9, no. 2, pp. 464–476, 2012.
- [159] A. Attar, C. Ripoli, E. Riccardi, P. Maiti, D. D. Li Puma, T. Liu, J. Hayes, M. R. Jones, K. Lichti-Kaiser, F. Yang, G. D. Gale, C. Tseng, M. Tan, C.-W. Xie, J. L. Straudinger, F.-G. Klärner, T. Schrader, S. A. Frautschy, C. Grassi, and G. Bitan, "Protection of primary neurons and mouse brain from Alzheimer's pathology by molecular tweezers," *Brain* , vol. 135 , no. 12 , pp. 3735–3748, Dec. 2012.
- [160] S. J. Sahl, L. E. Weiss, W. C. Duim, J. Frydman, and W. E. Moerner, "Cellular Inclusion Bodies of Mutant Huntingtin Exon 1 Obscure Small Fibrillar Aggregate Species," *Sci. Rep.*, vol. 2, Nov. 2012.